International Ocean Discovery Program Expedition 359 Preliminary Report

Maldives Monsoon and Sea Level

30 September–30 November 2015

Christian G. Betzler, Gregor P. Eberli, Carlos A. Alvarez Zarikian, and the Expedition 359 Scientists

IODP
INTERNATIONAL OCEAN DISCOVERY PROGRAM

Publisher's notes

Core samples and the wider set of data from the science program covered in this report are under moratorium and accessible only to Science Party members until 4 May 2017.

This publication was prepared by the International Ocean Discovery Program *JOIDES Resolution* Science Operator (IODP JRSO) as an account of work performed under the International Ocean Discovery Program. Funding for the program is provided by the following implementing organizations and international partners:

National Science Foundation (NSF), United States
Ministry of Education, Culture, Sports, Science and Technology (MEXT), Japan
European Consortium for Ocean Research Drilling (ECORD)
Ministry of Science and Technology (MOST), People's Republic of China
Korea Institute of Geoscience and Mineral Resources (KIGAM)
Australia-New Zealand IODP Consortium (ANZIC)
Ministry of Earth Sciences (MoES), India
Coordination for Improvement of Higher Education Personnel, Brazil (CAPES)

Portions of this work may have been published in whole or in part in other International Ocean Discovery Program documents or publications.

Disclaimer

Copyright

Citation

Betzler, C.G., Eberli, G.P., Alvarez Zarikian, C.A., and the Expedition 359 Scientists, 2016. *Expedition 359 Preliminary Report: Maldives Monsoon and Sea Level*. International Ocean Discovery Program. http://dx.doi.org/10.14379/iodp.pr.359.2016

ISSN

World Wide Web: 2372-9562

Expedition 359 participants

Expedition 359 scientists

Christian G. Betzler
Co-Chief Scientist
Institute of Geology
CEN, University of Hamburg
Bundesstrasse 55
Hamburg 20146
Germany
christian.betzler@uni-hamburg.de

Gregor P. Eberli
Co-Chief Scientist
Department of Marine Geosciences
Rosenstiel School of Marine & Atmospheric Science
University of Miami
Miami FL 33149
USA
geberli@rsmas.miami.edu

Carlos A. Alvarez-Zarikian
Expedition Project Manager/ Staff Scientist
International Ocean Discovery Program
Texas A&M University
1000 Discovery Drive
College Station TX 77845
USA
zarikian@iodp.tamu.edu

Montserrat Alonso-García
Paleontologist (foraminifers)
IPMA (Instituto Português do Mar e da Atmosfera)
Divisão de Geologia e Georecursos Marinhos
Avenida de Brasilia 6
1449-006 Lisboa
Portugal
montserrat.alonso@ipma.pt

Centro de Ciencias do Mar (CCMAR)
Universidade do Algarve
8005-139 Faro
Portugal

Nagender N. Bejugam
Sedimentologist
Geological Oceanography Division
CSIR—National Institute of Oceanography
Dona Paula Goa 403004
India
nagender@nio.org

Or M. Bialik
Sedimentologist
Dr. Moses Strauss Department of Marine Geosciences
The Leon H. Charney School of Marine Sciences
University of Haifa
Carmel 31905
Israel
obialik@campus.haifa.ac.il

Clara L. Blättler
Inorganic Geochemist
Department of Geosciences
Princeton University
Guyot Hall
Princeton NJ 08544
USA
blattler@princeton.edu

Junhua Adam Guo
Physical Properties Specialist
Department of Geological Sciences
California State University Bakersfield
9001 Stockdale Highway
Bakersfield, CA 93311
USA
jguo1@csub.edu

Sébastien Haffen
Physical Properties Specialist
Ecole Nationale Superieure de Geologie
Universite de Lorraine
2 rue du Doyen Marcel Roubault
Vandoeuvre-les-Nancy 54501
France
sebastien.haffen@gmail.com

Senay Horozal
Physical Properties Specialist
Petroleum and Marine Research Division
Korea Institute of Geoscience & Mineral Resources (KIGAM)
Gwahang-no 124, Yuseong-gu
Daejeon 305-350
Korea
shorozal@kigam.re.kr

Mayuri Inoue
Inorganic Geochemist
Department of Earth Sciences
Okayama University
3-1-1 Tsushima-naka 700-8530
Japan
inouem@cc.okayama-u.ac.jp

Luigi Jovane
Paleomagnetist
Instituto Oceanográfico da Universidade de São Paulo
Praça do Oceanográfico, 191
São Paulo, SP 05508-120
Brazil
jovane@usp.br

Dick Kroon
Paleontologist (foraminifers)
Department of Geology and Geophysics
University of Edinburgh
Grant Institute, The King's Buildings, James Hutton Road
Edinburgh EH9 3FE
United Kingdom
dick.kroon@ed.ac.uk

Luca Lanci
Paleomagnetist
Istituto di Scienze della Terra
Università di Urbino
Via S. Chiara 27
Urbino 61029
Italy
luca.lanci@uniurb.it

Juan Carlos Laya
Sedimentologist
Department of Geology and Geophysics and Berg-Hughes Center for Petroleum and Sedimentary Systems
Texas A&M University
Mail Stop 3115
College Station TX 77843-3115
USA
layajc@geos.tamu.edu

Anna Ling Hui Mee
Sedimentologist
Department of Marine Geosciences
University of Miami
RSMAS MGG N260
Key Biscayne FL 33149
USA
a.ling@rsmas.miami.edu

Thomas Lüdmann
Downhole Measurements
Institute of Geology
CEN, University of Hamburg
Bundesstrasse 55
Hamburg 20146
Germany
thomas.luedmann@uni-hamburg.de

Masatoshi Nakakuni
Organic Geochemist
Department of Environmental Engineering for Symbiosis
Soka University
1-236 Tangi-cyo
Hachioji-shi Tokyo 192-0003
Japan
e13d5702@soka-u.jp

Kaoru Niino
Paleontologist (radiolarians)
Graduate School of Science and Engineering
Yamagata University
1-4-12 Kojirakawa-machi
Yamagata City 990-8560
Japan
s14e510m@st.yamagata-u.ac.jp

Loren M. Petruny
Paleontologist (benthic foraminifers)
Environmental Science and Policy Department
David King Hall Rm 3005, MSN 5F2
George Mason University
4400 University Drive
Fairfax, VA 22030-4444
USA
lpetruny@gmu.edu

Santi D. Pratiwi
Paleontologist (nannofossils)
Faculty of International Resource Science
Akita University
1-1 Teagata-Gakuencho
Akita 010-8502
Japan
rhabdosphaera@gmail.com

John Reijmer
Sedimentologist
Faculty of Earth and Life Sciences
VU University Amsterdam
De Boelelaan 1085
1081 HV Amsterdam
Netherlands
j.j.g.reijmer@vu.nl

Jesús Reolid
Sedimentologist
Institute of Geology
CEN, University of Hamburg
Bundesstrasse 55
Hamburg 20146
Germany
jesus.reolid@uni-hamburg.de

Angela L. Slagle
Downhole Measurements
Lamont-Doherty Earth Observatory
Columbia University
Borehole Bldg. 61 Route 9W
Palisades NY 10964
USA
aslagle@ldeo.columbia.edu

Craig R. Sloss
Sedimentologist
Earth and Environmental Sciences
University of Technology Queensland
R-Block 317, 2 George Street
Brisbane Queensland 4001
Australia
c.sloss@qut.edu.au

Xiang Su
Paleontologist (nannofossils)
Key Laboratory of Marginal Sea Geology
South China Sea Institute of Oceanology
Chinese Academy of Sciences
164 West Xingang Road
Guangzhou 510301
P.R. China
suxiang@scsio.ac.cn

Peter K. Swart
Inorganic Geochemist
Department of Marine Geosciences
University of Miami
4600 Rickenbacker Causeway
Miami FL 33148
USA
pswart@rsmas.miami.edu

James D. Wright
Stratigraphic Correlator
Department of Geological Sciences
Rutgers, The State University of New Jersey
610 Taylor Road
Piscataway NJ 08854-8066
USA
jdwright@rci.rutgers.edu

Zhengquan Yao
Sedimentologist
Department of Marine Geology
First Institute of Oceanography (FIO) State Oceanic Administration (SOA)
6 Xian Xia Ling Road
Qingdao Shandong Province 266061
P.R. China
yaozq@126.com

Jeremy R. Young
Paleontologist (Nannofossil)
Earth Sciences
University College London
Gower Street
London WC1E 6BT
jeremy.young@ucl.ac.uk

Education and outreach

Juliet M. Crowell
Education/Outreach Officer
IODP-Ocean Leadership
1390 Bryant Street NE Apt 304
Washington DC 20018
USA
belize67@aol.com
crowelljuliet@gmail.com

Michelle D. Darrieu
Education/Outreach Officer
IODP-Ocean Leadership
Rue de la fauvette, 2
Bruxelles 1180
Belgium
michele_darrieu@hotmail.com

Siem Offshore AS Officials

Steve Bradley
Master of the Drilling Vessel

Wayne Malone
Offshore Installation Manager

Technical support

Robert Aduddell
Engineer

Timothy Blaisdell
Application Developer

Courtney Bouchard
Marine Laboratory Specialist (temporary)

Lisa Brandt
Chemistry Laboratory

Timothy Bronk
Assistant Laboratory Officer

Chad Broyles
Curatorial Specialist

Lisa Crowder
Laboratory Officer

Douglas Cummings
Publications Specialist

Benjamin Daniel
Thin Section Laboratory

William Davidson
Marine Laboratory Specialist (temporary)

Daniel Fields
Marine Laboratory Specialist (temporary)

Seth Frank
X-ray/Microbiology Laboratory

Timothy Fulton
Imaging Specialist

Clayton Furman
Logging Engineer

Randy Gjesvold
Marine Instrumentation Specialist

Rachael Gray
Chemistry Laboratory

Margaret Hastedt
Core Laboratory

Sandra Herrmann
Assistant Laboratory Officer

Michael Hodge
Marine Computer Specialist

Minh Nhut Huynh
Marine Computer Specialist

Mike Meiring
Electronics Specialist

Shawn Miller
Marine Laboratory Specialist (temporary)

Beth Novak
Paleomagnetism Laboratory

Michael Storms
Operations Superintendent

Garrick Van Rensburg
Marine Instrumentation Specialist

Hai (James) Zhao
Applications Developer

Abstract

International Ocean Discovery Program Expedition 359 was designed to address changes in sea level and currents, along with monsoon evolution in the Indian Ocean. Eight drill sites are located in the carbonate edifice of the Republic of Maldives, which bears a unique and mostly unread Indian Ocean archive of the evolving Cenozoic icehouse world. This tropical marine record is key for better understanding the effects of this global evolution in the Indo-Pacific realm. The bank geometries of the growing carbonate archipelago provide a physical record of changing sea level and ocean currents. The bank growth occurs in pulses of aggradation and progradation that are controlled by sea level fluctuations during the early and middle Miocene, including the mid-Miocene Climate Optimum. A dramatic shift in development of the carbonate edifice from a sea level–controlled to a predominantly current-controlled system appears to be directly linked to the evolving Indian monsoon. This phase led to a twofold configuration of bank development: bank growth continued in some parts of the edifice, whereas in other places, banks drowned. Drowning steps seem to coincide with onset and intensification of the monsoon-related current system and deposition of contourite fans and giant sediment drifts. Expedition 359 cores are intended for reconstructing the changing current system through time that is directly related to the evolution of the Indian monsoon. As such, the drift deposits will provide a continuous record of Indian monsoon development in the region of the Maldives.

Expedition 359 had two main focus points. The first was to date precisely the onset of the current system that is potentially in concert with the onset or the intensification of the Indian monsoon and coincides with the onset of the modern current system in the world's ocean. The second important outcome of Expedition 359 is groundtruthing the hypothesis that the dramatic, pronounced change in style of the sedimentary carbonate sequence stacking was caused by a combination of relative sea level fluctuations and ocean current system changes. These questions were directly addressed by the shipboard scientific data.

In addition, Expedition 359 cores will provide a complete Neogene $\delta^{13}C$ record of the platform and platform margin sediments and a comparison with pelagic records over the same time period. This comparison will allow assessment of the extent to which platform carbonates record changes in the global carbon cycle and whether changes in the carbon isotopic composition of organic and inorganic components covary and the implications this has on the deep-time record. This determination is important, as such records are the only type that exist in deep time.

Introduction

Changes in oceanic circulation and sea level, along with onset and fluctuations of the Indian monsoon characterize the Neogene. Located in the Indian Ocean, the Maldives carbonate edifice bears the tropical marine record of these changes. The archipelago is characterized by a double row of atolls encompassing a basin, the Maldives Inner Sea, connected to the open ocean through passages. The Maldives Inner Sea has served as a depositional center of current-controlled deposits (i.e., drifts) since the partial drowning of parts of the carbonate edifice during the middle Miocene. This sedimentary system of drowned platform parts and drifts was the target of International Ocean Discovery Program (IODP) Expedition 359, which aimed to reconstruct its paleoceanographic evolution over the past 23 My. The approach of Expedition 359 was to reconstruct this evolution from the combined physical record provided by the seismic data, the lithologic record in the neritic and hemipelagic deposits, and the chemical proxies within the sedimentary column. This reconstruction was achieved by drilling eight sites aligned into two transects covering shallow to deepwater deposits. Sites U1465, U1466, U1468, U1469, and U1470 were drilled to recover a sedimentary sequence encompassing a carbonate platform to drift succession (Oligocene to Pleistocene). Sites U1467, U1471, and U1472 recovered a Miocene to Pleistocene carbonate drift succession. The expedition built on a series of seismic data sets that image the different steps of carbonate platform evolution (R/V *Meteor* Cruise M74/4 NEOMA and R/V *Sonne* Cruise SO236 MALSTROM) and previously drilled Ocean Drilling Program (ODP) Site 716 (Leg 115) (Backman, Duncan, et al., 1988).

Background

Geological setting of the Maldives

The Maldives archipelago in the central equatorial Indian Ocean is an isolated tropical carbonate platform edifice constituting the central and largest part of the Chagos-Laccadive Ridge, which is located southwest of India (Figure **F1**). A north-south–oriented double row of atolls encloses the Inner Sea of the Maldives (Figure **F2**). The atolls are separated from each other by interatoll channels that deepen toward the Indian Ocean (Purdy and Bertram, 1993). The Inner Sea is a basin with water as deep as 550 m. The Maldives carbonate succession accumulated since the Eocene, away from any terrigenous input (Aubert and Droxler, 1992; Purdy and Bertram, 1993).

The modern archipelago comprises about 1200 smaller atolls that lie near or slightly above the sea surface. Discontinuous marginal rims formed by such small atolls surround lagoons with water depths up to 50–60 m. These rims are interrupted by deep passages, allowing strong currents within the atoll lagoons to rework and redeposit sediment and influence the growth of patch reefs (Ciarapica and Passeri, 1993; Betzler et al., 2015). Modern marginal reefs are composed of robust-branching corals and coralline algae, whereas the lagoonal reefs show domal corals and detrital sand and rubble facies (Gischler et al., 2008). Muddy sediments are present only in atoll areas that are protected by large marginal reefs (Ciarapica and Passeri, 1993; Gischler, 2006; Betzler et al., 2015).

The oceanward margins of the Maldives archipelago are generally steeply inclined, with dips of 20°–30° to 2000 m water depth. On the Inner Sea side, terraced atoll slopes have the same dip angles but reach to water depths of only 150 m, where the gradient rapidly declines (Fürstenau et al., 2010). The Inner Sea is characterized by periplatform ooze deposition that locally accumulates into sediment drift bodies (Droxler et al., 1990; Malone et al., 1990; Betzler et al., 2009, Lüdmann et al., 2013).

The climate and oceanographic setting of the Maldives are dictated by the seasonally reversing Indian monsoon system (Tomczak and Godfrey, 2003). Southwestern winds prevail during Northern Hemisphere summer (April–November), and northeastern winds prevail during winter (December–March). Winds generate ocean currents that are directed westward in the winter and eastward in the summer. Interseasonally, a band of Indian Ocean equatorial westerlies are established, enforcing strong eastward-flowing surface currents with velocities up to 1.3 m/s. Currents reach water depths of 200 m and more with only slightly reduced velocities (Tomczak and Godfrey, 2003). Within the modern atolls' passages,

currents can exhibit velocities up to 2 m/s at the surface (Preu and Engelbrecht, 1991), accounting for winnowing in the passages and lagoons, where hard bottoms form (Ciarapica and Passeri, 1993; Gischler, 2006; Betzler et al., 2015).

The Maldives formed on a lower Paleogene (60–50 Ma) volcanic basement (Duncan and Hargraves, 1990) (Figure F3). The long-term subsidence rate of the Maldives is roughly 0.03–0.04 mm/y based on deep core data from Well ARI-1 (Aubert and Droxler, 1996; Belopolsky and Droxler, 2004a). In contrast, sedimentological data from the Rasdhoo atoll indicate a much faster subsidence rate since the last interglacial, with a maximum subsidence rate of 0.15 mm/y during the past 135,000 y (Gischler et al., 2008).

Lower to middle Miocene

The Maldives comprise an approximately 3 km thick shallow-water carbonate succession (Belopolsky and Droxler, 2004a) (Figure F3). Carbonate production was established during the early Eocene when flat-topped carbonate banks began to form on topographic highs created by the volcanic basement during the Eocene to early Oligocene. During the late Oligocene, bank margins typically had elevated rims that separated bank-interior areas from the open ocean. During the early Miocene, these banks partially drowned and carbonate production became restricted to narrow bands at the respective most oceanward areas. During the Miocene, bank margins prograded toward the Inner Sea, as recognized in different versions of seismic reflection data, irrespective of seismic resolution (Purdy and Bertram, 1993; Aubert and Droxler, 1996; Belopolsky and Droxler, 2004a; Betzler et al., 2009, 2013a).

Ten seismic sequences are recognized in the lower and middle Miocene platform strata of the Maldives (Betzler et al., 2013a) (Figures F4, F5). These sequences are interpreted to have formed in response to sea level–driven accommodation space variations (Betzler et al., 2013a). Platform Sequences (PS) 1–6 show development from a shallow ramp to a steep-flanked, reef-rimmed carbonate platform. Bank-edge reefs protect the lagoon where backreef aprons occur. At the PS6–PS7 transition, a switch from dominantly aggrading to dominantly prograding bank margins occurs. PS7–PS10 are composed of deposits formed in response to forced regression and are overlain by deposits formed during reflooding of the bank margins.

Middle Miocene to Pleistocene

The upper middle Miocene is characterized by the appearance of large-scale lobate clinoform bodies, attesting to the onset of current amplification in the Inner Sea (Figures F4, F5) (Betzler et al., 2013a; Lüdmann et al., 2013). These bodies are attached to passages where parts of barrier reefs drowned while remaining banks and atolls grew elsewhere (Betzler et al., 2009, 2013a). Lobes are interpreted as "mega spillovers" fed by easterly currents and reworked by a current system flowing obliquely or normally to this main stream. This current pattern filled the Inner Sea from west to east (Lüdmann et al., 2013). Starting with Drift Sequence (DS) 6, the opening of a southern gateway introduced northward flow of bottom water into the Inner Sea, leading to deposition of giant elongated drifts at the eastern flank of the basin, filling it from east to west. Because the current swept away most of the material around the atolls, the system was not able to prograde and the steady subsidence was compensated by aggradation (Betzler et al., 2013a; Lüdmann et al., 2013).

DS1–DS9 are mostly conformable in the central part of the Inner Sea, but they display downlaps and onlaps at the basin margins. Two main types of bottom current–controlled deposits occur: (1) a prograding wedge to clinoform type near the passages between the atolls and (2) a mounded shape type located along the atoll flanks with a broad moat of 2.2–2.5 km in the updip direction (Lüdmann et al., 2013). The mounded shape type is interpreted as a plastered drift body of a giant elongated drift migrating along the basin flank under a weak current regime (Faugères et al., 1999). Narrower moats (500–800 m) at the western flank of the Inner Sea are interpreted as reflecting a high-velocity current focused in the west and a wider, slower current in the east. This partitioning is in line with monsoonal-triggered current reversals.

Two additional drowning steps affected the Maldives (Betzler et al., 2009, 2013a). Flat-topped and atoll-shaped banks are interpreted to have drowned quickly, whereas mound-shaped banks are interpreted to have undergone sequential drowning under elevated nutrient fluxes (Betzler et al., 2009), similar to banks described by Zampetti et al. (2004) offshore Malaysia. The drowned banks are elongated parallel to the extension of the Kardiva Channel, which is characterized by throughflow of monsoon-driven surface currents (Betzler et al., 2009). This shape is interpreted as reflecting current control, similar to the recent atolls that are elongated because of the action of waves and currents (Purdy and Bertram, 1993).

Partial drowning steps triggered by currents

The precise timing of current evolution in the Maldives is not well established, but some turning points are known. Marine records suggest onset of monsoonal-triggered marine upwelling at ~8.5 Ma (Kroon et al., 1991). An increase in sediment flux into the Indian Ocean occurred around 11 Ma (Rea, 1992; Zheng et al., 2004), and a peak in the sedimentation rates of the Indus Fan occurred between 16 and 10 Ma (Clift et al., 2008). Onset and monsoon-intensification steps correlate with the Maldives partial drowning steps (Betzler et al., 2013a). It is therefore proposed that currents and upwelling from monsoonal currents shaped the atolls in the past, controlling sediment production and reef growth. Thus, the timing of partial platform drowning and monsoon evolution is linked. Under monsoon conditions, upwelling injected nutrients into surface waters, affecting the carbonate banks (Betzler et al., 2009). This process caused the demise of the barrier reef system, which was replaced by a string of current-shaped relict reefs separated by passages accommodating the throughflow of currents (Betzler et al., 2009, Lüdmann et al., 2013).

Site summaries

Site U1465

Background and objectives

One goal of Expedition 359, in addition to retrieving the record of the Neogene sea level changes in the prograding Kardiva platform and the onset of the monsoon-related currents in drift deposits, was to establish the time and cause of the drowning of the Kardiva platform during the middle Miocene. Platform drowning–related questions were the focus of Site U1465, which is situated above the margin of the drowned Kardiva platform that is overlain by 70 m of sediment. It is the westernmost site of a four-site transect that runs from west to east in the Kardiva Channel. Site U1465 (proposed Site MAL-01A) is located at 4°55.9873′N, 73°0.6786′E in a water depth of 512.64 m between the Goidhoo and South Maalhosmadulu atolls (Figure F2).

Carbonate platforms are the only depositional system that can cease to exist. The mechanism of the platform demise is usually

drowning, but the reason(s) for drowning is still unresolved (Schlager, 1981). Many processes have been proposed, such as global anoxic events, tectonic breakup, and excess nutrients (Arthur and Schlanger, 1979; Hallock and Schlager, 1986; Philip and Schlager, 1990; Eberli, 1991). The close relationship between platform drowning and intensification of ocean currents has been proposed for the demise of the Miocene platforms on the Marion Plateau (Isern et al., 2004; John and Mutti, 2005; Eberli et al., 2010). Betzler et al. (2009, 2013a) and Lüdmann et al. (2013) document partial platform drowning in the Maldives and propose that, in the Maldives, the drowning of the platforms is the combined product of current activity and nutrient supply. Examining the drowning unconformity and the pre- and postdrowning succession in regard to age, composition, and diagenetic overprint was intended to provide evidence to link drowning directly to the onset of the monsoon-related current system and the concomitant excess nutrient supply from upwelling.

Principal results

The advanced piston corer (APC) deployed in Hole U1465A cored 76.6 m mainly in the drift sequence overlying the drowned platform, recovering 53.24 m (70% recovery). Hole U1465B was washed down to 65.9 meters below seafloor (mbsf), and 23 rotary core barrel (RCB) cores were recovered between 65.9 and 213 mbsf with a recovered length of 9.41 m (6% recovery) in the platform succession. Hole U1465C was washed down to 55 mbsf, and 26 half-length APC (HLAPC) and extended core barrel (XCB) cores were recovered from the drift and the platform succession, with a recovery of 24.6 m (14% recovery).

Three lithostratigraphic units were identified in the mostly unlithified drift deposits and the underlying lithified platform and slope-sediments of the Kardiva platform. Lithostratigraphic Unit I contains unlithified white/light gray to gray-brown and pale yellow packstone to grainstone and, locally, rudstone. The components are planktonic and benthic foraminifers, pteropods, red algae, *Halimeda* plates, bivalves, echinoid fragments and spines, otoliths, and rare solitary corals. Aggregate grains, yellow to brown grains, and black grains occur throughout the entire unit. All lithoclasts and some bioclasts are abraded, which is expected in this drift deposit. The underlying lithostratigraphic Unit II comprises a shallow-water platform margin facies with diverse coral fauna. The top of Unit II is well-lithified floatstone with corals, red algae, large benthic foraminifers, bivalves, and serpulid fragments that show evidence of exposure and subsequent submarine hardground formation. This thin drowning layer is partly dolomitized and silicified and contains large molds with two generations of dark-colored geopetal infillings that are likely phosphatic (Figure **F6**). Below this top layer coral boundstone and floatstone that can be rich in algal nodules alternate. The matrix of the floatstone is generally bioclastic grainstone with abundant benthic foraminifers. Pervasive meteoric diagenesis is indicated by moldic porosity, and marine diagenesis is seen in multiple stages of cements and partial dolomitization. Lithostratigraphic Unit III consists of an alternating lithified, very pale brown, coarse-grained dolomitic grainstone to packstone with varying degrees of cementation. The composition is similar to the matrix of the overlying floatstone, but coral fragments decrease and red algae and large benthic foraminifers increase. The main components are large benthic foraminifers (*Heterostegina* sp., *Lepidocyclina* sp. [*Nephrolepidina*], *Operculina* sp., *Amphistegina* sp., *Miogypsina* sp., and *Nummulites* sp.), bivalves, *Halimeda* plates, red algae, minor coral fragments (massive and branching), bryozoa, echinoid spines, gastropods, and abundant bioclasts (Figure **F7**). One characteristic of Unit III is the repetitive alternation of hard cemented layers with abundant moldic porosity and layers of loosely cemented grainstone to packstone with interparticle porosity. Unit III displays all the characteristics of a proximal slope facies, which fits the seismic facies that consists of steeply inclined reflections.

A robust age model was produced by combining the biostratigraphic data of the planktonic foraminifers and calcareous nannofossils in the ~70 m thick drift sediment succession recovered in Hole U1465A above the drowned platform. In the platform and the underlying slope section, the occurrence of planktonic foraminifers and nannofossils was not sufficient for biostratigraphic purposes. The 70 m thick drift sediments range in age from Late Pleistocene to early Pliocene. The large benthic foraminifer assemblage within the platform points to a middle Miocene age, indicating a long hiatus of ~10 My on the platform top.

Benthic foraminifers and ostracods were studied in selected samples above and within the platform to evaluate the paleoenvironmental conditions. Pliocene–Pleistocene benthic fauna in the drift samples generally indicate middle neritic to upper bathyal water depths (most likely <500 m) based on the presence of species such as *Borealis melo*, *Cycloclypeus mediterraneus*, *Planulina ariminensis*, *Planulina subtenuissima*, *Cibicidoides dutemplei*, *Sphaeroidina bulloides*, *Cibicidoides bradyi*, and small miliolids. Below 35.81 mbsf, there is a sand layer mainly composed of reworked reefal material (large benthic foraminifers, fragments of corals, and *Halimeda*). The upper Pliocene portion of the drift section also has abundant fragments of coral, well-preserved echinoderm spine fragments, fish teeth, and planktonic foraminifers, but no ostracods were observed. All samples contain reworked shallow-water taxa, indicating a range from reefal to middle neritic environments.

Interstitial water (IW) sampling was limited to the uppermost 70 m (i.e., the drift sediments overlying the platform) at Site U1465 by lithification and poor recovery. The concentrations of major anions and cations generally remain constant and close to the mean seawater values throughout the sampled interval. For example, Na^+ and K^+ concentrations range between 422–433 and 10.9–11.2 mM with no trends visible with increasing depth. Similarly stable values are reflected in Ca^{2+} and Mg^{2+} concentrations, and salinity also remains relatively constant at 34.5–35 throughout the measured interval. This general lack of variation could result from three possible situations: no significant diagenesis, high rates of advection, or contamination by seawater.

The lack of geochemical variation contrasts with the mineralogical changes shown by the X-ray diffraction (XRD) data, which reflect carbonate diagenesis during the burial of sediment at Site U1465. Above 45 mbsf, the sediment consists of 30%–80% aragonite, 6%–18% high-Mg calcite (HMC), and the remainder low-Mg calcite (LMC). From 45 to 85 mbsf, dolomite is present up to 7%, and aragonite and HMC continue to make up 30%–60% of the sediment (Figure **F8**). Thus, it is possible that the rate of advection dilutes the geochemical signal of diagenesis in the IW. In the carbonate platform portion, carbonate mineralogy is variable. Below 90 mbsf, the rocks are essentially composed of LMC and dolomite. Dolomite peaks at 57% at 143.50 mbsf and is otherwise present mostly <20%. Below 160 mbsf, aragonite is again present at abundances of <10%, with dolomite constituting <1% and the remainder (>90%) consisting of LMC. Quartz is often present in the XRD spectra but is never a significant component of the sediment (<1%).

Petrophysical analyses differentiate two physical properties units. The first unit encompasses the loose Pliocene–Pleistocene drift sediments and has high porosities. The lower unit corresponds to the platform carbonates, characterized by higher *P*-wave velocities and higher densities. *P*-wave velocities reflect a variety of pore types that possibly result from complex diagenetic processes in response to the diagenetic processes linked to platform drowning.

Seismic stratigraphy at Site U1465 shows excellent correlation with lithostratigraphic units. APC coring in Hole U1465A recovered DS7–DS9 and the platform top, and Hole U1465B and U1465C coring retrieved PS11 and parts of PS10 (Figure **F9**). The hiatus separating the platform top from the drifts encompasses DS1–DS6, is biostratigraphically dated at Site U1466 as middle Miocene to middle Pliocene (i.e., ~12–3.5 Ma), and corresponds to the boundary between lithostratigraphic Units I and II. The upper part of PS11 at Site U1465 consists of a package of gently basinward-dipping reflections that can be laterally traced over a distance of around 600 m. The lower boundary of the package coincides with sequence boundary PS11, which corresponds to the base of lithostratigraphic Unit II. The deepest hole at Site U1465 (Hole U1465C) was abandoned approximately 9 m above the basal boundary of PS10.

Site U1466

Background and objectives

Site U1466 (proposed Site MAL-02A) is positioned at 4°55.9880′N, 73°1.6894′E, in a water depth of 518 m 1880 m east of Site U1465 (Figure **F2**). The site is in front of the last prograding clinoform of the drowned carbonate platform that was the target of Site U1465. In this basinal position, a thick drift succession overlays the bottom- and foresets of the drowned Kardiva platform. The pulses of progradation are related to sea level changes, and the overlying drift succession is a current-controlled system that is likely related to the Indian monsoon (Belopolsky and Droxler, 2004a, 2004b; Betzler et al., 2013a, 2013b). The main goals of this site were (1) to date the transition from the sea level–controlled platform system to the current-controlled drift deposition and (2) to establish an age model for the early and middle Miocene sea level changes in the Indian Ocean and the changes in current evolution since the middle Miocene. The mid-Miocene to recent drift succession contains several sequences caused by fluctuations in the current system (Lüdmann et al., 2013). Dating these sequence boundaries will provide ages of changes in strength and direction of the currents and potentially serve as a proxy for changes in monsoon intensity. Dating of the platform sequence boundaries will provide ages of the sea level lowstands in the Indian Ocean that together with data sets from the Bahamas (ODP Leg 166) and offshore eastern Australia (ODP Legs 133 and 194) will allow testing of the global synchroneity of Neogene sea level changes (Betzler et al., 2000; Eberli et al., 2002, 2010). In addition, the age of the last platform sequence will provide the age of the platform drowning that potentially is linked to the onset of the current system. Site U1466 cores will also address another objective of Expedition 359: the periplatform sediments deposited at this site offer the opportunity to retrieve a complete record of $\delta^{13}C$ though the lower and middle Miocene that, together with other Expedition 359 sites, will provide another data set of the carbon isotopic record that is needed to calibrate the periplatform platform margin record against the pelagic record (Swart, 2008).

Principal results

Site U1466 is located in the Kardiva Channel, which connects the Inner Sea of the Maldives with the open Indian Ocean. Two holes were cored at Site U1466 using the APC, HLAPC, XCB, and RCB systems. Hole U1466A was cored to 317.9 mbsf (50 cores) and recovered 243.8 m of sediment (74% recovery). Hole U1466B was cored to 803.1 mbsf (50 cores) and recovered 88.5 m of sediment (17% recovery).

The sedimentary succession at Site U1466 penetrated 803.6 m of lower Miocene to Pleistocene carbonates. Seismic stratigraphy shows that this succession consists of a 254 m thick package of drift deposits overlying a 549 m thick succession consisting of the bottomsets and foresets of the middle Miocene prograding platform.

Seven lithostratigraphic units were identified in the drift and slope/basin deposits. Lithostratigraphic Unit I through Subunit IVC (0–248.3 mbsf) is from the sediment drift succession, Subunit IVD through Unit VI (248.3–715.34 mbsf) contains the lithologic record of the prograding tongues of the Kardiva platform, and Unit VII (715.34–803.61 mbsf) is composed of lower Miocene basinal carbonates from the Inner Sea.

Unit I is Pleistocene to recent in age and consists of an unlithified coarse-grained grainstone succession. The gray-brown to pale yellow carbonate sands consist almost exclusively of bioclasts, with planktonic foraminifers being the most abundant component with admixtures of benthic foraminifers, pteropods, otoliths, *Halimeda* plates, echinoid spines, bryozoa, and bivalves. The bioclasts are generally broken and show signs of abrasion indicative of current transport.

Unit II is an alternation of unlithified packstone and grainstone. The sediment ranges in grain size from very fine in the grainstone intervals to coarse grained in the packstone. The main components are planktonic foraminifers and minor benthic foraminifers, pteropods, red algae, *Halimeda* plates, bivalves, echinoid fragments and spines, and otoliths. Aggregate grains, yellow to brown stained grains, and black grains occur throughout the entire unit.

Unit III consists of very pale brown medium- to coarse-grained grainstone to packstone that is variably lithified. The main components are planktonic foraminifers, with common to present benthic foraminifers (e.g., *Lepidocyclina*), encrusting red algae, *Halimeda* plates, and bryozoan fragments. Lithification increases downhole to lithified rocks at 99.53 mbsf; below this depth, unlithified and lithified intervals alternate again.

Unit IV consists of four subunits based on the occurrence of textural changes from wackestones to packstones and/or grainstones. The overall lithology is similar throughout the entire unit and consists of skeletal and foraminiferal wackestone to packstone (Figure **F10**).

Unit V is marked by the occurrence of large benthic foraminifers in light gray to light brownish gray, lithified, medium- to coarse-grained, dolomitic grainstone and packstone.

Unit VI is characterized by a significant increase in the degree of bioturbation. It consists of an alternation of decametric intervals of lithified fine- to medium-grained packstones and wackestones with common planktonic and benthic foraminifers, echinoid fragments, and bioclasts.

Unit VII consists of a recurrent alternation of well-laminated black intervals with massive white chalk and gray-green intervals with moderate to abundant bioturbation (Figure **F11**). The top of the unit contains intervals with gravity-induced deposits (e.g., slump sediments, soft sediment deformation features, and turbidites).

The age model for Site U1466 (Figure **F12**) relies on the combination of planktonic foraminifer (Figure **F13**) and calcareous nannoplankton datums. The estimated sedimentation rate for the

Pliocene–Pleistocene sequence is ~1.41 cm/ky. Most of the upper Miocene is absent from the sedimentary record at this site. The hiatus occurs between the last occurrence (LO) of *Coronocyclus nitescens* (11.9 Ma) and the LO of *Globoquadrina dehiscens* (5.92 Ma). The middle Miocene is divided into two intervals; the basal one presents a moderately high sedimentation rate (~4.4 cm/ky), whereas the upper interval presents a very high sedimentation rate (~17.1 cm/ky). The early Miocene is divided into two intervals according to the preservation of microfossils, although the sedimentation rate does not change through those intervals and remains the same as values in the basal middle Miocene (~4.4 cm/ky).

Pore water studies at Site U1466 in the upper 85 mbsf indicate either relatively low rates of organic matter remineralization or rates of advection by bottom seawater that are faster than the rates of decomposition of organic matter. XRD analysis shows that the concentration of aragonite in the sediments remains relatively high throughout the Pleistocene and Pliocene (0–85 mbsf), reflecting either variations in the input from adjacent platforms during changes in sea level or diagenetic change to LMC. Although the hypothesis that aragonite is not being neomorphosed in the upper 85 mbsf is supported by the absence of large increases in the concentration of Sr^{2+} in the pore fluids, the possibility also exists that relative high rates of fluid advection remove evidence of dissolution and precipitation reactions. Below 85 mbsf, aragonite disappears, and at 97. 7 mbsf, the sediment contains up to 70% dolomite. Below ~150 mbsf, dolomite decreases again and up to 20% aragonite is present, and below 320 mbsf, dolomite disappears and is only barely detectable in trace concentrations through the remainder of the core (Figure **F14**).

The determination of paleomagnetic polarity based only on inclination data for Site U1466 is extremely weak because of the very low paleolatitude, possible inclination anomalies due to a nondipole field, and poor data quality. Nevertheless, paleomagnetic studies identify 21 magnetozones using the inclination data. These magnetozones are tentatively attributed to the lower and middle Miocene (C5A–C5E series and C6).

The variability of values in the downhole logs and the measured petrophysical properties in the pure carbonate strata of Site U1466 reflects changes in diagenesis/lithification and the amount of organic carbon rather than mineral composition. Downhole logging was limited to one run with the modified triple combo tool string to 345 m wireline log depth below seafloor (WSF) because the hole collapsed. In the pure carbonate succession, the natural gamma radiation (NGR) is low with two higher peaks related to increased organic carbon content. The resistivity most likely records the degree of cementation, with better-cemented intervals having higher resistivity.

Physical properties also reflect the pure carbonate composition (Figure **F15**). Magnetic susceptibility is very low throughout the section. Grain density is similar throughout the entire section. Velocity does not correlate well to porosity and displays abrupt increases and decreases downcore, as is typical in pure carbonates. Gamma ray peaks relate to increases in organic matter.

The correlation of the lithostratigraphy and age model from biostratigraphy to the seismic stratigraphy confirms and refines the predrilling interpretation (Figure **F16**). The continuous seismic reflections of the distal clinoforms of the sea level–controlled Kardiva platform are lithologically a regular alternation of intervals of lithified fine- to medium-grained packstones and wackestones. These alternations most likely are the result of high-frequency sea level changes. Turnover in the drift succession is recorded by a change in seismic and lithologic facies. The seismic reflection amplitudes decrease, and the lithology dominated by coarse-grained packstone and grainstone reflects a current-dominated sedimentation pattern.

Site U1467

Background and objectives

Site U1467 (proposed Site MAL-09A) is the easternmost site drilled in the Inner Sea of the Maldives during Expedition 359. It is located at 4°51.0274′N, 73°17.0223′E, at a water depth of 487.4 m 24.8 km east of the eastern end of the northern transect and 29.4 km east of the eastern end of the southern transect (Figure **F2**). Cores from this site record a 630 m thick succession of drift deposits lining the southern flank of the Kardiva Channel. The main objectives at this site were to constrain the timing of sequence boundaries in the drift succession and to precisely date the onset of the drift deposition; to analyze the cyclostratigraphy of carbonate drift deposits, providing reconstructions of changes in the current regime and monsoon cyclicity; and to recover an undisturbed sedimentary sequence for further paleoceanographic studies.

The mid-Miocene to recent drift succession contains several sequences that are likely caused by fluctuations in the current system flowing through the Kardiva Channel. Dating these sequence boundaries will provide the ages of changes in strength and direction of the currents. Further linking of these physical stratigraphic data with postcruise sedimentological and geochemical data will address the question of changes in the monsoon intensity (Kroon et al., 1991; Prell et al., 1992; Clift et al., 2008; Gupta et al., 2015). Moreover, the periplatform sediments deposited at this site offer the opportunity to retrieve a complete record of $\delta^{13}C$ through the middle Miocene that, together with the other Expedition 359 sites, will provide another data set of the carbon isotopic record that is needed to calibrate the periplatform record against the pelagic record.

Principal results

Five holes were drilled at Site U1467, one of them (Hole U1467E) as a dedicated logging hole. The sediment recovered at Site U1467 is a fine-grained succession of wackestone to packstone. Compositional changes are minor, but alternation of lighter and darker intervals of variable thickness persists downhole, even through the increasing degree of lithification to approximately 640 mbsf. Six lithostratigraphic units were differentiated.

Lithostratigraphic Unit I (0–110.0 mbsf) consists of unlithified, foraminifer-rich wackestone to packstone with a predominance of very fine- to fine-grained wackestone. The unit is characterized by thick (30–100 cm) to very thick (>100 cm) intervals defined by color changes ranging from light gray to grayish brown. The dark colored intervals correlate with low lightness L* reflectance values and display an inverse relationship with NGR trends, with higher NGR (counts/s) observed in the darker intervals.

Lithostratigraphic Unit II (110–215 mbsf) is defined by interlayered unlithified and partially lithified planktonic foraminifer–rich wackestone and mudstone with pteropods and particulate organic matter. The matrix of the sediment contains calcareous nannofossils and sponge spicules. Celestine is common as nodules and layers up to 3 cm thick and as disseminated crystals in the fine fraction.

Lithostratigraphic Unit III (215–303 mbsf) consists of partially lithified very fine–grained mudstone to wackestone with a dominance of wackestone. The unit also has thick to very thick packages with color changes, from light gray to light olive gray and light brownish gray. The sediment contains abundant planktonic fora-

minifers; echinoid spines and sponge spicules are common, but benthic foraminifers are rare. Celestine nodules and fragments, bioclasts, and particulate organic matter are common, especially in the darker intervals. Bioturbation is common with *Thalassinoides*, *Planolites*, *Palaeophycus*, and possibly *Zoophycos*. Traces appear better developed in the darker colored intervals.

The deposits of lithostratigraphic Unit IV (303–498.5 mbsf) are lithified, very fine– to medium-grained, planktonic foraminifer–rich wackestone to packstone. As with previous units, particulate organic matter is present and changes in abundance, which is linked to color variations from light gray to light brownish gray and pale yellow with gradational and commonly bioturbated contacts. Ichnofauna consist of *Thalassinoides*, *Planolites*, *Zoophycos*, *Chondrites*, and *Palaeophycus*.

Lithostratigraphic Unit V (498.5–607 mbsf) still consists of planktonic foraminifer–rich wackestone to packstone with alternating light and dark intervals, but lithostratigraphic Unit VI below 607 mbsf lacks dark layers within the fine-grained wackestone.

Biostratigraphic analyses show an apparently continuous succession of Holocene to middle Miocene age recovered at Site U1467 (Figure **F17**) that is divided into three intervals. The Pleistocene and upper Pliocene extends from the seafloor to ~130 mbsf. Throughout this interval, planktonic foraminifers are well preserved, whereas benthic foraminifers and calcareous nannofossils are well preserved at the top but are moderately well preserved below 40 mbsf. The lower Pliocene and much of the upper Miocene extends from ~130 to 540 mbsf. Preservation throughout this thick interval is poor to moderate for all microfossils, except in the deepest core in this interval (Core 359-U1467B-69X), from which very well preserved nannofossils were recovered from a few darker, probably clay-rich levels. The late Miocene and later part of the middle Miocene extends from 540 to 714 mbsf. In the upper part of this interval, all groups of calcareous microfossils are rare and poorly preserved; preservation improves downcore and in the lower part of the interval is moderate to good.

Decreases in SO_4^{2-} concentrations and alkalinity in the interstitial fluid geochemistry from Site U1467 indicate that significant remineralization of organic material occurred below 50 mbsf. An odor of H_2S was also noted upon core recovery and squeezing of the whole-round samples, suggesting that bacterial sulfate reduction probably accounts for the observed trend. As large amounts of NH_4^+ are released during decomposition of sedimentary organic matter, a negative correlation between SO_4^{2-} and NH_4^+ is also related to the oxidation of organic matter. Cl^- increases from the sediment surface to around 100 mbsf (Figure **F18**) are believed to be related to the last glacial period, when salinity was altered as a result of Northern Hemisphere glaciation.

Site U1467 sediments contain up to 60% aragonite in the upper 50 m of the core, as revealed by XRD analysis. Below 50 mbsf, aragonite content decreases to less than 10%–15% and drops to less than 10% by 500 mbsf. This decrease is interpreted to reflect aragonite dissolution, based on increases of Sr^{2+} concentrations in the pore fluids. Deposits are again richer in aragonite between 500 mbsf and the bottom of the hole; Sr^{2+} concentrations of the pore fluids decrease slightly in this interval, whereas Li^+ concentrations increase. The decrease in Sr^{2+} probably is controlled by a sink of Sr^{2+} located at a deeper interval that was not cored. XRD analyses also show several occurrences of celestine ($SrSO_4$) between 163 and 393 mbsf, indicating that the pore water concentrations of Sr^{2+} and SO_4^{2-} attain supersaturation with respect to this mineral. At Site U1467, celestine occurs in an interval of unusually high sedimentation. Hence, in spite of the reduction of SO_4^{2-} in this interval, there was sufficient Sr^{2+} to produce supersaturation in the pore waters with respect to celestine.

Organic carbon content in Site U1467 sediments fluctuates between 0 and 12 wt%, with the samples richest in organic carbon at 89, 112, and 168 mbsf. Methane remains at concentrations between 1.6 and 12.0 ppmv, increasing slightly from the surface to 300 mbsf and then remaining mostly stable around 5 ppmv with some scattering of values. Ethane is only present in measurable quantities (~1 ppmv) between 249 and 277 mbsf and at 324, 580, and 706 mbsf.

Natural remanent magnetization (NRM) analysis at Site U1467 was only possible on limited core sections because of pervasive contamination, presumably from rust in the drill pipe, that affected the first two to three sections of every core, despite cleaning the drill pipe interior while in Hole U1467C. Discrete samples showed less overprint than the archive section halves, and shore-based analyses should yield better quality results. Nevertheless, a series of magnetozones in the intervals between ~100 and 200 mbsf in Hole U1467C and between 195 and 255 mbsf in Hole U1467B were identified and interpreted as Chrons C2Ar to C3n.3n (Figure **F17**). Another series of possible normal and reverse polarity intervals based only on the analysis of inclinations, which are less than 20° and consistent with the paleolatitude for this site, was recognized between 580 and 714 mbsf in Hole U1467C (Cores 24X–37X) and interpreted to be Chrons C5n.2n to C5An.2n.

The physical properties of the sediment reflect the rather monotonous nature of the lithologic succession at Site U1467, whose main characteristic is the changes of color from darker to lighter intervals in generally fine grained, bioturbated wackestone. Four distinct physical properties units are identified. The first three units (0–465 mbsf) are divided mainly based on slightly higher variability of velocity in the second unit and a concomitant small step in the downhole increase in the density and a coeval decrease of porosity at 105 mbsf, as well as increased variability of density and porosity. Below 465 mbsf, where the formation is more lithified, density and velocity increase significantly and show large variations. High-frequency fluctuations in NGR also follow these color variations, which are likely produced by small admixtures of organic material (dark color) and more early marine cements (light color). In addition, NGR data display five longer term variations that loosely follow the lithostratigraphic units. Magnetic susceptibility is low throughout the entire core. Thermal conductivity, on the other hand, increases downhole. The rate of this increase is reduced in physical properties Unit 2.

In the dedicated logging Hole U1467E, three tool strings were deployed: the triple combo, Versatile Seismic Imager (VSI), and Formation MicroScanner (FMS)-sonic tool strings. The caliper log from the first logging run indicated that much of the borehole was ~14 inches in diameter and thus suitable for a vertical seismic profile (VSP) experiment. The VSI tool string recorded good sonic waveforms at 13 stations at a 50 m interval. After shore-based processing, logging data were analyzed and divided into four logging units. Logging unit boundaries correlate with some of the lithostratigraphic units (Figure **F19**). Most variations in the downhole logs are seen in the gamma ray values, triggered by differences in the uranium content, which correlate to variations in the amount of organic matter as revealed by smear slide analysis. The VSP experiment produced good stacks of sonic waveforms. VSP data and sonic velocity logs therefore helped to establish the conversion between depth and two-way traveltime (TWT) and thus allowed us to exactly tie in seismic and core data.

We attempted four formation temperature measurements in Hole U1467B; however, no evidence of frictional heating occurred upon insertion into the formation on any of them, so no reliable formation temperatures were obtained. The average mudline temperature appeared to range from 13.8° to 15°C.

Stratigraphic correlation, using available biostratigraphic and paleomagnetic age control points, allowed us to refine and establish a precise age model for Site U1467 that correlates the different physical property measurements and the downhole logging data. Results show that the bottom of the hole is in 12.7 Ma deposits. A composite depth scale and splice at Site U1467 were constructed from 0.0 to 220.25 m core composite depth below seafloor (CCSF-D) (from the "mudline" in Hole U1467C to the bottom of Core 359-U1467B-22H).

In the seismic profiles, the drift sequences at Site U1467 are represented by well-stratified, nearly horizontal, low- to medium-amplitude reflections and in the lower part by a succession of strong reflections separated by zones of weak echoes comprising DS1–DS3. The base of the drift succession lies at 1337 ms TWT and is underlain by the drilled distal bottomsets of the platform sequences. Site U1467 is located in a basinal position where all sequence boundaries appear as continuous parallel reflections, which are the correlative conformities to the unconformities along the basin margin that define the sequence boundaries. The thickness of the drift sequences varies from 24.5 m (DS7) to 104 m (DS6) and 173 m (DS4). Starting with DS1–DS3, the depocenter was situated at the western basin margin and dominated by southward bottom water inflow from the northeast Kardiva Channel and inflow from the newly opened northwest Kardiva Channel. DS4–DS7 mark the gradual eastward shift of the depocenters. The uppermost sequences (DS8–DS9) exhibit a more uniform thickness throughout the Inner Sea of the Maldives.

Site U1468

Background and objectives

Site U1468 (proposed Site MAL-03A) is located in the Kardiva Channel in the Inner Sea at 4°55.9823′N, 073°4.2834′E. This site is the easternmost site of the northern transect, 4.8 km east of Site U1466 (Figure **F2**). At Site U1468, seismic profiles indicate a succession with the Oligocene/Miocene boundary at 727 ms TWT followed by the basinal to lower slope deposits of the lower–middle Miocene Kardiva carbonate platform. The base of the overlying drift succession (reflection DS1) is a gently basinward-dipping horizon. The drift itself is 431 ms TWT thick, which equals 433 m. The modern current-swept seafloor is at 521.45 m water depth.

Site U1468, together with Site U1466, is a key site to (1) constrain the timing of the platform to drift turnover, (2) date the sequence boundaries of the Kardiva platform, and (3) reconstruct the platform evolution from the Oligocene/Miocene boundary onward (Aubert and Droxler, 1996; Belopolsky and Droxler, 2004a). With regard to the drift sequences, the position of Site U1468 was chosen because it bears an extended thickness of the DS1 succession and a greater thickness of DS2 compared to the succession at Site U1466. Because the sequences of the mid-Miocene drift succession are likely to be determined by fluctuations of the bottom-current regime (Lüdmann et al., 2013), dating such variations and understanding the drift depositional facies will help to address the paleoceanographic objective of the expedition to link the changes of the Maldives current regime to global Neogene ocean circulation. The succession recovered at Site U1468 also provides the opportunity to retrieve a complete record of $\delta^{13}C$ variations in periplatform carbonates through the lower and middle Miocene for establishing the carbon isotopic record needed to calibrate this hemipelagic record against the pelagic record.

Principal results

Two holes were drilled at Site U1468. Hole U1468A cored 873.7 m of carbonates (with 53% recovery) using a combination of the APC, HLAPC, and XCB coring systems. Hole U1468B was drilled as a dedicated logging hole with the RCB system to 874.7 mbsf. Sediments from a variety of depositional settings were recovered at Site U1468. The top formed a drift package that comprises lithostratigraphic Units I–IV, and the Miocene distal slope and the basinal deposits of the Kardiva platform form lithostratigraphic Unit V. A restricted basin environment defines lithostratigraphic Unit VI. Lithostratigraphic Units VII and VIII are shallow-water deposits.

Unit I (0–45.7 mbsf) is dominated by light gray and pale yellow to white unlithified to partially lithified packstone to grainstone. Deposits are rich in planktonic foraminifers and contain abundant benthic foraminifers, ostracods, pteropod fragments, *Halimeda* fragments, mollusk fragments, echinoid fragments and spines, otoliths, fish remains, and very rare bryozoans. Foraminifers and bioclasts are well preserved with aggregate grains, organic matter, and yellow- to brown-stained lithoclasts. The fine fraction contains aragonite needles (<5 µm), calcite crystals (5–10 µm), and calcareous nannofossils (coccoliths). Variations in grain size and texture, in particular the gradual change from packstone to grainstone layers, are interpreted to be the result of changing current strength.

Unit II (45.7–192.4 mbsf) mainly consists of unlithified to partially lithified rudstone to wackestone with abundant to frequent large benthic foraminifers (Figure **F20**). The matrix throughout the entire unit contains abundant calcite crystals and very rare dolomite rhombs and calcareous nannofossils. Rudstone layers containing rip-up clasts, other small lithoclasts, echinoid spines and fragments, and other large bioclasts often form the base of graded beds that have a slight erosional base and fine upward to a fine-grained grainstone (Figure **F21**).

Unit III (192.4–296.4 mbsf) is a light brownish gray to light gray wackestone succession with intercalations of packstone. This unit is characterized by the reappearance of planktonic foraminifers and the disappearance of large benthic foraminifers. Intraclasts are common, indicating early marine cementation and reworking. Most bioclasts are heavily overgrown with dogtooth calcite crystals. The matrix contains abundant calcite crystals, whereas sponge spicules are minimally present within the fine matrix. Calcareous nannofossils are extremely rare to absent.

Unit IV (296.4–427.7 mbsf) consists of lithified packstone to wackestone. Components in this unit include bioclastic fragments, as well as planktonic and benthic foraminifers that are severely overgrown by calcite cements. The degree of bioturbation in this unit allows the identification of several ichnotaxa, including *Thalassinoides*, *Palaeophycus*, *Planolites*, and *Chondrites*. Occasionally, some burrows are silicified.

Massive wackestone makes up lithostratigraphic Unit V (427.7–728.6 mbsf). Throughout the unit are alternations of light and dark intervals; the darker color is linked to a higher abundance of organic material. The main components in this unit are planktonic foraminifers, with benthic foraminifers, mollusk fragments, and bioclast fragments. The components found have calcite cement overgrowth. The well-preserved ichnotaxa identified within this unit include *Thalassinoides*, *Teichichnus*, *Asterosoma*, *Phycosiphon*, *Zoophycos*, *Palaeophycus*, *Planolites*, and *Chondrites*.

Unit VI (728.6–815.9 mbsf) is a wackestone to packstone succession that consists of light gray chalk with intercalations of dark gray to black layers with abundant organic matter (Figure **F22**). Planktonic foraminifers are abundant, and the rock matrix consists of calcareous nannofossils.

Unit VII is layered wackestone with floatstone intercalations containing large benthic foraminifers *Amphistegina*, *Lepidocyclina*, *Cycloclypeus*, and *Miogypsina*.

Unit VIII forms the lowest part of the cored succession at Site U1468. It is densely cemented limestone that contains abundant shallow-water biota such small and large benthic foraminifers, *Halimeda* plates, bivalve fragments, and bryozoan and coral fragments.

Biostratigraphic analysis of the microflora and microfauna allowed us to divide the succession into four intervals. Interval A reaches to ~45 mbsf and ranges in age from the late Pliocene to Quaternary. The lower part of the Pliocene is missing. The nannofossils are generally sparse, with the exception of well-preserved coccoliths in the uppermost sample. Planktonic and benthic foraminifers are moderately abundant in this interval. Interval B extends from about 45 to 429 mbsf. It comprises middle to late Miocene calcareous microfossils, which are generally sparse and poorly preserved throughout the succession. One sample at 40.59 mbsf contains a few late Miocene to Pliocene–Pleistocene specimens of planktonic foraminifers mixed with abundant abraded and recrystallized large foraminifers. The base of biostratigraphic Interval B corresponds to the base of the drift sequence as determined by seismic stratigraphy and lithostratigraphy. Interval C encompasses the middle Miocene to upper Oligocene between 447.3 and 827.4 mbsf with abundant and moderately to well-preserved calcareous nannoplankton. The lowest Interval D contains mainly large benthic foraminifers derived from the forereef environment.

Geochemical analyses of the sediments revealed that minimal changes in the SO_4^{2-}/Cl^- ratio and alkalinity of the interstitial fluids in the uppermost 200 m indicate either relatively low rates of organic matter remineralization or rates of advection by bottom seawater that are faster than the rates of decomposition of organic matter. Below 200 mbsf, a net decrease in the concentration of SO_4^{2-} is caused by bacterial sulfate reduction. The aragonite concentration in the sediments as measured by XRD remains between 20% and 40% throughout the uppermost 50 m, reflecting variations in input rather than diagenetic change to LMC. The sudden loss in aragonite below ~50 mbsf suggests a period of exposure to fluids that caused partial dolomitization. Neomorphism of the sediments to LMC and some limited amount of dolomitization is indicated by the rapid increase in the Sr^{2+}/Ca^{2+} ratio of the pore water below 200 mbsf. Although dolomite formation is supported by the decline in the Mg/Ca ratio of the pore fluid, the present dolomite formation indicated by pore water data is not responsible for the up to 25% dolomite found in the sediments. This indicates that dolomite must have formed during earlier time periods in a different fluid regime than observed at the present. The large increase in Sr^{2+} in lithostratigraphic Unit III causes the pore fluids to attain saturation with respect to $SrSO_4$ and precipitation of celestine, detected by XRD.

The influence of noncarbonate components on pore water chemistry can be seen between 450 and 500 mbsf, where the carbonate content of the sediments decreases to ~80%. Here, K^+ in the pore waters increases slightly. Increased Fe in the sediments and the marked increase in the Mn/Ca ratio below this depth clearly indicate the significance of this transition, which is reflected in a significant reduction in the rate of sedimentation as indicated by biostratigraphic data.

Paleomagnetic analyses show that contamination of the core sediment with highly magnetic material persisted at Site U1468, only slightly attenuated when compared to previous sites. This problem is unambiguously shown by the typical pattern of the NRM intensity that decreases from the upper to lower part of each core by 3 or 4 orders of magnitude. It has been noticed that APC and HLAPC cores drilled in the upper part of Hole U1468A seem more affected by this problem compared to XCB cores drilled in the deepest part of the same hole even though APC cores used nonmagnetic core barrels. The distribution of inclinations, despite the large scatter, has a single mode at 0°, suggesting that Site U1468 crossed the Equator during the early Miocene.

The strata at this site can be divided into five physical properties units. NGR has the most variability and basically defines the physical properties units, but other properties also contribute. For example, in physical properties Unit 1 (0–50 mbsf), bulk density is low and porosity is high. At this depth they shift abruptly to higher (density) and lower (porosity) values, and subsequently they only show a slight increase and decrease, respectively, to the bottom of the hole. Porosity remains very high even to great burial depths, with over 50% porosity at 800 mbsf. Likewise, velocity only displays a slight overall increase in physical properties Units 2–5 to about 2400 m/s, but high values of up to ~4000 m/s are measured in the more lithified beds. A velocity inversion occurs in physical properties Unit 4 that is lithologically the chalk interval of lithostratigraphic Unit VII.

Color reflectance quantifies the observed cyclic dark–light alternations in the rock but also captures the overall darker tones of lithostratigraphic Units II and IV. Magnetic susceptibility logger (MSL) values are like the other magnetic properties impacted by contamination. After filtering erroneous high values, most MSL values are very low with a range of –4–2 IU, and point magnetic susceptibility (MSP) values are –15 to –5 IU. Thermal conductivity values increase rapidly from 0.9 to 1.16 W/(m·K) above ~83 mbsf and more gradually below ~83 mbsf to 1.5 W/(m·K) at the bottom of Site U1468 with many fluctuations.

A dedicated logging hole was drilled at Site U1468 to ensure a complete set of downhole measurements. During the first logging run with the triple combo tool string, however, wireline tension increased at 485 m WSF and caliper measurements indicated a narrow borehole less than 7 inches in diameter. These collapsing hole conditions persisted to 280 m WSF, above which the logging run could be completed. No additional logging tool strings were run. In the narrow interval of the collapsing hole, the data quality was reduced but the lower and upper portion yielded good data. One characteristic of the logging suite is the low density and high porosity that are present in the deeper portion of the hole. Measurements on the discrete samples have shown porosities of 40%–50% for most of the logged interval. These high porosities are at the limit of what the logging tool can measure. This might explain the high values of 60%–80% for large portions of the hole.

Based on the electrical resistivity and gamma ray logs, four logging units were identified. Logging Unit 1 extends from the base of the drill pipe to 201 m wireline log matched depth below seafloor (WMSF) and is characterized by low gamma ray and resistivity values, both with low to moderate amplitude variability except for two peaks around 190 and 200 m WSF. Logging Unit 1 correlates mostly with lithostratigraphic Unit II, which in the logged interval displays an overall coarsening-upward trend and textures from mudstone to packstone at the base and grainstone to rudstone at the top. In logging Unit 2 (201–490 m WSF), the character of the resistivity changes with alternations of lower and higher resistivity over inter-

vals of meters to tens of meters. The gamma ray log is nearly flat, except at the base of the unit between 450 and 490 m WSF. This logging unit corresponds to lithostratigraphic Units III, IV and part of V. Units III and IV correspond to the drift sediments of DS1 (Figure **F23**), which is composed of wackestone with some packstone intervals (Unit III) and lithified packstone (Unit IV). Intervals of higher gamma ray and corresponding resistivity variations at the base of logging Unit 2, from 450 to 490 m WSF, capture alternations of submeter to multiple meter scale light and dark intervals deposited at the distal bottomsets of the prograding Kardiva platform. Logging Unit 3 is entirely within the bottomsets of the prograding platform characterized by the alternations of darker and lighter packstones to wackestones. The resistivity log reflects this rather uniform lithology with low variability values that slightly increase with depth. The gamma ray log displays more variability from low to moderate amplitude and also increases with depth. These variations in the gamma ray signature are mostly the result of uranium variations that are likely related to changes in the organic material that varies from the dark (high) to light (low) intervals. In logging Unit 4 (720–835 m WSF), the resistivity amplitude changes from low to moderate. Likewise, the gamma ray log exhibits the greatest variability compared to the other units. Again, the amplitude and variability of the gamma ray log are mainly caused by the uranium content. Lithologically, Unit 4 coincides with a thick upper Oligocene–lower Miocene package of chalky sediment with intercalations of dark organic-rich layers. These dark layers are taken as indicators of higher productivity and lower oxygenation during times of deposition.

Although no sonic log or VSP could be run at Site U1468, two high-impedance events identified by distinct lithology changes in the core helped us build a robust velocity model for the time-depth correlation on the seismic profiles. The first impedance event is generated by the top of the densely cemented shallow-water limestone of the Oligocene carbonate platform at 854.7 mbsf (1398 ms TWT) and the overlying wackestone–floatstone; the second is a densely cemented grainstone interval with a top surface at 540 mbsf (1198 ms TWT). These two surfaces are used as "check shots" for refining the velocity model.

The penetrated seismic section at Site U1468 displays four main seismic facies (Figure **F24**). At the bottom are near-horizontal seismic reflections with a distinct high-amplitude reflection that corresponds to a lithified bioclastic floatstone at the top of the Oligocene shallow-water carbonate platform, which produces the Oligocene/Miocene boundary (O/M) reflection. The O/M reflection was defined by Belopolsky and Droxler (2004a) as the Oligocene/Miocene boundary, but shipboard biostratigraphic analysis of the calcareous nannoplankton and planktonic foraminifers indicates that the Oligocene/Miocene boundary is located further upsection between 769.74 and 779.36 mbsf (i.e., between the O/M horizon and PS1). This interval is composed of a nannofossil chalk package with intercalations of organic-rich layers. Above this chalk package are near-horizontal low-amplitude reflections that are the distal bottomsets of Kardiva platform sequences PS1–PS11 (427.7–724.56 mbsf). These reflections are composed of bioturbated planktonic foraminiferal wackestone to packstone with meter-thick alternations of darker and lighter layers. Sections of alternating amplitude intensities are likely caused by pulses of deposition and intermittent slow sedimentation and associated diagenesis (Anselmetti et al., 2000; Malone et al., 2001). The age of these prograding sequences ranges from middle Burdigalian to Langhian or approximately from 21 to 12.7 Ma.

The onset of the drift sequences lies at 434 mbsf and is indicated by wavy high-amplitude reflections. Generally, DS1 displays a large mounded geometry with high-amplitude parallel reflections that conjugate basinward. The lower part of DS1 consists of lithified bioclastic packstones to wackestones. DS2 consists of high-amplitude, slightly inclined seismic reflections and is composed of a series of unlithified to partially lithified coarsening-upward packages of large benthic foraminiferal grainstone to rudstone. At the top of DS2, the reflections become nearly horizontal, marking the apex of the drift mound that continues into the base of DS9. At Site U1468, the sequence boundaries of DS3–DS9 merge into two horizontal reflections separated only by approximately 20 m. DS9 and DS10, the uppermost drift sequences, show undulating high-amplitude reflections and a facies of mud-poor bioclastic packstones and grainstones, similar to modern seafloor sediments.

Site U1469

Background and objectives

Site U1469 (proposed Site MAL-8A) lies 2.87 km (1.57 nmi) south-southwest of Site U1465, which is the westernmost site of the northern transect in the western part of the Kardiva Channel (Figure **F2**). It is located at 4°54.41′N, 73°0.48′E, at a water depth of 427 m. The Kardiva Channel is a wide west-east–oriented passage that dissects the north-south–running double row of the Maldives atolls (Purdy and Bertram, 1993; Aubert and Droxler, 1996). The Kardiva Channel formed as a result of the demise of larger carbonate banks during the Miocene (Belopolsky and Droxler, 2004a, 2004b; Betzler et al., 2009). The northern transect, including Site U1469, is in the approximately 12 km wide northwestern branch of the Kardiva Channel between the Goidhoo atoll and the Maalhosmadulu atoll. At present, this passage accommodates seasonally reversing and monsoonal-driven water throughflow. Currents affect the water column down to the sediment surface and trigger erosion at the seafloor and migration of large-scale carbonate sand and mud waves. This depositional regime has persisted since the Miocene, and the hypothesis to test is that the onset of current and partial drowning of the carbonate banks were intimately linked (John and Mutti, 2005; Betzler et al., 2009; Eberli et al., 2010). Seismic stratigraphy and facies indicate that the onset of this current was a rapid process and that the intensity of the currents varied through time (Lüdmann et al., 2013).

Site U1469 was selected to document and reconstruct the carbonate bank depositional system of the drowned Miocene bank and to link the seismic sequences to facies. This link is possible because the drowning unconformity (i.e., the surface that forms the top of the last growth episode of the carbonate bank) does not mask underlying geometries at this site. The target depth was 700 mbsf, which is the base of PS7, the first sequence after the Kardiva platform went from mostly aggrading growth to progradation.

The specific objectives of Site U1469 were (1) to provide a detailed reconstruction of the predrowning, drowning, and postdrowning evolution of the carbonate bank by linking the seismic stratigraphic record to the sedimentary record (i.e., depositional facies); (2) to constrain the timing of this evolution, thus allowing age assignments of unconformities, sedimentary interruptions, sedimentary turnovers, and onset of drift deposition; and (3) to reconstruct and date bank to drift turnover.

Principal results

The sedimentary succession at Site U1469 was expected to be comparable to that at Site U1465, with a package of loose drift car-

bonate sands overlying the limestones of the drowned platform. Although recovery was expected to be low, this site was cored with the RCB system because only faulty sleeves for XCB coring were available at the time of drilling.

Three lithostratigraphic units are defined at Site U1469 based on visual core descriptions and thin section analyses. Lithostratigraphic Unit I (0–93.0 mbsf) represents the youngest hemipelagic deposits, which consist of partly lithified to lithified, gray-brown to pale yellow, coarse-grained very well sorted grainstone to packstone. Bioclasts are typical open marine pelagic fauna and minor proportions of skeletal benthic fauna that may have originated close to the active atolls and transported by the currents to the Kardiva Channel.

During deposition of lithostratigraphic Unit II (93.0–141.7 mbsf), the coarse-grained grainstone to rudstone contained increased amounts of benthic foraminifers and admixtures of corals, bivalves, *Halimeda*, and echinoderm spines. The coarser grain size and the microfaunal assemblage indicate a shallower and higher energy current-dominated environment compared to Unit I. These deposits cover the top of a drowned carbonate platform that makes up lithostratigraphic Unit III (141.7–153.4 mbsf). The lithologies of Unit III consist of dolomitized coral-rich floatstone with massive and branching coral fragments, rhodoliths, gastropods, and other encrusting organisms interpreted as a shallow-marine reef to forereef depositional setting (Figure **F25**).

Because of poor recovery, no continuous record of core catchers could be obtained. As a result, the biostratigraphic age model for this site is limited, but both the planktonic foraminifers and the calcareous nannofossils indicate a Quaternary to early Pliocene age for sediments above the drowned platform. Planktonic foraminifer biostratigraphy identified two Pleistocene biohorizons, the last occurrences (LOs) of *Globigerinoides fistulosus* (1.88 Ma) and *Globorotalia limbata* (2.39 Ma), which were found at 44.57 and 63.96 mbsf, respectively. The Pliocene LOs of *Dentoglobigerina altispira* (3.47 Ma) and *Globorotalia margaritae* were found at 63.96 and 73.7 mbsf, respectively. The occurrence of nannofossils is sparse and poorly preserved. Thus, no assemblages are unambiguously datable. However, the presence of small *Gephyrocapsa* specimens in the upper part of the sequence (25–93 mbsf) indicates that these samples are Quaternary to middle Pliocene in age (Zones NN21 to NN14). Similarly, the consistent presence of *Sphenolithus* specimens in the lower part of the site (73.6–122.1 mbsf) suggests that this part of the sequence is middle Pliocene or older (Zone NN15 or older), although they could be reworked. No Miocene marker species were seen. The drowned platform does not contain any age-diagnostic benthic foraminifers, but seismic stratigraphic evidence places a middle Miocene age at the drowning surface.

At Site U1469, no IW samples were obtained. The carbonate content in seven sediment samples above the platform yielded carbonate contents between 94.95 and 97.95 wt%, and their total organic carbon is between 0.04 and 0.15 wt%. The mineralogy of the sediment consists of aragonite, HMC, LMC, and dolomite. HMC is present only to 25 mbsf and reaches a maximum of 8.9%. Aragonite occurs at concentrations between 10.7% and 49.0% from the surface to 73.6 mbsf. Below this depth, most of the aragonite and all of the HMC neomorphosed to LMC. Dolomite is present with a low abundance of <3.3% above 93 mbsf. Below 93 mbsf, dolomite increases to concentrations between 4.4% and 30.9%, and the concentration of aragonite decreases. C/N ratios of the samples collected for headspace analyses suggest organic matter with a marine origin. The platform carbonates at 153.22 mbsf are completely dolomitized. Sr/Ca ratios are high (1.26–3.32 mmol/mol) above 80 mbsf. Below that depth, they decrease to <1.2 mmol/mol.

Paleomagnetic measurements of intensity, declination, and inclination on platform carbonates below 151 mbsf yielded some magnetostratigraphic information. One reversal is recognized at 153.8 mbsf and is normal below. In addition, a possible short reversal occurs at 153.9 mbsf.

Physical properties fall into two groups that correspond to the Pliocene–Pleistocene drift sediments (physical properties Unit 1) and the carbonate platform succession (physical properties Unit 2). The slightly lithified grainstone to rudstone facies of the drift sediment displays low NGR that increases downhole. As in the drift sediments of the other sites, bulk density is low (1.5–2.0 g/cm^3), porosity is very high, ranging from 42% to 52%, and *P*-wave velocity reaches 2562 m/s. The dramatic facies change to platform carbonates at 141.7 mbsf is also reflected in the physical properties. The dolomitized limestone has high NGR values. Bulk density averages 2.5 g/cm^3, whereas grain density is 2.84 g/cm^3, confirming the complete dolomitization of this interval. Porosity is between 15.4% and 22.8%. Despite relatively high porosity, velocities are over 5000 m/s. This can be explained by the dominance of the moldic pore types that produce a rock with a stiff framework.

The time-depth conversion for correlating the seismic sequence to the lithology relied on the velocity model from Site U1465, which has a similar lithology. Similar to Site U1465, Site U1469 is at the margin of the drowned Kardiva platform and overlain by drift deposits (Figure **F26**). At this location, however, the sequence stratigraphic interpretation indicates a younger age for the top of the Kardiva platform. Additionally, the drift sequences overlying DS4 are more complete. The seismic facies of the drowned Kardiva platform displays a series of prograding clinoforms with slightly basinward inclined topsets and steep foresets that flatten out basinward. The overlying drift deposits are horizontal, semicontinuous, medium-amplitude reflections of DS4–DS10 and are interpreted to be late Miocene to recent in age. The drift succession consists of coarse-grained grainstones that are early Pliocene to recent in age in the upper part, but no age-diagnostic fossils were found in the portion directly overlying the drowned platform. The drowned platform top is part of PS11, which was interpreted to be middle Miocene in age. Shore-based radiometric dating will be needed to assess the exact age.

Site U1470

Background and objectives

The western Kardiva Channel that connects the open Indian Ocean with the Inner Sea of the Maldives is divided into northern and southern branches by the Goidhoo atoll. The second transect of sites drilled during Expedition 359 is located in this southern branch of the Kardiva Channel. Site U1470 (proposed Site MAL-08A) is the westernmost site of this southern transect (Figure **F2**) and has a geographical position of 4°45.9823′N, 72°59.0267′E, and a water depth of 399.7 m.

The site was positioned where seismic data indicated that a carbonate platform existed during the early stages of drift deposition. This seismic relationship implied that at this location the platform drowning is younger than in the northern Kardiva Channel. The main goal at Site U1470 was therefore to recover the drift to platform succession, which contains a platform that drowned at a later stage than the platforms in the northern transect. The specific objectives were (1) to provide a detailed reconstruction of the predrowning, drowning, and postdrowning evolution of the car-

bonate bank by linking the seismic stratigraphic record to the sedimentary record (i.e., depositional facies); (2) to constrain the timing of this platform drowning and the burial by drift sediments; and (3) to reconstruct the neritic carbonate factory of a bank growing in the current-dominated depositional system.

Principal results

Site U1470 penetrated 147.9 m of carbonate sands and 186.2 m of limestone from the underlying carbonate platform. The uppermost 59.1 m (lithostratigraphic Unit I) of the sheeted drift deposits was unlithified coarse-grained grainstone to packstone with abundant planktonic foraminifers but also benthic foraminifers, ostracods, pteropods, echinoderm spines, bryozoan fragments, and bivalves, as well as yellow-red–stained lithic grains and red algae fragments. In lithostratigraphic Unit II (59.1–147.8 mbsf), the grainstones become more lithified and the composition changes to a diverse assemblage of bioclasts (bivalve fragments, benthic foraminifers, echinoderm spines, planktonic foraminifers, and bryozoan and red algae). Crystal overgrowth and cementation is pervasive and was detrimental for biostratigraphy.

Three lithostratigraphic units were identified in the platform succession. Lithostratigraphic Unit III (147.9–188.4 mbsf) comprises coral-rich floatstone to boundstone, documenting a shallow-water reefal environment at the top of the drowned platform. Lithostratigraphic Unit IV (198–207.7 mbsf) is a bioclast-rich grainstone to rudstone that, with its composition of large benthic foraminifers, red algae, green algae (*Halimeda*), and coral fragments, resembles a reef-apron facies. Lithostratigraphic Unit V (207.7–334.11 mbsf) is a reef facies with interbedded grayish brown coral-rich boundstone and red algae floatstone. Coral fragments include massive, platy, and branching forms. Rhodoliths are present in different sizes up to 4 cm long with branching irregular shapes.

Micropaleontological analysis (Figure **F27**) of the core samples from the drift package above the platform carbonates allowed us to define a sequence of biostratigraphic events and a well-constrained age model for the upper part of the sedimentary succession that spans from the Quaternary to the lower Pliocene. As at other sites, however, throughout this interval the planktonic foraminifers consistently indicate older ages and lower sedimentation rates than the calcareous nannofossils. For the lower part of the cored interval, lower Pliocene and possibly uppermost Miocene, only a single planktonic foraminiferal event was identified. This suggests that the sedimentation rate remained constant throughout the Pliocene at ~2.2 cm/ky and that the base of the drift sequence is older than 5.92 Ma.

The concentrations of major anions and cations determined from interstitial water chemistry display near constant and close to seawater values through the uppermost 150 m of the unlithified drift sediments. This lack of gradient and thus indication of diagenetic alteration is in contrast to the changes in carbonate mineralogy across the same interval that document the disappearance of HMC and formation of small amounts of dolomite (Figure **F28**). This pattern was observed at several other sites during Expedition 359 and might be the result of massive advection that dilutes the signature of diagenesis in the pore water of highly porous drift sediment. The drowned platform cored at Site U1470 is mostly limestone with only a short interval with 20% dolomite and preserved aragonite between 200 and 250 mbsf. In the platform strata recovered at Sites U1469 and U1465, the drowned platform is considerably more dolomitized.

The paleomagnetic analysis was severely hampered by two problems: a persistent contamination that typically affected the first two sections of each core (this problem was already observed at the other sites) and a novel artifact that mostly affected measurements below 60 mbsf in Hole U1470A. Starting from Core 359-U1470A-8H, the measured paleomagnetic directions of the "uncontaminated" portion of each core show a constant direction toward east with a subhorizontal inclination (~090/00), independent of the actual core orientation. A correction was applied to this second problem, and the corrected values looked more credible, even suggesting the presence of some reversals in the declination record. Inclination values were rather high, however, and given all the uncertainties associated with these measurements, we did not attempt to interpret these results as a record of geomagnetic polarity changes.

The sedimentary succession from Site U1470 is divided into three physical properties units based on the changes observed in NGR, *P*-wave velocity, bulk density, and porosity measurements. Physical properties Units 1 and 2 (0–148 mbsf) comprise upper Miocene to recent drift sediments. The entire package has very high porosity, although in Unit 1 porosity decreases from 80% to 60% with a more gradual decrease ranging from 60% to 40% in physical properties Unit 2. Sonic velocity is low (average = 1725 m/s) and increases slightly to the bottom of Unit 2. NGR fluctuates with high frequency throughout these two units but has a low at the unit boundary. Physical properties Unit 3 (148–334.1 mbsf) consists of samples from the carbonate platform succession identified by the abrupt increase of velocity and density values and a concomitant decrease in porosity. Velocity varies widely from 2000 to 5000 m/s.

The interpreted seismic data show that the drift sequences overlying the drowned platform are mostly subparallel, semicontinuous reflections, mainly of medium amplitude. The top of the drowned carbonate platform is indicated by strong reflections of a lower frequency (Figure **F29**). To the west, at a distance of around 400 m, this platform package thins out and DS3 and DS2 almost merge. DS1 and DS2 at this locality therefore bear a platform succession that postdates the drowning event recognized at Sites U1465 and U1469. The DS2 relict bank package is characterized by an elevated top and shows basinward-dipping reflections in its eastern part. To the west, these reflections abut the basal sequence boundary of DS3, which can be explained by two processes. This stratal pattern could show a late-stage predrowning reef package or it might reflect erosion of the reef-related strata.

DS10 and DS9 correspond to lithostratigraphic Unit I, which consists of an unlithified planktonic foraminifer–rich grainstone. This package is followed by the partly lithified bioclastic grain- to packstone of lithostratigraphic Unit II, which comprises DS3–DS8. The bounding unconformity of DS3 corresponds to the top of the shallow-water platform limestone (lithostratigraphic Unit III). The top of the coral-rich boundstone and floatstone in lithostratigraphic Unit V is the reflector for DS1.

Site U1471

Background and objectives

Site U1471 (proposed Site MAL-07A) is the eastern end of the southern transect at 4°45.9828′N, 073°08.1146′E, in a water depth of 419.3 m in the Inner Sea (Figure **F2**). Geologically, the site is positioned on the distal portion of the prograding drift where it thins and is overlain by the sheeted drift deposits. The target depth is in the distal bottomsets of the sea level–controlled platform sequences underneath the drift, estimated to be at about 950 mbsf (Figure **F5**).

At this location, all sequence boundaries are conformable; therefore, cores from this site were expected to provide a continuous and expanded record of current evolution from the middle Miocene throughout the Pleistocene.

The specific objectives for Site U1471 were (1) to constrain the age of onset of current-dominated sedimentation; (2) to analyze the cyclostratigraphy of drift deposits, therefore providing reconstructions of changes in the current regime and monsoon cyclicity; and (3) to constrain the timing of sequence boundaries within the drift and the youngest platform sequence.

Principal results

An 889 m thick succession of drift deposits above 110.9 m thick distal platform bottomsets was retrieved at Site U1471. Seven lithostratigraphic units are distinguished in the drift deposits that reflect the degree of current-controlled winnowing and diagenetic overprint. Lithostratigraphic Unit VIII comprises the periplatform deposits in the distal bottomsets. Lithostratigraphic Units I–III (0–180.1 mbsf) consist of planktonic foraminifer–rich packstone to wackestone that is heavily bioturbated, often producing a mottled appearance. All three units contain benthic foraminifers, echinoderm spines, pteropods, sponge spicules, calcareous nannofossils, and mollusk fragments in addition to abundant planktonic foraminifers. The degree of lithification was used to distinguish unlithified Unit I from partly lithified Unit II, and the predominance of the wackestone texture was taken as the criteria to separate Unit III. All three units contain alternations of intervals with darker and lighter colors. These alternations range from ~1 to 10 m, and the darker portion of the alternation is generally much thinner (~20% of the total). The dark intervals comprise higher amounts of organic material and tunicates but fewer benthic foraminifers compared to the lighter intervals.

Lithostratigraphic Units IV (180.1–254.6 mbsf) and V (254.6–588.2 mbsf) have a similar texture and consist predominantly of planktonic foraminifer–rich packstone. These units differ in the amount of lithification rather than composition, with alternating lithified and unlithified layers in Unit IV. Unit V contains densely cemented layers and also layers with moldic porosity. Lithostratigraphic Unit IV has some wackestone intercalations that are generally less lithified than the packstone. In both units, overgrowth of bioclasts was prevalent. Several intervals in Unit V exhibit visible porosity, including intraparticle, moldic, and vuggy porosity. At times, celestine is present, forming large crystals spanning adjacent pores (Figure **F30**).

Lithostratigraphic Unit VI was defined by the occurrence of alternations of very fine to medium-grained dark brownish packstone and dark brownish gray to light gray wackestone/packstone. In addition to planktonic foraminifers, sponge spicules, radiolarians, and calcareous nannofossils were identified, as well as rare dolomite crystals. Packstone intervals are thinner than those comprising wackestone. Packstone intervals are thicker and more prevalent downhole. Packstone intervals are less bioturbated than wackestone intervals, individual burrows are discernable, and lamination-like structures are present. The burrows are in some cases completely flattened, and some of the noncontinuous lamination-like structures may be highly compacted burrows, possibly with organic matter. *Planolites, Chondrites*, *Palaeophycus, Phycosiphon, Thalassinoides, Teichichnus*, and *Zoophycos* ichnofossils were identified, in that order of abundance. Fractures in incompletely cemented beds occur as both open and cemented fractures.

Lithostratigraphic Unit VII contains thin, loosely cemented grainstone layers in a background sediment of fine-grained foraminifer-rich packstone. The light brownish gray to light gray coarse-grained bioclastic-rich grainstone is between 2 and 78 cm thick (average = 14.0 cm). The layers often (but not always) have sharp lower boundaries and a more gradational top. The grain size does not vary much within the grainstone layers. These layers were interpreted as reflecting high-energy current events within this first drift sequence.

In the distal bottomsets of the prograding clinoforms of lithostratigraphic Unit VIII, the facies changes considerably from very fine to fine-grained, white to light gray, foraminifer-rich packstone to wackestone and from very fine grained and finer dark gray wackestone to mudstone. Calcareous nannofossils are abundant in both end-members; planktonic foraminifers are abundant in the lighter packstone to wackestone and rare in the dark wackestone to mudstone (Figure **F31**). Benthic foraminifers and glauconite are present only in the lighter packstone to wackestone. In the lighter intervals, bioturbation is common with ichnofossils, including *Planolites*, *Thalassinoides*, *Zoophycos*, and *Chondrites*.

Biostratigraphic and paleoenvironmental analyses were conducted in Holes U1471A, U1471C, and U1471E and provide a robust age model at Site U1471 in the expanded section of younger drift sequences and the tops of underlying bottomsets. Pleistocene and late Pliocene sediments extend from the seafloor to ~150 mbsf and are defined by a succession of well-constrained events and reasonably good agreement of the data. The implied sedimentation rate is 4.0 cm/ky. However, there is a consistent offset between the ages inferred from calcareous nannofossil events and those from planktonic foraminifers, with the planktonic foraminifers suggesting ages about 0.5 My older than the calcareous nannofossils. This pattern was also seen in this interval at Sites U1465, U1466 and U1467, so possibly the age calibrations of these events may need revision, at least for this area.

In the lower Pliocene to middle Miocene sediments and rocks within the top of underlying bottomsets, preservation of planktonic foraminifers is generally moderate to very poor, with mostly poor to very poor preservation in the samples from Hole U1471E. Benthic foraminifers are moderately preserved throughout this interval, with preservation decreasing downhole. Nannofossil preservation is poor to moderate throughout most of the core. In the lower part of Hole U1471E (Cores 37R–44R), nannofossils are generally more abundant and better preserved. The planktonic foraminiferal and nannofossil events recognized in this lower Pliocene to mid-Miocene section reasonably agree with each other. They provide an inferred sedimentation rate of 8.0 cm/ky.

The concentrations of major anions and cations in interstitial water of the upper 40 mbsf exhibit negligible changes, reflecting either low rates of organic matter remineralization or fast rates of advection by seawater. Below this interval, pore water profiles of many elements start to vary, indicating numerous diagenetic processes occurring in the sediment column. The inflection points of these profiles, however, did not coincide with boundaries between lithostratigraphic units.

A decrease of sulfate coincided well with an increase in alkalinity, indicating that bacterial sulfate reduction is occurring in the sediment column. However, a greater increase in alkalinity was expected from the ~4 mM decrease in sulfate than was observed; the difference is explained by the authigenic precipitation of calcite. The decrease in Mg^{2+} and concurrent increase in Ca^{2+} reflects dolo-

mitization by replacement of calcium carbonate. However, only a minor amount of dolomite was found at this site, with the dolomite peak at 105.55 mbsf occurring close to the maximum decrease in Mg^{2+} concentrations. A rapid increase in the Sr^{2+}/Ca^{2+} ratios of the pore water occurs below 40 mbsf, documenting the neomorphism of aragonite sediments to LMC, which is also evident in the changes in carbonate mineralogy based on the XRD data (Figure **F32**). The large increase in Sr^{2+} caused the pore fluids to attain saturation with respect to celestine ($SrSO_4$). The presence of celestine based on XRD spectra and high sedimentary Sr/Ca ratios extends to approximately 700 mbsf. Changes in the Mn content of the pore waters and sediments were related to the redox state. The higher Pliocene–Pleistocene Mn/Ca and Fe/Ca ratios may reflect a more reducing environment during this time interval relative to the late Miocene. The small increase in Mn/Ca and Fe/Ca in the middle Miocene may be coincident with the development of the Oxygen Minimum Zone (OMZ) as proposed by Dickens and Owen (1994).

A cyclic pattern in carbonate content is visible when the data are smoothed with a five-point moving average, with alternations of ~5 wt% between higher and lower values. The upper 300 mbsf has a period of ~40 m with seven or eight maxima within this depth interval. Where recovery was poor, from 300 to 400 mbsf, the smoothing was not effective, but cycles with an amplitude of ~5 wt% carbonate were again apparent between 400 and 1000 mbsf. The apparent cycles in carbonate content may be related to changes in climate or currents, which influenced sediment supply and probably carbonate dissolution at Site U1471.

For establishing a magnetostratigraphy at Site U1471, the core orienting device was used in the upper 19 cores drilled in Hole U1471C and in Cores 359-U1471D-6H and 7H. The magnetostratigraphy is based on the interpretation of the declinations in the oriented APC cores that show relatively consistent directions within each core, with most of the reversals occurring within a single core.

The Brunhes/Matuyama boundary was tentatively placed between Cores 359-U1471C-4H and 359-U1471D-6H (36–39 mbsf) based on the short reversal found in Core 359-U1471D-5H, which was interpreted as the Jaramillo Event. Additional reversals were identified at 79, 84, 112, 152, 169, and 172 mbsf (Cores 359-U1471C-9H, 10H, 12H, 16H, and 19H). For unoriented Hole U1471A cores, a smoothing moving average (six points) was used for the inclination, and a series of magnetozones were defined as intervals with multiple consecutive sections with the same polarity. The magnetostratigraphy based on inclination only, however, has a high degree of uncertainty because of the subequatorial paleolatitude of Site U1471.

Analysis of physical properties allowed us to divide the sedimentary formation into six units primarily based on porosity and NGR measurements and not necessarily following lithostratigraphic unit boundaries. In physical properties Unit 1 (0–68 mbsf), sediments have high porosity values of 60%–75% decreasing downhole within the unit. Porosity, however, increases again downhole in physical properties Unit 2 (68–138 mbsf) to reach 75%. A similar reversal of the porosity trend occurs in the lower part of the succession in physical properties Unit 6 (700–1003 mbsf), where porosity values reach around 50% and are on average higher than in physical properties Unit 5 (320–700 mbsf). NGR counts reach values higher than 80 counts/s in physical properties Unit 4 (180–320 mbsf) and are the highest NGR values measured on Expedition 359 cores.

Three logging runs were conducted at Site U1471, but only the triple combo tool string reached the bottom of the hole. The VSI tool string encountered an unpassable obstruction at ~615 m WSF and the Formation MicroScanner (FMS)-sonic tool string did the same at 454 m WSF. The triple combo tool string produced good quality data, except in three intervals where the borehole diameter was too large. Gamma ray values are dominated by uranium, as at other sites. The porosity log confirmed the high porosities measured in the laboratory and the unusual high porosities of the drift deposits. Resistivity and magnetic susceptibility display similar trends and increase slightly downhole between 50 and 400 m WSF. They decrease from there to the bottom of the hole but have a small but abrupt decrease at the bottom of the drift. In the short interval velocity was measured, it displays a gradual increase with depth to 400 m WSF with a few higher peaks. In the deepest 40 m of the log data (400–440 m WSF), velocity fluctuates dramatically and reaches as high as 3.5 km/s. These fluctuations match the alternating lithified and unlithified lithologies observed in the cores. Four formation temperature measurements documented a low geothermal gradient of 15.3°C/km.

Determining the relative positions of core gaps among the various holes at Site U1471 during coring was accomplished using gamma ray attenuation (GRA) density data collected at 5 cm resolution on the Whole-Round Multisensor Logger. NGR was also used to evaluate sedimentary completeness for Holes U1471A, U1471C, and U1471D. High-resolution compositing was based on the 2.5 cm interval color reflectance parameter L* for all but one interval where L* lacked distinct patterns. The composite depth scale and splice at Site U1471 are constructed from 0.0 to 195.71 m CCSF-D; deeper cores from Hole U1471A are appended with a constant affine value.

The upper 30 m of the L* records from Sites U1467 and U1471 were compared to assess Late Pleistocene sections at each site. This interval was correlated to 0–800 ka at Site U1467. Based on the L* records, the latest Pleistocene is slightly more expanded at Site U1467 than Site U1471 over the interval correlated to marine isotope Stages (MIS) 1–11. Below this level, the reflectivity L* highs are more expanded at Site U1471 than Site U1467. The change in relative thickness of the reflectivity highs between Site U1467 and U1471 sedimentation may indicate subtle changes in the location of current-controlled sedimentation at ~450 ka.

Seismic stratigraphy and core data were correlated using three stations of the check shot survey with the VSI tool string in the upper part of the hole. To anchor our velocity model in the interval below 604.6 mbsf, where hole collapse prevented further lowering of the tool, we used the boundary between lithostratigraphic Units VII and VIII (Core 359-U1471E-33R), which marks the change from drift to platform sequences at 898 mbsf, as a tie point. The three oldest drift sequences (DS1–DS3) at Site U1471 show a pronounced clinoform prograding reflection pattern. DS5–DS10 are classified as elongated mounded separate drifts. Site U1471 penetrated the bottomsets of the prograding drift bodies, calibrating the seismic facies with the depositional facies. For example, high-amplitude reflections, especially in DS3, are related to strong impedance contrasts produced by the alternation of partly lithified and lithified beds. In DS3 and DS4, small-scale wavy reflections are interpreted as cyclic steps or bottom current–related features.

Correlation of the seismic sequences and the biostratigraphic age model shows that DS9 encompasses the Pleistocene. The pronounced change in lithology between lithostratigraphic Units IV and V at 254.6 mbsf correlates with the base of DS4 (261.5 mbsf) and roughly coincides with the boundary between the Pliocene and Miocene. The bottom of the drift that is the base of DS1 at 898 mbsf lithologically expresses the last occurrence of grainstone layers at 898 mbsf in the upper middle Miocene.

Site U1472

Background and objectives

Site U1472 (proposed Site MAL-06B) is in the middle of the southern transect at 4°46.2653′N, 073°04.0111′E, at a water depth of 379.34 m (Figure F2). The site is located well within the middle part of the west to east prograding contourite fan. The target for coring at this site was the lower sequence boundary of DS1, but it was not reached because of time constraints at the end of the cruise. Coring penetrated to 251.9 mbsf and recovered 233.75 m (93%), providing a valuable data set for understanding drift deposition in the Inner Sea and the contourite fan depositional system. The specific objectives at this site were to (1) constrain the ages of the drift depositional sequences; (2) analyze the cyclostratigraphy of drift deposits, therefore providing reconstructions of changes in the current regime and monsoon cyclicity; and (3) retrieve the lithology of the wavy seismic facies to confirm their current-controlled deposition.

Principal results

The succession at Site U1472 is divided into four lithostratigraphic units. Lithostratigraphic Unit I (0–52.70 mbsf) consists of unlithified packstone and grainstone texture and mud-lean fine to medium sand. Deposits contain abundant fairly well preserved planktonic foraminifers, pteropods, otoliths, echinoid fragments, and shell fragments. This facies is similar to the top units of all the sequences drilled during Expedition 359. Layers of floatstone contain large bioclasts such as pteropods and solitary corals (Figure F33). Light gray to brownish gray sediment was interpreted to reflect the presence of organic matter and also of iron in reduced form. This sediment provides evidence for suboxic conditions at the seafloor, as does the NGR measured on the cores. Varying gray-brown color changes associated with a cyclic pattern of L* color reflectance and NGR likely indicate that these conditions fluctuated through time.

Lithostratigraphic Unit I has grainstone to packstone textures, whereas lithostratigraphic Unit II (52.70–195.20 mbsf) consists of packstone to wackestone. The composition of the sediment is similar to lithostratigraphic Unit I sediments, with the difference that Unit II does not contain pteropods. NGR values in Unit II are distinctly lower than in Unit I, and the top of Unit II contains large bioclasts and shells, suggesting a phase of intensified bottom current.

The transition from packstone to grainstone texture and the grain size change from predominantly medium- to coarse-grained sand defines the top of lithostratigraphic Unit III. Unit III is characterized by the appearance of large benthic foraminiferal assemblages typical of neritic environments. Foraminiferal shells have extensive overgrowths, masking their original shape. The textural, grain size, and biota assemblage changes collectively imply that this unit represents a shallowing-upward succession.

Lithostratigraphic Unit IV (224.22–249.24 mbsf) is marked by a change toward a grainstone texture and coarse-grained sand. The bioclast assemblage is composed of corals, red algae, large benthic foraminifers, and bivalves. Texture, grain size, and inclined layers indicate that these sediments were deposited under high-energy conditions that existed on the top of the contourite fan drift sequence.

Calcareous microfossils are present throughout the sequence, showing good preservation in the upper 100 m and poor to very poor preservation below. The calcareous nannofossil biostratigraphy suggests a late Miocene age for the bottom of the sequence. A useful sequence of biostratigraphic events through the Quaternary and early Pliocene provides a fairly clear age model that indicates a sedimentation rate of 2.6 cm/ky throughout the succession. As observed at other Expedition 359 sites, planktonic foraminifers in this interval consistently indicate older ages and therefore lower sedimentation rates than those based on calcareous nannofossils.

IW analysis indicates that the slight increase in chloride in pore waters at Site U1472 is higher than the increase observed at Site U1471 but not as strong as that at Sites U1466 or U1468. This may be a relict signal of Last Glacial Maximum seawater that has not yet diffused. Negligible rates of bacterial sulfate reduction relative to advection of seawater at Site U1472 are indicated by the constant alkalinity concentrations with depth. XRD analysis of the sediments showed that neomorphism of aragonite to LMC does not appear to occur with the same intensity as at other Expedition 359 sites. The high abundance of aragonite even at 200 mbsf is unique to this site and may be related to the general lack of modern, active diagenesis inferred from constant pore fluid profiles. The constant alkalinity at Site U1472 also implies that the small amounts of dolomite present in the sediments are the result of previous episodes of alteration and are not actively forming in the modern sediment column. Carbonate diagenesis and dolomitization must have occurred in previous time intervals but unusually do not seem to have resulted in aragonite neomorphism to LMC.

Measurements of the magnetic sediment properties exhibit early vertical and negative inclinations in the uppermost 30 mbsf of Hole U1472A that could be interpreted as a coring disturbance in these soft and fluid-rich sediments. The rest of the inclination record, although it shows generally shallower inclination, still has a rather erratic behavior that was not easily interpretable as a sequence of reversals.

Because of time constraints at the end of the expedition, only a reduced suite of physical property measurements was performed on Site U1472 cores (primarily whole-round and split core track measurements). Four physical properties units are observed and correlate well with the lithostratigraphic units. Physical properties Units 1 and 2 have high NGR values in their lower parts and decreasing values toward the top. Physical properties Units 2–4 generally show lower NGR values with little variation but some isolated peaks of higher values. Sediment bulk density at Site U1472 increases continuously downhole, whereas there is an inversion of the *P*-wave velocities below 185 mbsf. As at other sites, porosity is very high at the top (>70%) and decreases to ~50% at 200 mbsf.

Site U1472 comprises a complete succession of all drift sequences (DS1–DS10) in the southern transect. For a time to depth conversion, the check shot information from Site U1470 was used because the sediments had similar characteristics at both sites. Sheeted DS7–DS10 are imaged by well-stratified continuous reflections of medium to low amplitude. The subhorizontal reflections of the topsets of DS4–DS6 are discontinuous to wavy at Site U1472, but the reflections become more continuous in a distal direction to the east. Whereas DS5 and DS6 are sheet-like, DS3 and DS4 have a divergent pattern and thicken basinward. The calibration of these seismic facies was one of the objectives for Site U1472.

Lithostratigraphic Unit I corresponds to Pleistocene DS10 and DS9. Underlying DS8–DS5 are dominated by packstones, which become increasingly lithified with depth. Large benthic foraminifers in DS4 indicate shallow-water conditions. The transition from lithostratigraphic Units III to IV at 224 mbsf is within DS3 and is accompanied by a significant increase in benthic foraminifers and by more diverse skeletal components. Both DS3 and DS4 show a characteristic chaotic reflection pattern of high amplitude that correlates well to the abundance of coarse material in Units III and IV

and layers with downcutting erosion. Both features indicate a high-energy depositional regime within this drift sequence.

Preliminary scientific assessment

Eight sites were drilled along two transects in the Kardiva Channel in the Inner Sea of the Maldives during Expedition 359. The recovered cores retrieved material to achieve all of the objectives set for the expedition. Beyond the acquisition of these data, coring also revealed a series of unexpected discoveries.

Drilling the carbonate platforms and drifts in the Maldives aimed to recover the marine tropical record of the Neogene sea level changes and the onset of the monsoon-related current system in the Indian Ocean. The recovered cores and log data elucidate both aspects with great detail. The most arresting accomplishment is the documentation of how the sea level–controlled carbonate platform system thrived during the mid-Miocene Climate Optimum and abruptly transitioned into a current-dominated system in the late middle Miocene. This transition is linked to the onset of an early intensification of the Indian monsoon and the coeval demise of some of the Maldivian platforms. In addition to accomplishing all of the primary objectives, four major discoveries were made, and all are major contributions to the fields of paleoceanography, sedimentology, biostratigraphy, and geochemistry. How these objectives and the additional discoveries were achieved is outlined below.

Objectives

1. *To decipher the record of Neogene environmental changes in the Maldives sediment archive.*

Cores and downhole logs allowed us to produce a solid record and reconstruct Neogene environmental changes in the central Indian Ocean. Site U1468 cored the entire succession from the upper Oligocene to Pleistocene. Deeper cores recovered illustrate how an Oligocene neritic carbonate platform drowned and how sedimentation turned to a hemipelagic mode. Coinciding with the Oligocene to Miocene transition, the sedimentary regime changed to a pelagic system characterized by events of high organic accumulation. The record of the sea level–controlled lower and middle Miocene carbonate platform was cored at Sites U1466 and U1467. The onset of the monsoon wind–driven depositional system was cored at Sites U1466, U1467, U1468, and U1471. Preliminary shipboard analyses allow precise dating of this major paleoclimatological and paleoceanographical change, as it also applies to the extension of the OMZ into this part of the Indian Ocean. Coring produced a solid framework to foster postcruise research of these distinct topics. We therefore regard this objective as fully accomplished.

2. *To place the Maldives current system into the larger scale ocean current framework present during Neogene global cooling and monsoon evolution.*

Seismic data from the Maldives document mounded drift packages deposited by the ocean currents that sweep through the Inner Sea. Today these currents are linked directly to the monsoon as they flow from west to east during the summer monsoon and reverse direction with the onset of the winter monsoon. This changing current also occurred during Expedition 359 and served as a good illustration of the sedimentary and oceanographic dynamics of the archipelago. Based on seismic stratigraphy, the onset of drift deposition coincides with cessation of sea level–controlled platform progradation during the late middle Miocene global cooling phase. If the Miocene drift deposits are related to the monsoon, as they are today, the onset of the drift deposits give strong evidence of the onset or at least major strengthening of the monsoon at this time. The biostratigraphic age model of Expedition 359 indicates a late middle Miocene age for the onset.

Complete spliced sections and logging at key sites during Expedition 359 provide the potential to assemble a cycle-based astrochronology for the Neogene section in the Maldives. This high-resolution chronology will allow (1) assignment of independent ages to key biostratigraphic events in the Maldives for comparison with those from other tropical regions; (2) assignment of more precise ages for the major sequence boundaries and unconformities; and (3) evaluation of higher resolution sedimentation rate variations.

The age of the onset of the drift deposition and thus the current system in this part of the Indian Ocean is essentially the same as the onset of the Santaren Drift in the Bahamas that is formed by the Florida Current. Initial comparison shows that not only the onset but also the changes in sedimentation rates within the two drift bodies are coeval. Likewise, the onset of the current across the Marion Plateau, northeast Australia, is only slightly younger based on data from ODP Leg 194. The synchronous evolution of the drifts indicates that the onset of the current in the Atlantic, Pacific, and Indian Oceans was basically simultaneous. Postcruise research will have to establish the extent of the lead and lag in each ocean.

3. *To obtain a continuous carbon isotopic record to calibrate a platform and platform margin record with the pelagic record.*

This objective was achieved by coring the platform tops at three sites (U1465, U1469, and U1470) and the entire Neogene periplatform strata at several sites at varying distances from the platform (U1468, U1467, and U1471). Together, the cored intervals will provide a complete record of the carbon isotopic record of the platform and platform margin sediments. Because sedimentation rates are high to very high in these settings, these cores provide an expanded record that will be suitable for high-resolution carbon isotope stratigraphy. In the distal portions of the prograding clinoforms, sedimentation rates were between 3.2 and 4.4 cm/ky, and in the drift deposits, they reached 17 cm/ky. The base of the Neogene was penetrated at Site U1468, where the earliest Miocene succession was a shallow-water carbonate lagoonal environment that developed into a somewhat deeper basin, the paleo–Inner Sea of the Maldives, with fine-grained carbonates that also contain numerous dark organic-rich intervals. Together with the sediments of the overlying distal bottom set from the Kardiva platform in the west, these sediments will provide a continuous carbon isotopic record to the late middle Miocene. The overlying late middle Miocene to recent drift deposits were cored at Sites U1466, U1467, U1468, and U1471. Each of these sites covered a different age interval with a high sedimentation rate. Thus, the entire Neogene is cored, and therefore we obtained an ideal candidate for shore-based analysis of carbon isotopes on both the organic and inorganic fractions. This will allow the record of carbon isotope change to be extended back in time from the approximate 8 My record, which was already measured on sediments from ODP Site 716, to ~25 Ma at Site U1467. A complete comparison will be possible not only with ODP Site 1007, which penetrated the entire Miocene, but also in relation to other platform and pelagic records over the same time period. This comparison will allow assessment of the extent to which platform carbonates record changes in the global carbon cycle and determine whether changes

in the carbon isotopic composition of organic and inorganic components covary and the implications this has on the deep-time record.

Additional discoveries

1. *Organic-rich layers indicate early Miocene oxygen minima*

At Site U1466, coring recovered an upper Oligocene to lower Miocene alternation of chalky white wackestone and black organic-rich layers in the lower Miocene. At Site U1468, the same facies was recovered above neritic carbonates with large benthic foraminifers. Here, the succession with nannofossil chalk and black organic-rich sediments is approximately 90 m thick. Based on their position within the stratigraphic succession and the estimated water depth of the Inner Sea at the time, the presumed oxygen minima conditions necessary for their formation must have formed a relatively shallow basin.

2. *The shallow nature of a carbonate contourite fan*

Although the drift package in the Kardiva Channel was identified based on the geometries seen on the seismic data, the cores revealed a facies evolution that has far-reaching implications for interpretations of neritic carbonates. Together with lithologies from the cores, this drift is best classified as a contourite fan. No such system has been previously reported for carbonates. The reason this discovery will have major implications for carbonate sedimentology is that the facies within this drift is very similar to what has hitherto been described as, for example, neritic shoals, prograding delta lobes, and so on. For example, Site U1468 cores from the apex of the drift mound contain large benthic foraminiferal floatstones that resemble benthic foraminiferal shoals. Likewise, the prograding lobes of this contourite fan are very reminiscent of what might be called a tidal delta front. The documentation of this carbonate contourite fan will thus trigger reinterpretation of deposits with these characteristics.

3. *Advection dominance of fluid flow*

Early diagenesis is thought to be controlled by diffusion of seawater into the underlying sediments. This diffusion-related diagenesis generally produces a characteristic depth profile of the major anions and cations. This general lack of variation may result both from high rates of advection in the high-permeability drift sediments and from different geochemical profiles and carbonate diagenesis being present during the sedimentary history. Many workers assume that the present measured pore water profile might have been similar throughout the history of a particular site and used gradients in various elements and isotopes to calculate rates of neomorphism and recrystallization (e.g., Baker et al., 1982; Richter and DePaolo, 1987). Therefore, the findings made during Expedition 359 question one of the basic assumptions inherent in such modeling studies.

4. *Planktonic foraminiferal and nannofossil biostratigraphy*

During Expedition 359, age models were constructed with a succession of well-constrained events of calcareous nannofossils and planktonic foraminifers, which generally were in good agreement. However, through much of the Pleistocene and Pliocene intervals in all cores there was a consistent offset between the ages inferred from calcareous nannofossil events and those from planktonic foraminifers, with the planktonic foraminifers suggesting ages about 0.5 My older than the calcareous nannofossils. This persistent pattern indicates that possibly the age calibrations of these events need revision, at least for the Maldives (i.e., the central Indian Ocean).

Operations

The Expedition 359 hole summary is presented in Table **T1**. A diagram of Expedition operations and core recovery is presented as Figure **F34**.

Port call and transit

Expedition 359 officially began with the first line ashore Fort Hill Wharf, Berth 2W, Darwin, Australia, at 1013 h on 30 September 2015. The initial week of Expedition 359 consisted entirely of port call activities in Darwin, including routine resupply of consumables, offloading the previous expedition's freight, and refueling. Unfortunately, no work could be conducted after dark because of noise restrictions.

IODP *JOIDES Resolution* Science Operator (JRSO) staff and the Expedition 359 Co-Chief Scientists boarded the vessel at 1100 h on 30 September and immediately started crossover meetings with the previous expedition's participants. Other activities on the first day included loading the ship operator's air freight, the Schlumberger logging sources, and local fresh food. In addition, a press conference with the Expedition 356 Co-Chief Scientists and a public relations tour were conducted. The second day of port call (1 October) included the ship crew change, the arrival of Expedition 359 scientists, and a tour for VIPs and media. We also offloaded Expedition 356 cores, loaded frozen food, and started loading drilling mud. On 2 October, loading continued with drilling mud, drill collars, arriving sea freight, and locally-sourced laboratory supplies. Expedition 356 outgoing shipments were dispatched, including remaining cores, scientists' personal samples, and JRSO/Schlumberger airfreight.

Completion of activities on 3 October was critical to an on-time departure for Expedition 359 because the port side aft crane could not be used during the refueling process planned for the following day. Therefore, all loading and storing of supplies that required the aft crane had to be completed before moving the ship to the bunkering pier. This was further complicated because we were not able to operate the cranes after dark and were only able to operate one crane at a time in the afternoon.

On 4 October, the *JOIDES Resolution* was relocated to the East Arm Wharf refueling dock in Darwin, where bunkering activities commenced and the final loading of reentry cones and a box of operations hardware (Motion Decoupled Hydraulic Delivery System [MDHDS]) was completed. Bunkering continued through the night and was completed at 1024 h on 5 October.

The port pilot came aboard, and with tugs on-site, the last line was cast away at 1206 h on 5 October. The pilot was discharged at 1306 h, and the sea passage to the Maldives began. As part of the agreement with the Republic of Maldives, the vessel was required to report to anchorage in Malé and clear into the country. Two Maldivian coastal observers were also scheduled to board the vessel and participate on the expedition. In addition, Overseas Drilling Limited (ODL) planned to have one of their drillers board the ship in Malé.

The ship was favored with good weather and calm seas during the two weeks of transit. The drilling department took advantage of the stable platform to conduct routine drilling equipment maintenance. Three time changes took place during the first week of transit with the clocks being turned back a total of 2.5 h, placing the vessel on UTC + 8 h time or 13 h ahead of College Station, Texas (USA). As of 2400 h on Sunday, 11 October, the vessel had transited 1869 nmi at an average speed of 11.9 kt. With 1737 nmi remaining

to our destination and a projected time of arrival at the Malé pilot station of 1200 h on 18 October, the ship was approximately 18 h ahead of schedule.

Already on the third week of the expedition, the ship continued to make good time in transit to Malé. At 1813 h on 15 October, the vessel crossed the Equator, entering into the Northern Hemisphere. Time was changed two more times, with the last change taking place at 0200 h on 16 October, placing the ship on Maldives time (UTC + 5 h or 10 h ahead of College Station) for the remainder of the operational period prior to the final transit of the expedition from Malé to Colombo (Sri Lanka).

The vessel arrived at the Malé pilot station at 0630 h on Sunday, 18 October, completing the 3594 nmi transit from Darwin at an average speed of 11.6 kt. The harbor pilot boarded the ship at 1030 h, and the ship proceeded to anchorage. By 1142 h, the ship was securely anchored. Maldivian Customs and Immigration personnel cleared the ship by 1300 h, and there was a brief visit by the Maldivian Coast Guard. During the Malé stopover, the ship was cleared into Maldivian waters to conduct scientific coring operations over the next 6 week period. In addition, the Minister of Fisheries and Agriculture from the Republic of the Maldives, accompanied by an entourage of local news media personnel, took a brief tour of the ship's laboratory facilities and held a press conference with the expedition Co-Chief Scientists. A limited amount of fresh food and supplies were brought aboard, including some spare parts. Finally, two coastal observers from the Republic of Maldives Ministry of Defense joined the ship to sail with us until the end of coring operations. The ship was scheduled to return to Malé on 28 November to clear the Republic of Maldives waters and disembark the two observers.

At 2048 h on 18 October, the harbor pilot arrived on board, and we proceeded out of the Malé harbor. After discharging the pilot at 2142 h, we began our sea passage to the first site (U1465). At 0418 h the next day, Monday, 19 October, the vessel completed the 65 nmi to Site U1465 at an average speed of 9.9 kt.

Site U1465

Hole U1465A

Thrusters/hydrophones were lowered, and by 0456 h on Monday, 19 October 2015, full control of the vessel was shifted to the dynamic positioning (DP) system operator. A positioning beacon was deployed at 0611 h. The bottom-hole assembly (BHA) and the outer core barrel assembly were made up, and APC/XCB space-out was checked. A precision depth recorder (PDR) reading indicated the seafloor was at ~514.4 meters below rig floor (mbrf). The sinker bars were made up, and an APC core barrel was run in the hole with the bit positioned at 509.4 mbrf, or 5.0 m above the PDR depth. This core barrel was recovered empty, so the pipe was lowered an additional 9.0 m for a second attempt. This time the barrel was again recovered empty; however, the core barrel may have hit the seafloor because the gap at the base of the core liner contained a small amount of coarse sand. At this point, the drill string compensator was opened, and the bit was lowered until it hit something hard at ~524.4 mbrf and again at ~528.0 mbrf. A third attempt at starting Hole U1465A was successful at 1405 h with the bit positioned at 523.4 mbrf. Core 1H recovered 7.3 m and established a seafloor depth of 525.8 mbrf. It was later determined that the original PDR measurement had a 10 m error.

Coring in Hole U1465A continued to a total depth of 76.6 mbsf. Nine APC cores were obtained and recovered 77% of the 64.4 m penetrated. One HLAPC core was taken and recovered 71% of the 4.7 m advance, and a single XCB core was cut at total depth, advancing 7.5 m and recovering a mere 0.42 m (6%). Coring was problematic from the start due primarily to the highly sandy formation and a few interspersed hard layers. The APCT-3 temperature shoe was deployed three times; however, analysis indicated that all measurements were suspect. The formation conditions were not good for core recovery or formation temperature measurement. Therefore, we halted coring when the depth objective, the ancient carbonate platform, was reached. As planned, we transited in DP mode to the next site (U1466). The strategy was to save time by using the same BHA on both holes to recover and date the thick prograding drift succession at Site U1466 and then return to Site U1465 to rotary core down to the target depth.

Overall recovery for Hole U1465A was 70%. The drill string was pulled clear of the seafloor and secured for a move in DP mode to Site U1466. At 0230 h on 20 October, the ship began moving east with the thrusters down.

Hole U1465B

Hole U1466B was completed at 1220 h on 26 October 2015, officially ending operations at Site U1466. The ship was moved in DP mode ~1 nmi back to Site U1465 while a new RCB bit/BHA was assembled. Once on station, the drill string was lowered to the sea bottom and a seafloor depth was established as 512 meters below sea level (mbsl). The top drive was picked up, and after spacing out the drill string, Hole U1465B was spudded at 0655 h. The hole was drilled to 65.9 mbsf before deploying an RCB core barrel. Continuous rotary coring began at that point and continued through Core 23R to 221.3 mbsf. Recovery was poor through the high-porosity carbonate sedimentary unit. RCB half-cores were used a few times in an attempt to improve recovery with very limited success. Ultimately, the inability to effectively clean the hole, high drilling torque, and occasional stuck pipe led us to abandon the hole at 0215 h on 27 October. The drill string was pulled with the top drive to 63.5 mbsf before becoming stuck for 0.75 h. Once the drill string was freed, the bit was pulled clear of the seafloor at 0610 h and the top drive was set back. The ship was offset 20 m east of Hole U1465B to start Hole U1465C.

Hole U1465C

A third hole at this site was not originally planned, but because of the exceptionally poor recovery in Hole U1465B we decided to make another attempt to core the formation using the HLAPC and XCB coring systems. The target depth was reduced from the original 720 to 500 mbsf because given the sedimentological properties of the formation it was highly unlikely that hole conditions would allow penetrating even that deep. In this hole, the cores were not oriented and no temperature measurements were taken. An APC/XCB BHA was assembled with a mechanical bit release (MBR) system above the bit even though no logging was planned. The MBR was included to have the option of releasing the bit in case the pipe became stuck in the hole. After spacing out the wireline core barrels, the drill string was lowered to the bottom, where a seafloor tag established a mudline depth of 510 mbsl. Hole U1465C was spudded at 1330 h on 27 October 2015. The hole was drilled to 55 mbsf before coring began. Recovery was poor; however, the objective was to reach ~500 mbsf (or into the sediment drifts below the drowned reef complex). APC/XCB coring was ultimately suspended at 233.2 mbsf because, just as in Hole U1465B, all circulation began going downhole into the formation and the drillers were no longer able to get the drill cuttings pumped out of the hole. After discussion, the

general consensus was that most likely both holes were drilled into an area of very high porosity within the ancient reef formation, which made it impossible to further deepen either hole. Therefore, at 1430 h on 28 October, we stopped further cleaning attempts in Hole U1465B and ended operations at this site.

Site U1466

Transit to Site U1466

After the ~1 nm transit from Site U1465 to Site U1466, the ship was positioned over the new location by 0430 h on 28 October 2015 and rig floor activities began. The top drive was picked up, and the drill string was spaced out.

Hole U1466A

At 0625 h on 20 October 2015, Hole U1466A was started, recovering 5 m of core and establishing a seafloor depth of 528.9 mbrf. Coring was problematic in this hole because of the abundance of sand in the surface layers of the formation. Nevertheless, coring with the APC and HLAPC coring systems proceeded to 100.5 mbsf (Core 12F). Three formation temperature measurements (APCT-3) were attempted; however, all the values were considered suspect because the characteristic friction curves did not occur. At this point, we decided to make a wiper trip because of high drilling torque. At 1730 h on 20 October, the drill string was pulled back to 63.1 mbsf and then washed back to bottom. With all drilling parameters back to normal, coring resumed at 1930 h and continued through Core 20F to 155.0 mbsf. Once again, high drilling torque necessitated a wiper trip. At 0100 h on 21 October, the drill string was recovered to 63.1 mbsf and then washed back to the bottom of the hole at 155.0 mbsf. As on the first wiper trip, the hole cleaned up, and all drilling parameters returned to normal. Coring resumed at 0400 h and continued through Core 50X to a total depth of 326.2 mbsf. All three coring systems (APC, HLAPC, and XCB) were used interchangeably and with great effectiveness during this cored interval. Coring was terminated at 0400 h on 22 October because the depth objective was achieved and we decided the formation could be cored at that point with the RCB coring system. The drill string was recovered and pulled back to the rig floor at 1000 h on 22 October, officially ending Hole U1466A and initiating Hole U1466B.

Hole U1466B

An RCB BHA was lowered to the seafloor, and with the compensator open, the driller physically tagged the seafloor with the bit at 528.0 mbrf. Drilling without coring in Hole U1466B started at 1620 h on 22 October 2015 at the seafloor and continued to 158 mbsf. A wiper trip to 61 mbsf and back to bottom was conducted with no overpull or drag experienced and no fill noted on bottom. Drilling resumed, and 313.9 mbsf was reached by 0600 h on 23 October. A second wiper trip was conducted, and again there was no overpull or drag noted. At the bottom, 2 m of fill was circulated out with a high-viscosity mud sweep. At 1045 h, we started RCB coring at 314.0 mbsf. Coring continued with nonmagnetic core barrels. Poor recovery through the highly interbedded hard/soft formation led to a combination of full and half RCB cores. As the hole progressed and the scientific data grew, the scientists decided that the scientific objectives had essentially been reached and terminated the hole so that downhole logging could start. At 1150 h on 25 October, the last RCB core (57R) was recovered at 809.7 mbsf. Hole conditions remained good. The bit was released, and the hole was displaced with heavy mud. The drill string was pulled up, and the end of the pipe was placed at 106.0 mbsf. At 1800 h, rig-up of the first wireline logging tool string was initiated. The triple combo tool string, without the source installed, was run in the hole. However, the tools would not pass 894.0 mbrf (366.0 mbsf). Log data were collected up from there, but constant tool drag indicated the hole was rapidly deteriorating. The triple combo was back on deck at 2100 h, and the decision was made to abandon any further logging attempts in Hole U1466B. The drill string was pulled out of the hole, clearing the seafloor at 2250 h. Hole U1466B was completed at 1220 h on 26 October, officially ending operations at Site U1466.

Total recovery for Site U1466 was 243.8 m (75%) in Hole U1466A and 88.54 m (18%) in Hole U1466B. Of the total 106 cores recovered, 20 were full APC cores, 20 were half-length APC cores, 10 were XCB cores, and 56 were RCB cores.

Site U1467

Transit to Site U1467

The short transit from Site U1465 to Site U1467 was completed in 2 h at 8.5 kt. At 2045 h on 28 October 2015, the ship was under DP control over Site U1467. We prepared an APC/XCB BHA including a nonmagnetic drill collar for oriented piston coring and a MBR for eventual wireline logging and as insurance for freeing a stuck BHA.

Hole U1467A

Hole U1467A was spudded at 0055 h on 29 October 2015 with the bit positioned at 481 mbsl. Core 1H recovered 3.5 m and established a seafloor depth of 487 m. Oriented piston coring continued through Core 4H to 32.0 mbsf; a single formation temperature measurement (APCT-3) was made while taking Core 3H at 22.5 mbsf. Right from the start, the coring system was not behaving normally. Barrels were seating high and then dropping down while under 300–400 psi pressure; the resultant jarring impact caused the shear pins to shear and the barrels to fully stroke. To free the core barrels, 5000 lb of overpull was necessary. In an attempt to determine whether there was some sort of blockage or a broken flapper valve, an XCB core barrel was deployed. This barrel also landed high and also experienced an initial 5000 lb overpull. Convinced that something was wrong in the BHA, we decided to abandon the hole, recover the drill string, and inspect the coring assembly. The bit arrived back on the rig floor at 0900 h on 29 October. Upon inspection of the coring tools, the MBR, float valve, and landing shoulders were all determined to be in good shape, but further inspection determined that the XCB latch sleeve was damaged, which was why the wireline barrels were jamming upon deployment and recovery. The latch sub and sleeve were replaced. The drill string was deployed back to the seafloor, and Hole U1467B was spudded at 1430 h.

Hole U1467B

In Hole U1467, Core 1H recovered 3.46 m and established a water depth of 487 m. Oriented APC coring continued through Core 37H to 338 mbsf. Formation temperature measurements (APCT-3) were made while taking Cores 3H, 5H, 7H, and 9H (22.5, 41.5, 60.5, and 79.5 mbsf, respectively); however, all the temperature measurements appear to be erroneous. At 2100 h on 29 October 2015, after reaching refusal with the HLAPC (Core 42F at 361.4 mbsf), coring was suspended in order to test the MDHDS and Electronic RS (ERS) overshot system.

The MDHDS is being developed for use when deploying the temperature dual-pressure tool (T2P); however, it can also be used to deploy the Sediment Temperature Tool (SET), SET2, and sedi-

ment temperature/pressure tool (SETP). The ERS will also be useful for deploying future CORK thermistor strings. Both systems are deployed with the conductor cable or "wireline" that is used primarily for downhole logging. The MDHDS system was assembled and hung off at the rig floor, and the ERS was attached to the top of the MDHDS. The system was deployed into the hole using the wireline, but all communication with the ERS was lost and the tool had to be recovered back to the rig floor. Subsequent testing indicated that a component had failed in the ERS electronic module. This was subsequently repaired, and the tool was deployed back into the hole. During the descent, however, a concern was raised about the compatibility of the MDHDS/SET system with the standard MBR and float valve assembly in the deployed BHA. The MDHDS is designed to be deployed through a lockable float valve (LFV) and has been deployed in this manner on a previous expedition. In this case, a MBR was being run in lieu of a LFV because it provided another way to free up the drill string should it become stuck in the hole. The test was suspended, and after an assessment it appeared the MDHDS system was compatible. The SET tool being deployed was also compatible as long as the shear pins were not sheared in the SET tool, as would be the case when taking a normal temperature measurement. There was no plan to do this during the MDHDS test; however, there was some concern that if the shear pins accidentally sheared and the SET tool scoped out, it would have been impossible to recover it inside the BHA because the float valve flapper engages a square shoulder. Because of this potential risk to a high-value hole, the test was suspended and the tools were pulled out of the hole. The system was back at the rig floor just before 0300 h on 31 October.

Continuous oriented APC coring resumed and continued until 0615 h on 31 October, when Core 45H reached 389.9 mbsf. Core 45H achieved a full stroke, but at 100,000 lb overpull the barrel required drillover with the XCB core bit. Coring then continued using the HLAPC through Core 61F to 465.1 mbsf. Coring with the HLAPC was suspended when the last two cores each had 100,000 lb overpull and required drillover. At 1530 h, we switched to the XCB coring system. Coring continued through Core 77X to 617.2 mbsf. At that time, the assistant driller noted that he was getting high (10,000 lb) overpull when recovering the XCB core barrels. An HLAPC was deployed, and this barrel landed high. After pressuring up the drill string, the shear pins prematurely sheared at 400 psi (upon impact) after being pushed through the XCB double window latch sleeve. These were the same symptoms experienced earlier in Hole U1467A with the XCB latch sleeve. With the hole only 97 m from the desired total depth, a meeting was called with the Co-Chief Scientists and technical personnel to discuss options. We decided to stop coring Hole U1467B, recover/repair the BHA, and modify the plan for Hole U1467C. APC coring to 200 m was already planned for Hole U1467C, so we planned to add drilling to ~610 m, XCB coring to the target depth, and wireline logging.

Hole U1467C

The drill string was recovered, the XCB latch sleeve was replaced, the ship was offset 20 m north of Hole U1467B, and Hole U1467C was started at 1620 h on 1 November 2015. Core 1H established a seafloor depth of 487 m. By 0000 h on 1 November, we extended coring to 111.2 mbsf (Cores 2H–12H). Coring continued the next day using the APC coring system through Core 22H to 198.7 mbsf. The XCB was then used to drill ahead to 325.8 mbsf before a center bit had to be deployed. The XCB with center bit advanced to 578.6 mbsf, and the center bit was recovered via wireline. At 2030 h on 2 November, XCB coring was initiated, and it continued through Core 37X to 714.0 mbsf, the Environmental Protection and Safety Panel–approved depth for the site. A mud sweep was circulated to clean the hole one final time, and the drill string was recovered and spaced out for wireline logging with the bit placed at 101.8 mbsf.

At 1400 h on 3 November, wireline logging began. As the triple combo tool string was being made up, the rig crew noted backflow of water coming from the tool joint at the rig floor. The triple combo tool string was removed so we could add heavy mud in the drill pipe to prevent further backflow. While attempting to reinsert the tool string, a fiberglass connection on the bottom of the magnetic susceptibility tool broke off and the connected LFV go-devil fell through the drill string. This was not a significant concern because these go-devils were free-fall deployed in the past. After manufacturing a new fiberglass connector sleeve and changing out the magnetic susceptibility sonde with the onboard spare, the triple combo tool string was redeployed. The tool string was run to the total depth of the hole (714 mbsf) without any problems. After completing the first logging run, it was determined that the borehole diameter was too large (>17 inches) for collecting useful data with the FMS-sonic and VSI tool strings. Therefore, the triple combo tool string was recovered and the tools were rigged down. We then decided to drill a dedicated logging hole utilizing a 9⅞ inch tricone drill bit after completing one additional APC hole to ~200 mbsf. The drill string was pulled clear of the seafloor at 0010 h on 4 November.

Hole U1467D

The top drive was picked up, the drill string was spaced out to 1.5 mbsf, and coring in Hole U1467D started at 0130 h on 4 November 2015. This space-out was used to spread out the breaks between cores in adjacent holes to enable the recovery of a complete section for paleoceanographic studies. APC coring (not orientated) continued through Core 22H to 201.0 mbsf. The drill string was then recovered on ship with the bit arriving on the rig floor at 1325 h on 4 November.

Hole U1467E

Our final operation at Site U1467 was to drill a dedicated logging hole. The ship was offset 20 m east of Hole U1467A. The BHA was changed to a noncoring drill bit, and the drill string was lowered back to the seafloor. The top drive was picked up, and the drill string was spaced out using an offset seafloor depth of 498.4 mbsf taken from Hole U1467A. Drilling in Hole U1467E started at 1710 h on 4 November 2015. This dedicated logging hole was drilled without coring to 714.0 mbsf in 25 h. A mud sweep was circulated to clear cuttings out of the hole, and two wireline runs were made to release the bit at the bottom of the hole and reverse shift the MBR sleeve. Because of the stability seen in the previous holes at this site and while drilling the hole, we decided that a wiper trip was not necessary and there was no need to displace the hole with heavy mud. The drill string was raised up the hole, and the end of the pipe was placed at 98.6 mbsf. We started rigging up for wireline logging at 2230 h on 5 November. The triple combo was run into the hole and reached the total depth at 714.0 mbsf. Caliper logs from this deployment indicated a hole diameter of 11–17 inches. The triple combo tool string was recovered and rigged down by 0600 h 6 November. Taking advantage of daylight and following the marine mammal protection protocol, the VSP experiment was conducted next. The VSI tool was able to reach ~684 mbsf or ~30 m off bottom, apparently because of fill in the borehole, and data were col-

lected up from there. A very good signal was received at each VSP station, thus providing the necessary information for an accurate time-depth conversion for comparison of seismic and downhole (core and logging) data. The FMS-sonic tool string was deployed at 1200 h on 6 November and reached 664 mbsf, where it stopped because of further fill at the bottom of the borehole. One of the four FMS pads was not recording accurate data because it was covered with grease, which prevented good contact between the pad and the borehole wall. After the FMS-sonic data were obtained, the tool string was recovered and rigged down by 1900 h on 6 November.

The rig floor was secured from logging operations by 2000 h, and by 2015 h the upper guide horn was raised in preparation for pressure testing the new fiber optics–based subsea camera system. The camera was deployed down the drill string to the seafloor. This system was installed prior to the last expedition (356); however, because all of the shallow-water operating depths during Expedition 356, the system has only been tested to ~90 mbrf. We needed to test this system prior to the next expedition (360), which will require multiple deployments of the system for making bit changes in the course of drilling a single 1500 m RCB hole into gabbro in ~700 m of water. Testing the camera system at Site U1467 (473 m) indicated that the system is 100% operational. The camera was back on board and secured within 1 h, and the drill string was pulled clear of the seafloor and recovered to the ship. After the seafloor positioning beacon was recovered and the ship was secured for transit, we began the ~13.6 nmi transit to Site U1468 at 0024 h on 7 November.

Total recovery for Site U1467 was 31.49 m (98%) in Hole U1467A, 560.4 m (91%) in Hole U1466B, 266.15 m (80%) in Hole U1467C, and 203.7 (102%) in Hole U1467D. Of the total 137 cores recovered, 86 were full APC cores, 21 were half-length APC cores, and 30 were XCB cores.

Site U1468

Transit to Site U1468

The 13.6 nmi transit from Site U1467 to Site U1468 required only 1.5 h, and by 0232 h on 7 November 2015, the ship arrived over the site coordinates and switched to the DP system. Soon after, the rig crew began assembling the APC/XCB BHA. A positioning beacon was deployed, and the drill string was lowered to the seafloor.

Hole U1468A

For Site U1468, we obtained an extension for the total EPSP approved penetration depth to 1000 mbsf to ensure the achievement of the site's main scientific objective of coring thorough the Oligocene/Miocene boundary. Ultimately, coring with the XCB system terminated with Core 359-U1468A-111X at a total depth of 874.7 mbsf when the biostratigraphers confirmed the Oligocene age of the recovered core.

Hole U1468A was spudded at 0830 h on 7 November 2015, establishing a seafloor depth of 521.5 m. Nonoriented APC coring continued through Core 13H to 112.6 mbsf. Coring using the HLAPC followed until APC refusal on Core 38F at 225.6 mbsf. Coring with the XCB coring system continued. Hole stability was maintained throughout by circulating 20 bbl high-viscosity mud sweeps every other core. This resulted in little or no fill on connections, normal drilling torque, and no overpull or drag with the drill string. After laying out the final core barrel, the bit was raised to 795.5 mbsf and the top drive was set back. The drill string was pulled out of the hole, clearing the seafloor at 2215 h, and the bit arrived on the rig floor at 2400 h on 11 November.

Hole U1468B

We offset the ship 20 m east of Hole U1468A and started assembling the tricone drill bit with a MBR to drill the dedicated logging hole. An extra stand of 8¼ inch drill collars was added to the existing drilling BHA to place the bit at ~130 mbsf or slightly deeper to allow the end of the pipe to be below a potentially problematic sand package. We lowered the bit to the seafloor and started drilling without coring in Hole U1468B at 0810 h on 12 November 2015. During the course of drilling the dedicated logging hole, the driller noted elevated drilling torque and hole cleaning problems at 131.7 mbsf. At 1345 h, we spent nearly 2 h conducting a wiper trip by raising the bit to 43.5 mbsf and then running it back to the bottom of the hole. At 1530 h, drilling resumed and continued without incident until the bit reached a total depth of 874.7 mbsf at 2030 h on 12 November. We circulated a high-viscosity mud sweep, released the bit in the bottom of the hole, and at 0115 h on 13 November the end of the pipe had been positioned at 140.5 mbsf in preparation for wireline logging. We rigged up the triple combo tool string and ran it into Hole U1468B at 0240 h. The tool string reached ~835 mbsf, where it tagged bottom, indicating ~40 m of infill in the hole. A short pass logged from the bottom of the hole up to ~735 mbsf showed reasonable hole diameter. The tool string was run back to total depth, and the main pass started at 835 mbsf, recording gamma radiation, density, porosity, electrical resistivity, and magnetic susceptibility. Borehole diameter varied smoothly, ranging from ~17 to 12 inches, until a narrow section (<6 inches) was encountered at ~465 mbsf. Significant overpull was required to continue pulling the tool string up to ~290 mbsf, suggesting the borehole had deteriorated in this interval. Above ~290 mbsf, hole diameter increased, and the main pass continued up to the base of the drill pipe at 140 mbsf. Logging data were recorded continually throughout the main pass with the triple combo tool string, but further logging operations could not be carried out because of the state of the borehole. The tool string was returned to the rig floor and rigged down, and logging operations in Hole U1468B were completed by 0915 h on 13 November.

After rigging down from wireline logging, the pipe was pulled out of the hole, clearing the seafloor at 0935 h. Hole U1468B ended when the bit arrived back on the rig floor at 1125 h.

Site U1469

Transit to Site U1469

Site U1469 was only a 4 nmi transit from Site U1468, so the DP system was used to move the ship to the new coordinates. During the transit, the drill string was recovered and a new RCB BHA was assembled and lowered to the seafloor.

Hole U1469A

We tagged the seafloor with the drill bit and established a seafloor depth of 427 mbsl. RCB coring in Hole U1469A started at 1825 h on 13 November 2015. Coring was extremely challenging because of the loosely cemented carbonate sand formation. High torque and overpull occurred when pulling the bit off the bottom of the hole. However, we were able to penetrate to 122.1 mbsf before making a wiper trip up. At 0245 h on 14 November, with the bit back on bottom again, RCB coring continued, but hole conditions continued to be problematic. We suspected that drilling had encountered a zone of high permeability within the buried reefal carbonate rocks, causing a loss of circulation uphole that was required to clean the drilled cuttings off the hole. At 0630 h, we decided to abandon Hole

U1469A and try a new hole after offsetting the ship 40 m west. The drill string was pulled clear of the seafloor at 0810 h on 14 November, ending Hole U1469A.

Hole U1469B

Drilling in Hole U1469B started at 0850 h on 14 November 2015 after using the drill bit to tag the seafloor (427 mbsl). Hole U1469B was drilled without coring to 122 mbsf without incident, and it appeared that this hole would be considerably better than the previous hole. This optimism was short lived, as the same hole cleaning problems occurred again after cutting just three RCB cores to 151.4 mbsf. Convinced that the hole could not be deepened any further because of lost circulation, Hole U1469B was also abandoned. The drill string was retrieved back on board, the positioning beacon was picked up, the thrusters were raised, and we started the transit to the next site (U1470) at 2045 h on 14 November.

Site U1470

Transit to Site U1470 and Hole U1470A

After a 17.8 nm transit from Site U1469, we arrived at Site U1470 at 2306 h on 14 November 2015. We lowered the thrusters and hydrophones and switched to DP mode. We assembled an APC/XCB BHA and lowered it to the seafloor. After establishing a PDR depth of 367.0 mbrf, the first APC core barrel was deployed, recovering just a water core. The bit was lowered to 403.5 mbrf, and a second APC core barrel was deployed, recovering 2.17 m of core and establishing a seafloor depth of 410.8 mbrf (400.3 mbsl). APC coring continued through Core 17H to 148.4 mbsf before a lithologic change in the formation to hard reef material led us to switch to the XCB coring system. Cores 18X and 19X had very poor recovery (0.17 and 0 m, respectively). The material was hard but very friable, and rock pieces would break and jam in the core catcher. The HLAPC system was deployed for Cores 20F and 21F, which recovered 1.76 and 1.90 m, respectively. The improved recovery was welcome, but the time required to deepen the hole was a concern. We therefore attempted another XCB core, this time using an "extended" XCB cutting shoe that placed the cutting structure even further ahead of the main drill bit. Recovery with the extended XCB shoe was not better, and because of the higher risk associated with the longer extension of the XCB shoe, it was not run again. Coring was terminated after Core 24X at 190.0 mbsf in favor of starting a new hole using the RCB system. The drill string was pulled clear of the seafloor at 1910 h, and the bit arrived on the rig floor at 2055 h on 15 November, ending Hole U1470A.

Hole U1470B

By 2400 h on 15 November 2015, we finished making up an RCB BHA and spacing out the core barrels in preparation for lowering the drill string back to the seafloor. The ship was offset 20 m west of Hole U1470A, and Hole U1470B was started at 0230 h on 16 November. An offset seafloor depth of 410.8 mbsl was utilized from adjacent Hole U1470A. Drilling proceeded to 150.0 mbsf before the formation stiffened up enough to warrant deploying a RCB center bit. Drilling continued to 168.9 mbsf, and at 0930 h on 16 November, RCB coring was initiated. Only a single core was cut to 178.6 mbsf before high torque and overpull forced the need for a wiper trip. The drill string was pulled back to 90.2 mbsf, placing the top of the tapered drill collar above seafloor before drilling parameters returned to normal. The hole was washed/reamed to total depth, and at 1345 h on 16 November, RCB coring resumed. Cores 3R–8R to 227.1 mbsf were cut before high torque and overpull indicated cuttings again were not being properly flushed from the hole, perhaps aggravated by zones of lost circulation within the cavernous reefal limestone. Another 3 h wiper trip was made, and at 2030 h, RCB coring restarted. Coring continued through Core 19R to 343.7 mbsf, and coring was terminated shortly after 0400 h because of need to wireline log the hole. Downhole logging was considered to be of greater importance than deepening a challenging hole. The shifting tool was run in the hole; however, there were problems shifting the MBR sleeve to release the bit. Repeatedly jarring on the sleeve with the wireline jars eventually knocked the sleeve loose, and the bit was released at 0530 h. The sleeve was reverse shifted without incident, and the drill string was pulled to logging depth at 100.2 mbsf.

Because of the uncertainty about hole conditions and stability, a single logging run was planned with a tool string designed to measure the highest priority data (gamma ray, sonic velocity, electrical resistivity, and borehole diameter). Rig-up for wireline logging began at 0730 h on 17 November. We ran this sonic-resistivity tool string into the hole without installing the nuclear source, but unfortunately, resistance was encountered almost immediately as the tools reached 10 m below the end of the pipe and we were not able to securely pass a collapsing section of the borehole just 52 m below the end of the pipe at 100.2 mbsf. The winch operator eventually pulled the tool string back into the pipe and up to the rig floor, where it was rigged down, and logging operations in Hole U1470B were concluded by 1215 h on 17 November. The drill string was pulled clear of the seafloor at 1230 h, and the drill string was recovered back onboard the ship with the end of the pipe clearing the rig floor rotary table at 1355 h. The positioning beacon was recovered on deck at 1410 h. Thrusters were pulled, and the rig was secured for transit to the next site.

Site U1471

Transit to Site U1471

At 1448 h on 17 November 2015, we started the transit to Site U1471. We covered the short 9.1 nmi distance in 1 h, arriving over the site coordinates at 1548 h. Thrusters were lowered, and heading control was switched over to DP at 1636 h. This process took a little longer than usual because the captain had to turn the ship around and change heading prior to getting back on the location coordinates. The APC/XCB BHA was built, and at 1707 h we deployed the same positioning beacon recovered from Site U1470. We lowered the drill string to the seafloor, picked up the top drive, and spaced out the bit at 414.6 mbsl.

Hole U1471A

We started Hole U1471A at 2050 h on 17 November 2015 by cutting Core 1H and recovering 4.62 m of sediment, thus establishing a seafloor depth of 419.5 mbsl. Uninterrupted oriented APC coring continued through Core 32H to 295.1 mbsf, where high overpull and an incomplete stroke with the APC system led us to switch to the HLAPC coring system. We continued to core with the HLAPC system through Core 37F to 318.6 mbsf. All HLAPC cores were incomplete strokes, and penetration continually decreased. The high content of sand in the formation caused the flapper valve in the core barrel to lock up, leading to occasional misfires of the APC and HLAPC coring systems. We therefore switched to XCB coring and continued through Core 44X to 384.0 mbsf, but because of poor recovery, we attempted another HLAPC core. Core 45F recovered only 0.51 m, indicating the formation had become more lithified and therefore too hard for piston coring. In addition, the driller noticed that the wash pipe assembly on top of the top drive

was seriously leaking, leading to an impromptu wiper trip to condition the hole and position the tapered drill collar above the seafloor. The standpipe assembly was replaced, and the bit was washed back to bottom. At 0030 h on 19 November, we resumed XCB coring and continued through Core 59X to 515.1 mbsf. Recovery was extremely poor, averaging just 9% (2%–27%). Only 2 of 14 cores were recovered with more than 1 m of sediment. Cores 60F and 61F were HLAPC cores in an attempt to improve recovery. These cores recovered 1.91 and 1.16 m, respectively. It was deemed too risky to drill out the rat hole with the pipe open ended and no core barrel in place. Core 63F was the final HLAPC core attempted, and it recovered 1.74 m. Continuous XCB coring began with Core 64X at 531.5 mbsf and continued through Core 82X to 685.1 mbsf. XCB coring the interbedded hard/soft material was difficult, and recovery was marginal because the lithified limestone jammed in the XCB cutting shoe and the softer material washed away. Although hole conditions remained good throughout and core recovery improved significantly over the last 100 m interval (averaging 44.5% and ranging between 19% and 88%), we decided to stop coring before reaching our depth and age objectives because of the slow rate of penetration (<8 m/h) and in favor of reaching our target depth in an RCB hole to be drilled after completing two more APC holes. Therefore, at 2300 h on 20 November, we stopped coring Hole U1471A and pulled the drill string back, clearing the seafloor.

Holes U1471B and U1471C

After offsetting the ship 20 m west, we started coring Hole U1471B at 0440 h on 21 November 2015. The mudline core recovered 6.62 m, but the core liner was shattered and much of the material was lost. Therefore, we started Hole U1471C another 20 m west at 0555 h. Core 1H recovered 7.85 m and established a seafloor depth of 419.3 mbsl. APC coring continued through Core 19H to a total depth of 178.8 mbsf. Successful temperature measurements were made using the APCT-3 at 26.8, 45.8, 64.8, 83.8, and 169.3 mbsf and were 11.4°C, 11.6°C, 12°C, 12.2°C, and 13.5°C, respectively. The downhole temperature trend defined a very low temperature gradient of 15.3°C/km. In addition, as a result of one APCT-3 cutting shoe arriving late to the rig floor, the shoe was inadvertently installed without a core catcher, resulting in Core 5H (36.3–45.8 mbsf) being recovered empty. The drill string was pulled clear of the seafloor at 2000 h, ending Hole U1471C.

Hole U1471D

The ship was moved another 20 m west, and we initiated Hole U1471D at 2105 h on 21 November 2015. For this hole, the bit was advanced to 1 mbsf before taking the first core to optimally position the core breaks for a reliable stratigraphic correlation. Cores 2H–7H were recovered to 59.0 mbsf. The last two cores were not oriented.

Testing of the Motion Decoupled Hydraulic Delivery System

After completing coring operations in Hole U1471D, the planned test of the MDHDS took place with mixed results. Handling of the tool at the rig floor was vastly improved, reducing deployment time from the 1.5 h required during the first test at Site U1467 to 30 min. The ERS was opened and closed numerous times and worked flawlessly each time. The SET2 functioned as designed and successfully recorded data although it was not inserted into the formation because the MDHDS became stuck in the LFV. A round trip of the drill string was completed, and the bit cleared the rig floor at 0545 h on 22 November 2015, ending Hole U1471D.

The MDHDS tool was removed without incident at the rig floor, and the LFV was discovered packed with sand. It appeared that entrained sand was restricting removal of the MDHDS tool downhole and was flushed from the system during the pipe trip, which also explained several unusual piston core sequences where the pressure profile was atypical.

Hole U1471E

After making up a new RCB coring bit with a MBR and a four-stand BHA, the drill string was once again lowered to the seafloor. The ship was offset another 20 m west, and at 1110 h on 22 November 2015, we started drilling Hole U1471E. Our initial goal was to drill this hole to ~610 mbsf and then continuously RCB core to ~950 mbsf. Once coring operations were completed, downhole logging would follow with the three suites of wireline tools: the triple combo, FMS-sonic, and VSI tool strings. By midnight on Sunday, 22 November, Hole U1471E was drilled to 421.4 mbsf. Drilling ahead continued to 596.3 mbsf. Several deployments of the RCB bit deplugger were required to clear debris from the float valve flapper, resulting in drill string backflow. Drilling was halted because of the slow penetration rate and a concern for possible damage to the RCB center bit in the hard formation. The center bit was recovered via wireline, and an RCB core barrel was deployed. At 1045 h on 23 November, RCB coring was initiated. Coring continued through Core 44R to 1003.7 mbsf. The original EPSP-approved depth was 950 mbsf, but because of concerns about the reliability of the velocity depth model used, we requested to deepen the hole and received a depth extension approval from the EPSP to 1050 mbsf to ensure penetration to the target seismic reflector. This also provided a small amount of rat hole below the target depth, which allowed for logging data across the target facies. Additional depth would also accommodate any cuttings that might settle out of the hole annulus or cave-in during subsequent logging runs. Core recovery was adequate for most of the hole but continually improved with depth. Overall recovery for the hole was 42%; however, this increased to an average of 57% over the last 100 m (37%–89%). Toward the end of the cored interval, multiple deployments of the bit deplugger were made because of excessive backflow during drill string connections. Although these were unsuccessful, the coring process was not impacted. This suggested that the spring in the float valve was either broken or weakened and no longer able to fully seal the end of the pipe. There were no indications of hole stability issues through the course of drilling/coring in the hole. There was no filling identified on bottom between connections, no elevated drilling torque noted, and no wiper trips required during the course of the drilling/coring effort. As a result, the hole was not displaced with heavy mud and there was no prelogging wiper trip conducted in preparation for wireline logging.

Downhole logging

The RCB bit was released at the bottom of the hole, and the pipe was pulled up to a logging depth of 99.7 mbsf. The triple combo tool string was rigged up and deployed in the hole at 0545 h on 26 November 2015. A downlog was completed to 1003.7 mbsf (the total drilled depth), a short repeat pass was logged, and the main pass of the tool string was recorded from the bottom of the hole up past the seafloor. Borehole diameter in the upper section of the hole was at the maximum reach of the caliper arm (~17 inches), but much of the lower section was in gauge. The VSI tool string was rigged up next and run into the hole at 1245 h for a VSP experiment. The tool

string reached an unpassable obstruction at ~615 mbsf, where the borehole had been observed to be very narrow during the triple combo run. Therefore, only shallow VSP stations could be reached; clear waveforms were recorded at three depth stations between 233 and 606 mbsf. The VSI tool string was run one more time into the hole to attempt one deeper station, but on this second attempt, an obstruction was encountered at 454 mbsf, another narrow section observed during the triple combo run. A third logging run was made with a sonic tool string, measuring gamma ray and sonic velocity, with the aim of recording velocity data in the available open hole interval. The FMS tool that is usually combined with the sonic tool has a maximum caliper reach of ~15 inches and would not have made contact with the borehole walls in sections where the diameter exceeded 17 inches; thus, it was not included in the third logging tool string. The sonic tool string was run into the hole at 1620 h, and a downlog was recorded down to 454 mbsf, the same location where an obstruction blocked passage of the VSI tool string. After several unsuccessful attempts to pass the blocked section, the sonic tool string was pulled up from 454 mbsf to record a main pass through the shallow section of open hole up to the seafloor. The sonic tool string was rigged down, and logging operations for Hole U1471E and Expedition 359 were completed by 1940 h. The drill string was pulled on board and the seafloor-positioning beacon was recovered as the ship began to move using the DP system to the next site (U1472) at 2120 h on 26 November.

Site U1472

Hole U1472A

With limited time available because we needed to depart for Malé no later than 0200 h on Saturday 28 November 2015, we decided to move to Site U1472 and core one final APC hole as deep as possible with the remaining expedition time. Site U1472 was originally a primary drill site for the expedition, but it was downgraded to alternate status as a result of a higher scientific priority to core at Site U1471.

An APC/XCB BHA was made up as the ship moved 4.1 nmi in DP mode to Site U1472. The drill string was run to the seafloor, and Hole U1472A was started at 0415 h. We cut and recovered Cores 1H–34F from 0 to 251.9 mbsf, recovering 233.75 m of core (93%). None of the cores were oriented. The last core of Expedition 359 arrived on deck at 2015 h, and the final drill string trip of the expedition began. All drilling equipment was secured. The seafloor-positioning beacon was released, but it did not come to the surface. Thrusters were pulled, and at 0212 h on 28 November we began the transit to Malé.

Transit to Malé

The transit ended at 0718 h on 28 November 2015, and at 0720 h the pilot came on board. The anchor was ultimately dropped in the Malé anchorage at 0806 h. As part of the Republic of Maldives drilling clearance, the ship was required to check in at Malé. Two observers were discharged, and the agent took everyone's passports ashore again to clear out of Maldivian waters. In addition, Maldivian Minister of Fisheries and Agriculture came onboard for a meeting with the Co-Chief Scientists, who gave him a briefing on the expedition results. Passports were returned, and the pilot came aboard at 1430 h. At 1448 h on 28 November, the anchor was weighed, and at 1512 h, the pilot departed the ship, marking the beginning of the sea transit to Colombo, Sri Lanka.

Transit to Colombo

The transit to Colombo was quick and uneventful. Shipboard clocks were advanced 30 min at 1400 h on 29 November 2015. Although the pilot was scheduled for 0700 h, it was not until 1013 h that the pilot actually boarded the ship. The first line went ashore at the Unity Container Terminal berth at Colombo (Sri Lanka) at 1100 h on 30 November, officially ending Expedition 359.

References

Anselmetti, F.S., Eberli, G.P. and Ding, Z.-D. (2000) From the Great Bahama Bank into the Straits of Florida: a margin architecture controlled by sea-level fluctuations and ocean currents Bull. Geol. Soc. America, 112, 829-844.

Arthur, M.A., and Schlanger, S.O., 1979. Cretaceous "oceanic anoxic events" as causal factors in development of reef-reservoired giant oil fields. *AAPG Bulletin,* 63:870–885.

Aubert, O., and Droxler, A.W., 1992. General Cenozoic evolution of the Maldives carbonate system (equatorial Indian Ocean). *Bulletin Des Centres de Recherches Exploration-Production Elf-Aquitaine,* 16(1):113–136.

Aubert, O., and Droxler, A.W., 1996. Seismic stratigraphy and depositional signatures of the Maldive carbonate system (Indian Ocean). *Marine and Petroleum Geology*, 13(5):503–536. **http://dx.doi.org/10.1016/0264-8172(96)00008-6**

Backman, J., Duncan, R.A., et al., 1988. *Proceedings of the Ocean Drilling Program, Initial Reports,* 115: College Station, TX (Ocean Drilling Program). **http://dx.doi.org/10.2973/odp.proc.ir.115.1988**

Baker, P.A., Gieskes, J.M. and Elderfield, H. (1982) Diagenesis of carbonates in deep-sea sediments; evidence from Sr/Ca ratios and interstitial dissolved Sr2+ data. J. Sed. Pet., 52, 71-82

Belopolsky, A.V., and Droxler, A.W., 2004a. Seismic expressions and interpretation of carbonate sequences: the Maldives platform, equatorial Indian Ocean. *AAPG Studies in Geology,* 49. **http://archives.datapages.com/data/specpubs/study49/images/st49.pdf**

Belopolsky, A.V. and Droxler, A.W., 2004b. Seismic expressions of prograding carbonate bank margins: middle Miocene, Maldives, Indian Ocean. *In* Eberli, G.P., Masaferro, J.L., and Sarg, J.F. (Eds.), *Seismic Imaging of Carbonate Reservoirs and Systems.* AAPG Memoir, 81:267–290. **http://archives.datapages.com/data/specpubs/memoir81/CHAPTER12/CHAPTER12.HTM**

Betzler, C., Fürstenau, J., Lüdmann, T., Hübscher, C., Lindhorst, S., Paul, A., Reijmer, J.J.G., and Droxler, A.W., 2013a. Sea-level and ocean-current control on carbonate-platform growth, Maldives, Indian Ocean. *Basin Research*, 25(2):172–196. **http://dx.doi.org/10.1111/j.1365-2117.2012.00554.x**

Betzler, C., Hübscher, C., Lindhorst, S., Reijmer, J.J.G., Römer, M., Droxler, A.W., Fürstenau, J., and Lüdmann, T., 2009. Monsoon-induced partial carbonate platform drowning (Maldives, Indian Ocean). *Geology,* 37(10):867–870. **http://dx.doi.org/10.1130/G25702A.1**

Betzler, C., Kroon, D., and Reijmer, J.J.G., 2000. Synchroneity of major late Neogene sea level fluctuations and paleoceanographically controlled changes as recorded by two carbonate platforms. *Paleoceanography,* 15(6):722–730. **http://dx.doi.org/10.1029/1999PA000481**

Betzler, C., Lüdmann, T., Hübscher, C., and Fürstenau, J., 2013b. Current and sea-level signals in periplatform ooze (Neogene, Maldives, Indian Ocean). *Sedimentary Geology*, 290:126–137. **http://dx.doi.org/10.1016/j.sedgeo.2013.03.011**

Betzler, C., Lindhorst, S., Lüdmann, T., Weiss, B., Wunsch, M., and Braga, J.C., 2015. The leaking bucket of a Maldives atoll: implications for the understanding of carbonate platform drowning. *Marine Geology,* 366:16–33. **http://dx.doi.org/10.1016/j.margeo.2015.04.009**

Ciarapica, G., and Passeri, L., 1993. An overview of the Maldivian coral reefs in Felidu and North Malé atoll (Indian Ocean): platform drowning by ecological crises. *Facies*, 28(1):33–65. **http://dx.doi.org/10.1007/BF02539727**

Clift, P.D., Hodges, K.V., Heslop, D., Hannigan, R., Long, H.V., and Calves, G., 2008. Correlation of Himalayan exhumation rates and Asian monsoon intensity. *Nature Geoscience,* 1(12):875–880. **http://dx.doi.org/10.1038/ngeo351**

Dickens, G.R., and Owen, R.M., 1994. Late Miocene–early Pliocene manganese redirection in the central Indian Ocean: expansion of the intermediate water oxygen minimum zone. *Paleoceanography,* 9(1):169–181. **http://dx.doi.org/10.1029/93PA02699**

Droxler, A.W., Haddad, G.A., Mucciarone, D.A., and Cullen, J.L., 1990. Pliocene–Pleistocene aragonite cyclic variations in Holes 714A and 716B (The Maldives) compared with Hole 633A (The Bahamas): records of climate-induced $CaCO_3$ preservation at intermediate water depths. *In* Duncan, R.A., Backman, J., Peterson, L.C., et al., *Proceedings of the Ocean Drilling Program, Scientific Results,* 115: College Station, TX (Ocean Drilling Program), 539–577. **http://dx.doi.org/10.2973/odp.proc.sr.115.179.1990**

Duncan, R.A., and Hargraves, R.B., 1990. $^{40}Ar/^{39}Ar$ geochronology of basement rocks from the Mascarene Plateau, the Chagos Bank, and the Maldives Ridge. *In* Duncan, R. A., Backman, J., Peterson, L.C., et al., *Proceedings of the Ocean Drilling Program, Scientific Results,* 115: College Station, TX (Ocean Drilling Program), 43–51. **http://dx.doi.org/10.2973/odp.proc.sr.115.141.1990**

Eberli, G.P., 1991. Growth and demise of isolated carbonate platforms: Bahamian controversies. *In* Müller, D., McKenzie, J., and Weissert, H. (Eds.), *Controversies in Modern Geology: Evolution of Geological Theories in Sedimentology, Earth History and Tectonics:* London (Academic Press), 231–248.

Eberli, G.P., Anselmetti, F.S., Isern, A.R., and Delius, H., 2010. Timing of changes in sea-level and currents along Miocene platforms on the Marion Plateau, Australia. *In* Morgan, W.A., George, A.D., Harris, P.M., Kupecz, J.A., and Sarg, J.F., *Cenozoic Carbonate Systems of Australasia.* Special Publication - SEPM (Society for Sedimentary Geology), 95:219–242. **http://www.eawag.ch/forschung/surf/publikationen/2010/2010_eberli.pdf**

Eberli, G.P., Anselmetti, F.S., Kroon, D., Sato, T., and Wright, J.D., 2002. The chronostratigraphic significance of seismic reflections along the Bahamas Transect. *Marine Geology,* 185(1–2):1–17. **http://dx.doi.org/10.1016/S0025-3227(01)00287-0**

Faugères, J.-C., Stow, D.A.V., Imbert, P., and Viana, A., 1999. Seismic features diagnostic of contourite drifts. *Marine Geology*, 162(1):1–38. **http://dx.doi.org/10.1016/S0025-3227(99)00068-7**

Fürstenau, J., Lindhorst, S., Betzler, C., and Hübscher, C., 2010. Submerged reef terraces of the Maldives (Indian Ocean). *Geo-Marine Letters*, 30(5):511–515. **http://dx.doi.org/10.1007/s00367-009-0174-2**

Gischler, E., 2006. Sedimentation on Rasdhoo and Ari atolls, Maldives, Indian Ocean. *Facies*, 52(3):341–360. **http://dx.doi.org/10.1007/s10347-005-0031-3**

Gischler, E., Hudson, J.H., and Pisera, A., 2008. Late Quaternary reef growth and sea level in the Maldives (Indian Ocean). *Marine Geology*, 250(1–2):104–113. **http://dx.doi.org/10.1016/j.margeo.2008.01.004**

Gupta, A.K., Yuvarja, A., Prakasam, M., Clemens, S.C., and Velu, A., 2015. Evolution of the South Asian monsoon wind system since the late middle Miocene. *Palaeogeography, Palaeoclimatology, Palaeoecology,* 438:160–167. **http://dx.doi.org/10.1016/j.palaeo.2015.08.006**

Hallock, P., and Schlager, W., 1986. Nutrient excess and the demise of coral reefs and carbonate platforms. *Palaios,* 1(4):389–398. **http://dx.doi.org/10.2307/3514476**

Isern, A.R., Anselmetti, F.S., and Blum, P., 2004. A Neogene carbonate platform, slope, and shelf edifice shaped by sea level and ocean currents, Marion Plateau (northeast Australia). *In* Eberli, G.P., Masaferro, J.L., and Sarg, J.F. (Eds.), *Seismic Imaging of Carbonate Reservoirs and Systems.* AAPG Memoir, 81:291–307. **http://archives.datapages.com/data/specpubs/memoir81/CHAPTER13/CHAPTER13.HTM**

John, C.M., and Mutti, M., 2005. Relative control of paleoceanography, climate, and eustasy over heterozoan carbonates: a perspective from slope sediments of the Marion Plateau (ODP Leg 194). *Journal of Sedimentary Research,* 75(2):216–230. **http://dx.doi.org/10.2110/jsr.2005.017**

Kroon, D., Steens, T., and Troelstra, S.R., 1991. Onset of monsoonal related upwelling in the western Arabian Sea as revealed by planktonic foraminifers. *In* Prell, W.L., Niitsuma, N., et al., *Proceedings of the Ocean Drilling Program, Scientific Results,* 117: College Station, TX (Ocean Drilling Program), 257–263. **http://dx.doi.org/10.2973/odp.proc.sr.117.126.1991**

Lüdmann, T., Kalvelage, C., Betzler, C., Fürstenau, J., and Hübscher, C., 2013. The Maldives, a giant isolated carbonate platform dominated by bottom currents. *Marine and Petroleum Geology*, 43:326–340. **http://dx.doi.org/10.1016/j.marpetgeo.2013.01.004**

Malone, M.J., Baker, P.A., Burns, S.J., and Swart, P.K., 1990. Geochemistry of periplatform carbonate sediments, Leg 115, Site 716 (Maldives Archipelago, Indian Ocean). *In* Duncan, R.A., Backman, J., Peterson, L.C., et al., *Proceedings of the Ocean Drilling Program, Scientific Results,* 115: College Station, TX (Ocean Drilling Program), 647–659. **http://dx.doi.org/10.2973/odp.proc.sr.115.184.1990**

Malone, M.J., Slowey, N.C. and Henderson, G.M. (2001) Early diagenesis of shallow-water periplatform carbonate sediments, leeward margin, Great Bahama Bank (Ocean Drilling Progr.Leg 166) Bull. Geol. Soc. America, 113, 881-894.

Philip, J., and Schlager, W., 1990. Cretaceous carbonate platforms. *In* Ginsburg, R.N., and Beaudoin, B. (Eds.), *Nato Science Series C* (Volume 304): *Cretaceous Resources, Events and Rhythms: Background and Plans for Research:* Dordrecht, The Netherlands (Springer), 173.

Prell, W.L., Murray, D.W., Clemens, S.C., and Anderson, D.M., 1992. Evolution and variability of the Indian Ocean summer monsoon: evidence from the western Arabian Sea drilling program. *In* Duncan, R.A., Rea, D.K., Kidd, R.B., von Rad, U., and Weissel, J.K. (Eds.), *Synthesis of Results from Scientific Drilling in the Indian Ocean.* Geophysical Monograph, 70:447–469. **http://dx.doi.org/10.1029/GM070p0447**

Preu, C., and Engelbrecht, C., 1991. Patterns and processes shaping the present morphodynamics of coral reef islands—case study from the North-Male atoll, Maldives (Indian Ocean). *In* Brückner, H., and Radtke, U. (Eds.), *From the North Sea to the Indian Ocean*: Stuttgart, Germany (Franz Steiner), 209–220.

Purdy, E.G., and Bertram, G.T., 1993. *Carbonate Concepts from the Maldives, Indian Ocean.* AAPG Studies in Geology, 34.

Rea, D.K., 1992. Delivery of Himalayan sediment to the northern Indian Ocean and its relation to global climate, sea level, uplift, and seawater strontium. *In* Duncan, R.A., Rea, D.K., Kidd, R.B., von Rad, U., and Weissel, J.K. (Eds.), *Synthesis of Results from Scientific Drilling in the Indian Ocean.* Geophysical Monograph, 70:387–402. **http://dx.doi.org/10.1029/GM070p0387**

Richter, F.M. and DePaolo, D.J. (1987) Numerical models for diagenesis and the Neogene Sr isotopic evolution of seawater from DSDP Site 590B. Earth Planet. Sci. Lett., 83,27-38

Schlager, W., 1981. The paradox of drowned reefs and carbonate platforms. *Geological Society of America Bulletin,* 92(4):197–211. **http://dx.doi.org/10.1130/0016-7606(1981)92<197:TPODRA>2.0.CO;2**

Swart, P.K., 2008. Global synchronous changes in the carbon isotopic composition of carbonate sediments unrelated to changes in the global carbon cycle. *Proceedings of the National Academy of Sciences of the United States of America,* 105(37):13741–13745. **http://dx.doi.org/10.1073/pnas.0802841105**

Tomczak, M., and Godfrey, J.S., 2003. *Regional Oceanography: An Introduction* (2nd ed.): Delhi (Daya Publishing House).

Zampetti, V., Schlager, W., van Konijnenburg, J.-H., and Everts, A.-J., 2004. Architecture and growth history of a Miocene carbonate platform from 3D seismic reflection data: Luconia province, offshore Sarawak, Malaysia. *Marine and Petroleum Geology*, 21(5): 517–534. **http://dx.doi.org/10.1016/j.marpetgeo.2004.01.006**

Zheng, H., Powell, C.M., Rea, D.K., Wang, J., and Wang, P., 2004. Late Miocene and mid-Pliocene enhancement of the East Asian monsoon as viewed from the land and sea. *Global and Planetary Change*, 41(3–4):147–155. **http://dx.doi.org/10.1016/j.gloplacha.2004.01.003**

Table T1. Expedition 359 hole summary.

Hole	Latitude	Longitude	Water depth (m)	Penetration DSF (m)	Cored interval (m)	Recovered length (m)	Recovery (%)	Drilled interval (m)	Drilled interval (*N*)	Total cores (*N*)	Date started (UTC)	Date finished (UTC)	Time on hole (days)	Comments
359-														
U1465A	4°55.9873′N	073°0.6786′E	515.01	76.6	76.6	53.37	70		0	11	10/18/2015 2318	10/19/2015 2115	0.91	Two water cores
U1465B	4°55.9862′N	073°0.6897′E	512.64	221.3	155.4	9.41	6	65.9	1	22	10/26/2015 1220	10/27/2015 0850	0.85	Offset 20 m east of Hole U1465A
U1465C	4°55.9865′N	073°0.7002′E	510.12	233.2	178.2	24.60	14	55.0	1	25	10/27/2015 0850	10/28/2015 1818	1.39	Offset 20 m east of Hole U1465B
		Site U1465 totals:		531.1	410.2	87.38		120.9	2	58				
U1466A	4°55.9888′N	073°1.6785′E	518.09	326.2	326.2	243.79	75		0	50	10/19/2015 2115	10/22/2015 0500	2.32	
U1466B	4°55.9883′N	073°1.6893′E	517.14	809.7	495.7	88.54	18	314.0	1	56	10/22/2015 0500	10/26/2015 1220	4.31	
		Site U1466 totals:		1135.9	821.9	332.33		314.0	1	106				
U1467A	4°51.0139′N	073°17.0200′E	487.49	32.0	32.0	31.49	98		0	4	10/28/2015 1518	10/29/2015 0400	0.53	
U1467B	4°51.0255′N	073°17.0204′E	487.49	617.2	617.2	560.39	91		0	77	10/29/2015 0400	11/1/2015 0605	3.09	Offset 20 m north of Hole U1467A
U1467C	4°51.0362′N	073°17.0197′E	487.28	714.0	332.1	266.15	80	381.9	2	35	11/1/2015 0605	11/3/2015 1910	2.55	Offset 20 m north of Hole U1467B
U1467D	4°51.0475′N	073°17.0201′E	487.23	201.0	199.5	203.29	102	1.5	1	21	11/3/2015 1910	11/4/2015 0825	0.55	Offset 20 m north of Hole U1467C
U1467E	4°51.0137′N	073°17.0312′E	487.42	714.0			0	714.0	1	0	11/4/2015 0825	11/6/2015 1924	2.46	Offset 20 m east of Hole U1467A
		Site U1467 totals:		2278.2	1180.8	1061.32		1097.4	4	137				
U1468A	4°55.9832′N	073°4.2780′E	521.50	874.7	873.7	458.70	53	1.0	1	110	11/6/2015 2106	11/10/2015 1900	3.91	
U1468B	4°55.9823′N	073°4.2888′E	521.45	874.7			0	874.7	1	0	11/10/2015 1900	11/13/2015 0625	2.48	
		Site U1468 totals:		1749.4	873.7	458.70		875.7	2	110				
U1469A	4°54.4143′N	073°0.4910′E	426.93	161.1	161.1	4.14	3		0	17	11/13/2015 0625	11/14/2015 0310	0.86	
U1469B	4°54.4166′N	073°0.4694′E	426.91	151.4	29.4	0.72	2	122.0	1	3	11/14/2015 0310	11/14/2015 1548	0.53	
		Site U1469 totals:		312.5	190.5	4.86		122.0	1	20				
U1470A	4°45.9828′N	072°59.0324′E	399.70	190.0	190.0	139.78	74		0	24	11/14/2015 2230	11/15/2015 1555	0.73	
U1470B	4°45.9818′N	072°59.0210′E	399.72	343.7	174.8	7.35	4	168.9	1	18	11/15/2015 1555	11/17/2015 1448	1.95	
		Site U1470 totals:		533.7	364.8	147.13		168.9	1	42				
U1471A	4°45.9825′N	073°08.1358′E	419.40	685.1	685.1	366.08	53		0	82	11/17/2015 1048	11/20/2015 0528	2.78	
U1471B	4°45.9825′N	073°08.1263′E	420.29	6.7	6.7	6.62	99		0	1	11/20/2015 0528	11/20/2015 2345	0.76	
U1471C	4°45.9831′N	073°08.1147′E	419.19	178.8	178.8	170.19	95		0	19	11/20/2015 2345	11/21/2015 1500	0.64	
U1471D	4°45.9828′N	073°08.1035′E	419.19	58.0	57.0	56.76	100	1.0	1	6	11/21/2015 1500	11/22/2015 0045	0.41	
U1471E	4°45.9829′N	073°08.0929′E	419.19	1003.7	407.4	171.54	42	596.3	1	43	11/22/2015 0045	11/26/2015 1620	4.65	
		Site U1471 totals:		1932.3	1335.0	771.19		597.3	2	151				
U1472A	4°46.2653′N	073°04.0111′E	379.34	251.9	251.9	233.75	93	0	0	34	11/26/2015 1620	11/27/2015 2112	1.2	
		Site U1472 totals:		251.9	251.9	233.75		0	0	34				
		Expedition 359 totals:		8725.0	5428.8	3096.66		3296.2	13	658				

Figure F1. Location map of the Maldives in the central equatorial Indian Ocean. The Maldives carbonate platform consists of 22 atolls on the Laccadive–Maldives Ridge, a volcanic ridge that formed when the Indian plate moved over the Réunion hotspot.

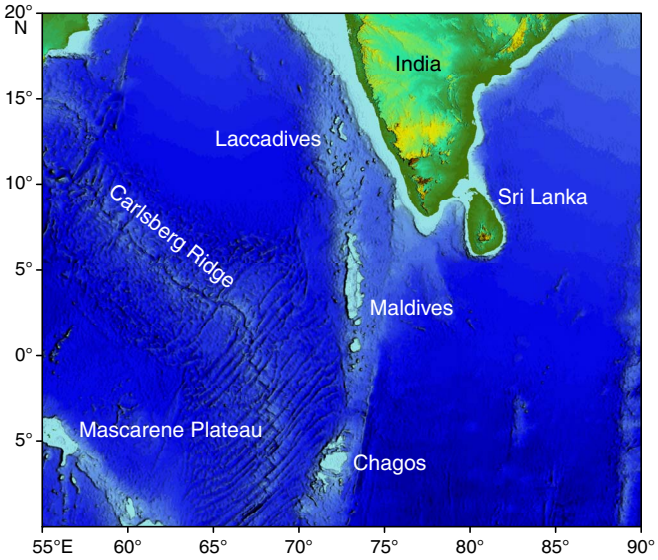

Figure F2. Location map of Expedition 359 sites in the Inner Sea of the Maldives with line plan of site survey seismic lines for ARI 1, an existing industrial well that served for pre-expedition seismic stratigraphic interpretation.

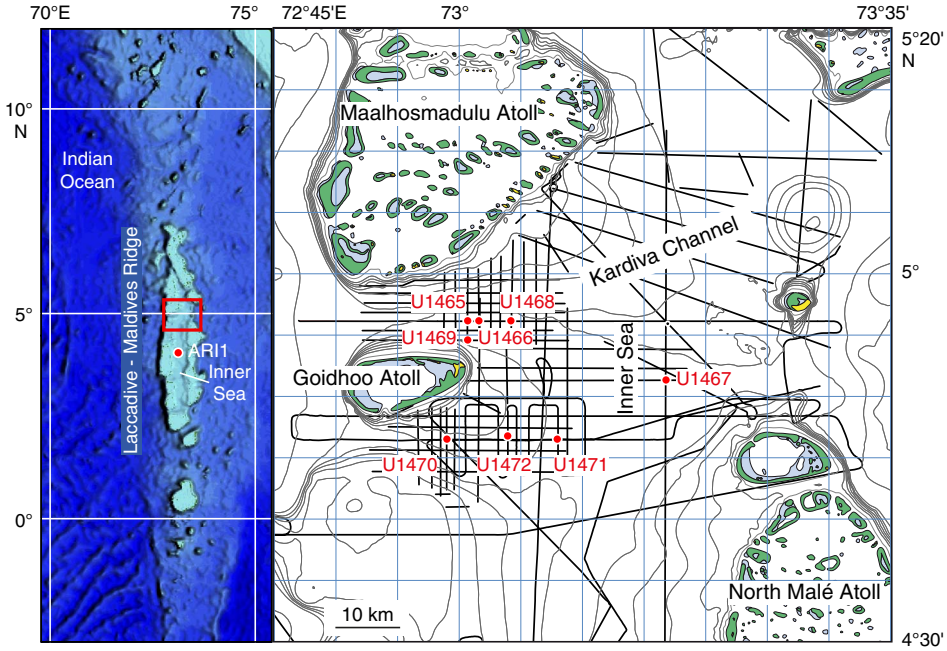

Figure F3. Sketch of the Maldives carbonate platform stratigraphy. The volcanic basement is overlain by Eocene and Oligocene neritic carbonates. During the Oligocene, the platform areas shrank and two north-south–trending carbonate banks developed. During the Miocene, shallow-water carbonate banks partly drowned, whereas other platform areas grew further on. Contemporaneously, the carbonate platform was affected by an intensification of currents, as registered by the onset of widespread drift sedimentation in the Inner Sea of the Maldives. The research strategy for Expedition 359 was to drill two transects of sites going from the inner part of the drowned platforms toward the Inner Sea, where the drifts accumulated in more current-protected settings.

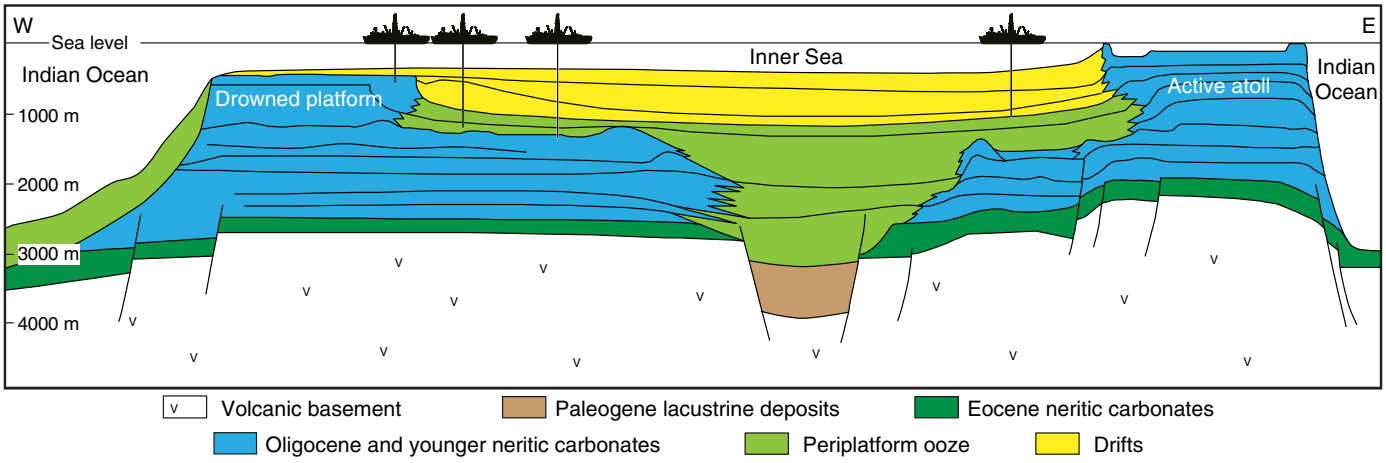

Figure F4. Expedition 359 northern transect with location of sites. Close view of the western part of seismic Line NEOMA-P65 (vertical exaggeration = 6×) running west–east through northern Kardiva Channel with sequence stratigraphic interpretation (Betzler et al., 2013a; Lüdmann et al., 2013) and age assignments.

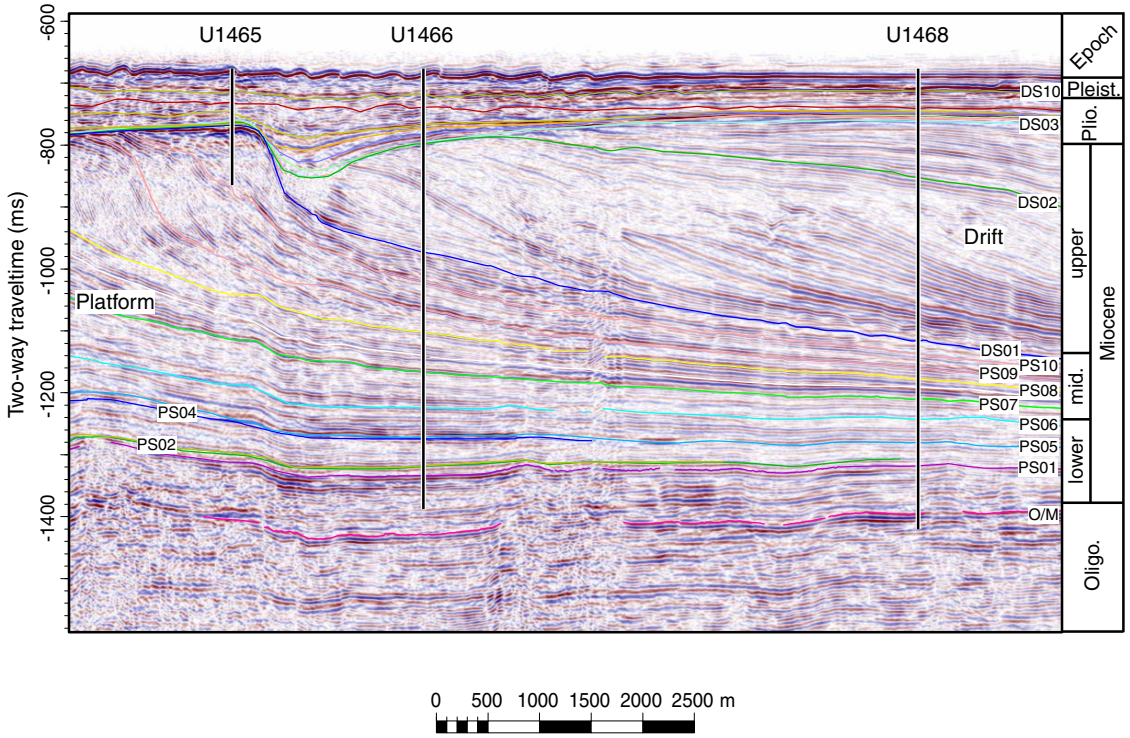

Figure F5. Expedition 359 southern transect with location of sites along seismic Line NEOMA-P62 (vertical exaggeration = 6×) running west–east through southern Kardiva Channel. The position of Site U1472 is projected onto the line; the site is located 400 m north of the line.

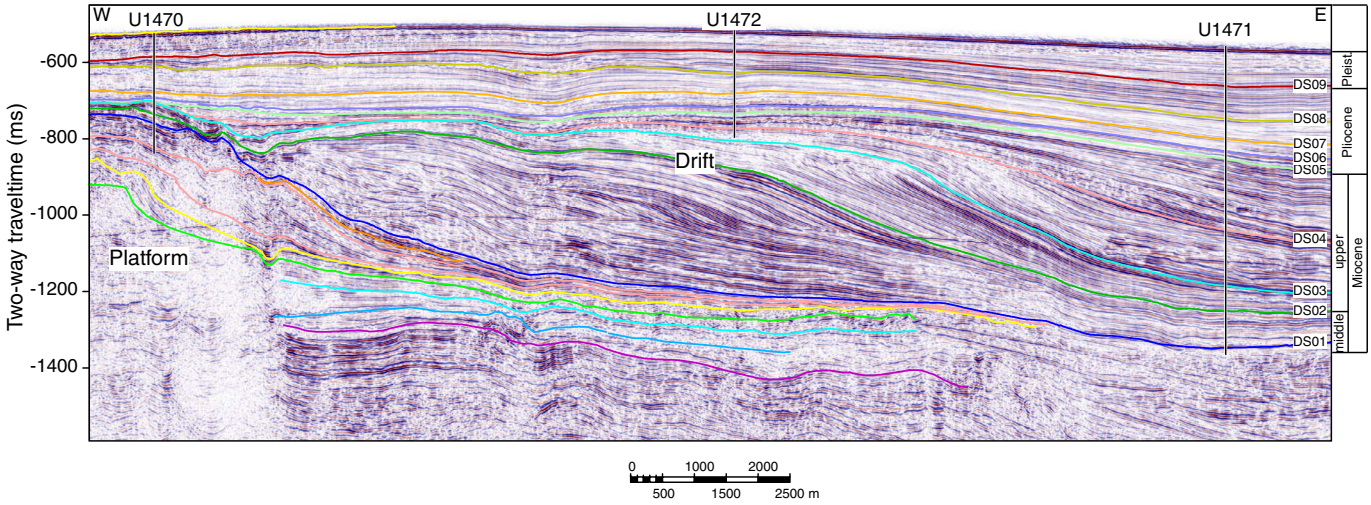

Figure F6. A. Floatstone facies of Unit II with abundant bioclastic molds, some of them with geopetal infills (yellow box), Site U1465. Scale bar = 5 mm. B. Close-up of geopetal infill in a mold (yellow box = contact between original rock and infill). Two different generations of geopetal infill are marked by different brown shades. The uppermost part of the infill displays evidences of bioerosion (scale bar = 1 mm). C. Close-up of contact between original rock and geopetal infill. Contact surface shows extensive dolomitization marked by sucrosic dolomite. Small planktonic foraminifers floating in a micritic matrix, locally showing porostromate structures, are present in the infill (scale bar = 1 mm).

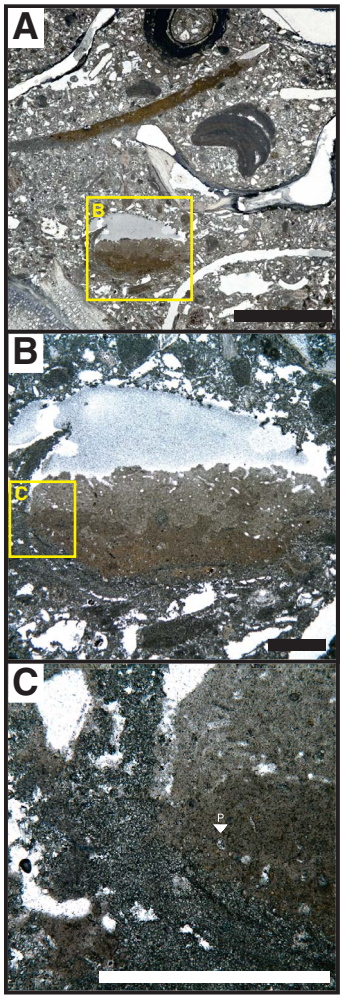

Figure F7. Thin section photographs showing the main benthic foraminifers in Units II and III, Hole U1465A. Scale bars = 1 mm. A–B. *Nummulites* sp. (TSB 11X-CC, 29–31 cm). C. *Amphistegina* sp. (TSB 23R-1W, 21–25 cm). D. *Heterostegina* sp. and *Nummulites* sp. (TSB 21R-1W, 83–86 cm). E. *Lepidocyclina* sp. (TSB 21R-1W, 83–86 cm). F. *Miogypsina* sp. (TSB 23R-1W, 21–25 cm).

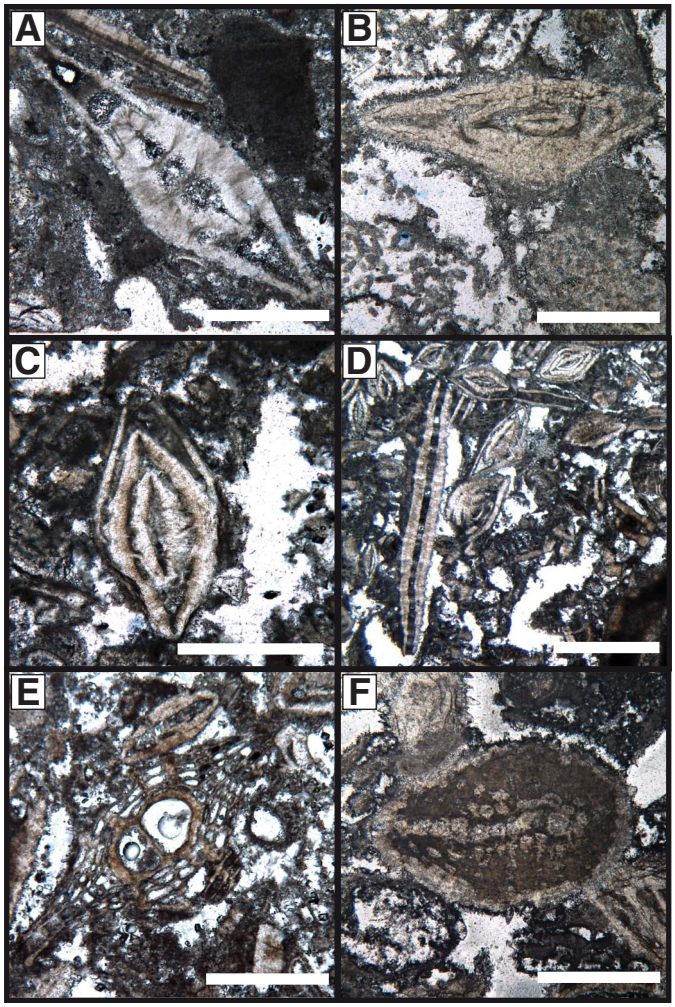

Figure F8. Relative concentration of aragonite (Arag), high-Mg calcite (HMC), low-Mg calcite (LMC), dolomite (Dol), and quartz (Qtz) as determined using X-ray diffraction, Site U1465. Dotted line = depth of the drowned platform top as inferred by the disappearance of aragonite.

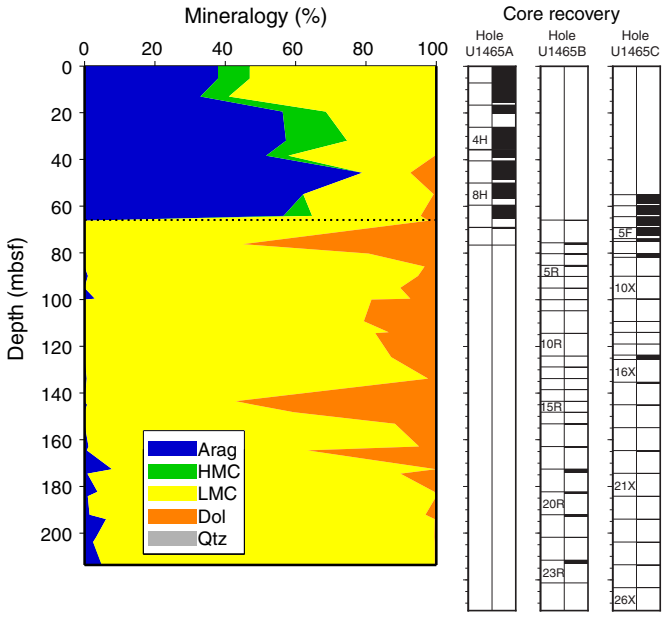

Figure F9. Seismic section showing the drowned Kardiva platform and the onlap and burial by drift sequences, Site U1465. Light blue lines = platform sequence (PS) boundaries, orange lines = drift sequence (DS) boundaries, dark blue line = horizon that separates PSs and DSs. O/M = Oligocene/Miocene boundary.

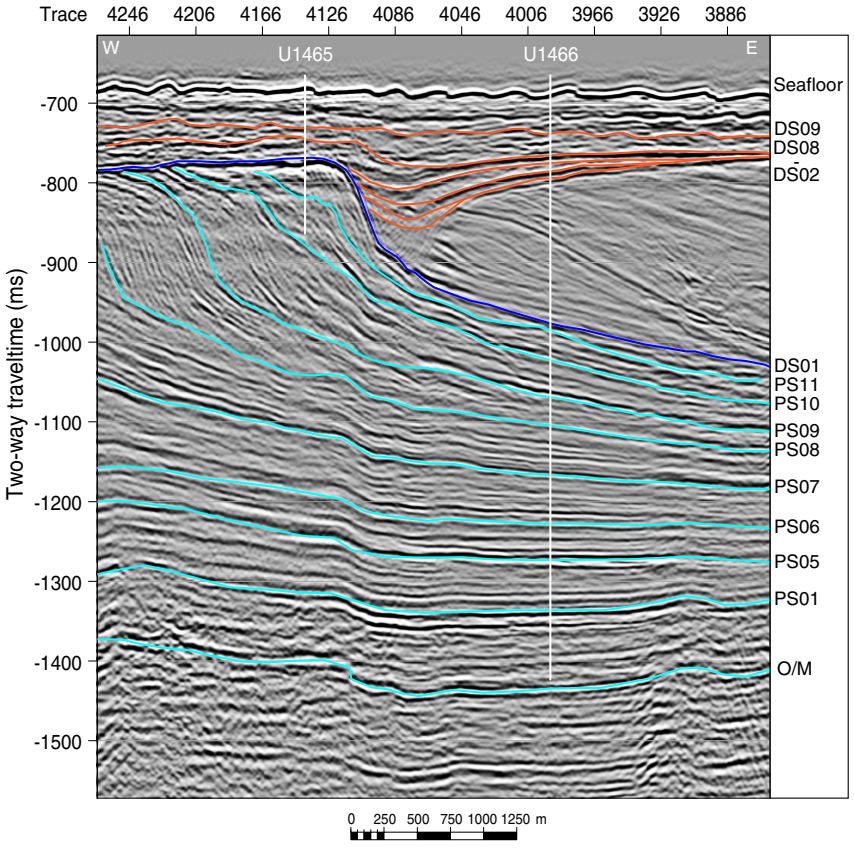

Figure F10. Photomicrograph of fine-grained packstone with common planktonic foraminifers, a few benthic foraminifers, some mollusk fragments, and abundant bioclasts in a micritic (partially recrystallized) matrix (359-U1466A-50X-CC, 30–33 cm; 317.72 mbsf). Scale bar = 1 mm.

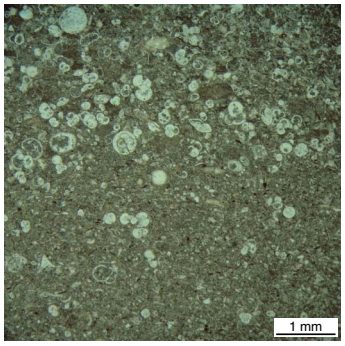

Figure F11. Typical black organic-rich and white chalk alternation present within Unit VII (359-U1466B-56R-1 [top = 789.60 mbsf] and 56R-2).

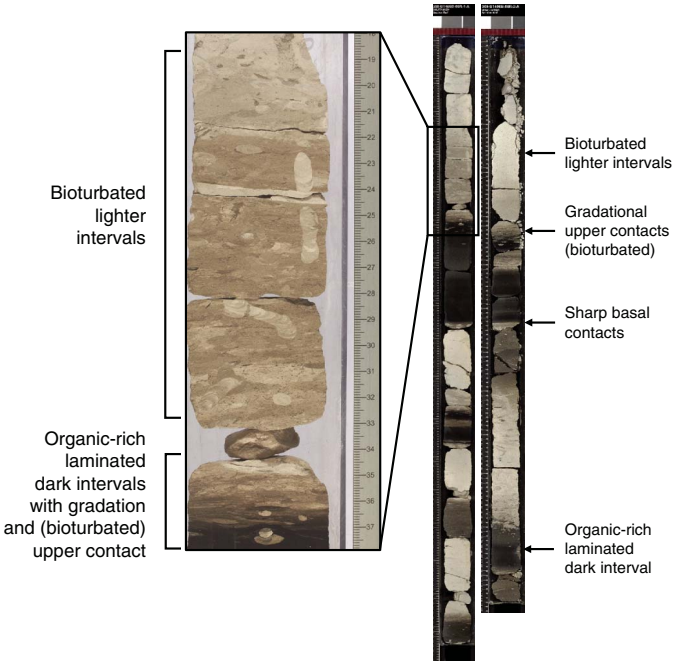

Figure F12. Age-depth plot, Site U1466. L = last occurrence, F = first occurrence. *G.rp* = *Globigerinoides ruber* pink, *E.h* = *Emiliania huxleyi*, *P.l* = *Pseudoemiliania lacunosa*, *G.f* = *Globigerinoides fistulosus*, *D.b* = *Discoaster brouweri*, *D.p* = *Discoaster pentaradiatus*, *G.l* = *Globorotalia limbata*, *D.a* = *Dentoglobigerina altispira*, *S.a* = *Sphenolithus abies*, *D.q* = *Discoaster quinqueramus*, *G.d* = *Globoquadrina dehiscens*, *C.n* = *Coronocyclus nitescens*, *F.f* = *Fohsella fohsi*, *S.h* = *Sphenolithus heteromorphus*, *O.s* = *Orbulina suturalis*, *S.p* = *Sphenolithus pseudoheteromorphus*, *P.k* = *Paragloborotalia kugleri*, *S.d* = *Sphenolithus delphix*.

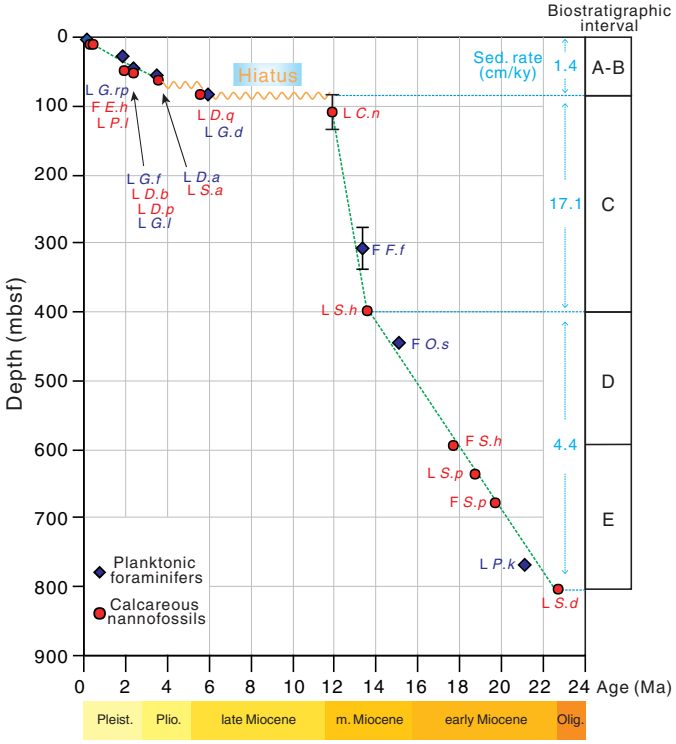

Figure F13. Selected planktonic foraminifers, Site U1466. Scale bars = 250 µm, unless other scale is provided. 1. *Globigerinoides ruber* pink (two specimens on the left) and white (one specimen on the right). 2–3. *Globorotalia limbata*. 4. *Orbulina suturalis*. 5–6. *Globorotalia truncatulinoides*. 7. *Praeorbulina sicana*. 8. *Dentoglobigerina altispira*. 9. *Pulleniatina obliquiloculata*. 10–11. *Paragloborotalia kugleri*. 12. *Globigerinatella insueta*. 13. *Globigerinoides fistulosus*. 14–15. *Fohsella fohsi*.

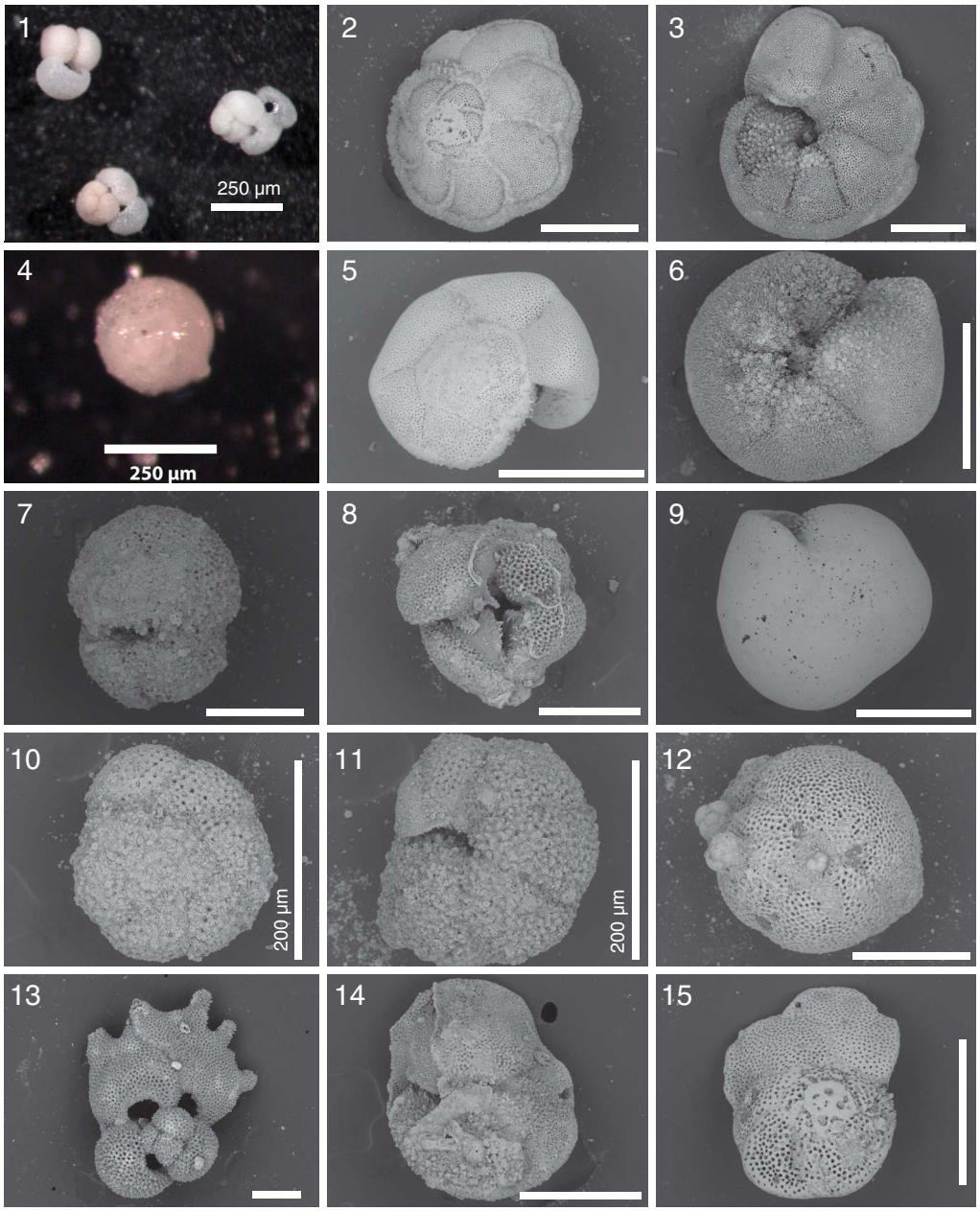

Figure F14. Relative concentrations of aragonite (Arag), calcite (Calc), dolomite (Dol), and quartz (Qtz) as determined using X-ray diffraction, Site U1466. Depths of peaks in dolomite are noted.

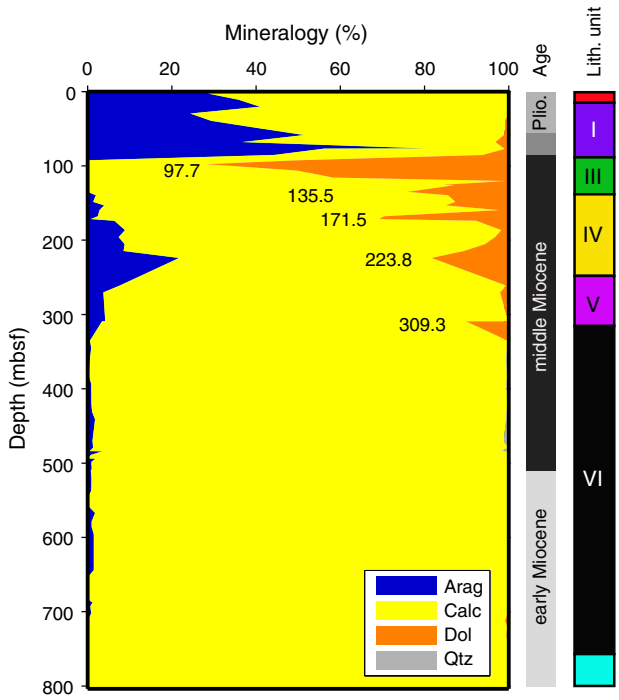

Figure F15. Physical property measurements, Site U1466. Bulk density = GRA density from the Whole-Round Multisensor Logger (WRMSL) and discrete wet bulk density. Porosity was measured using moisture and density (MAD) mass/volume Method C.

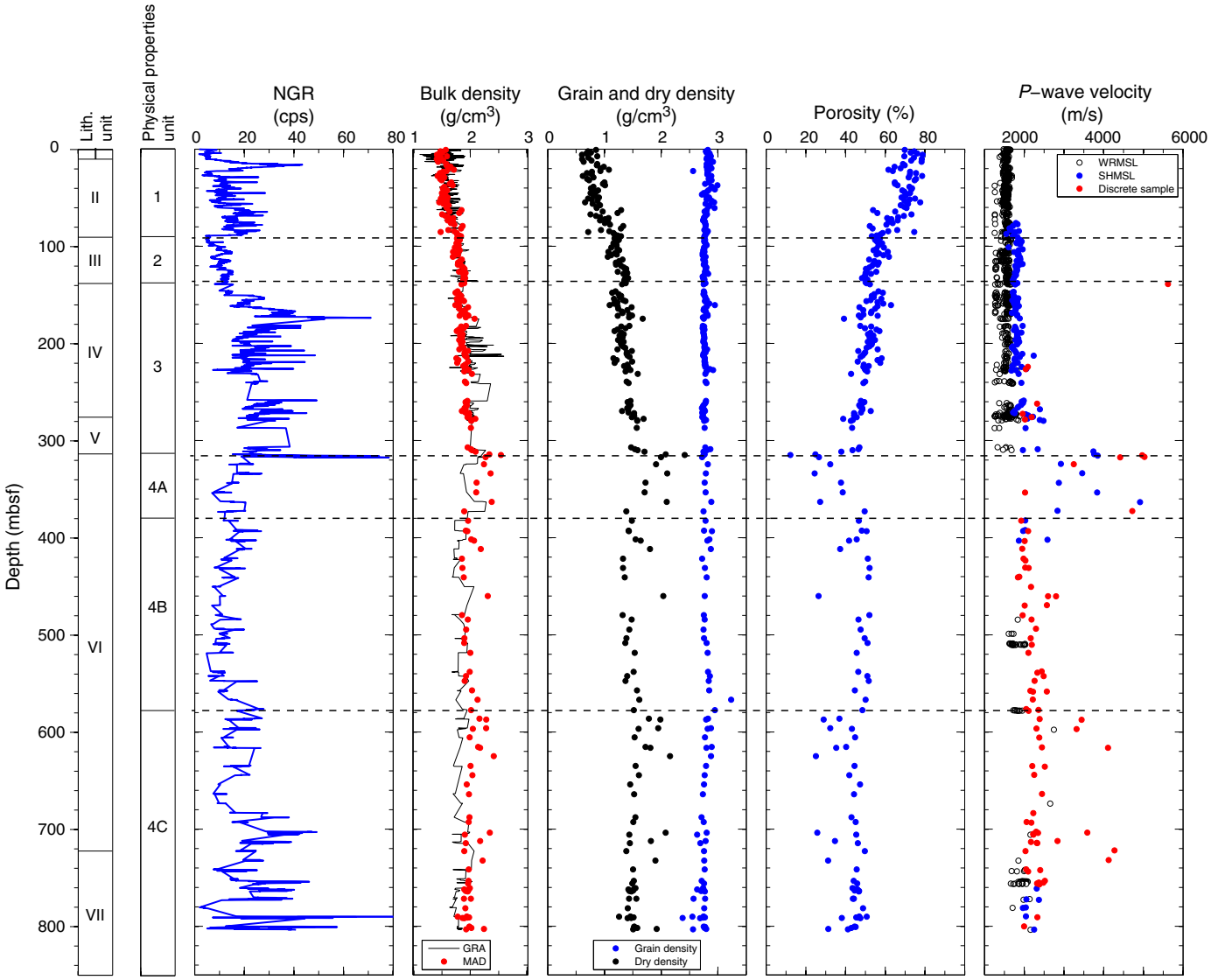

Figure F16. Physical property measurements, Site U1466. Seismic Line 65 (M74) shows position of Site U1466 and bases of seismic megasequences (DS = drift sequence, PS = platform sequence). *P*-wave caliper (PWC), NGR, and HSGR data are from downhole logging. Interval velocity is the model for time-depth conversion. Dashed lines indicate sequence boundaries.

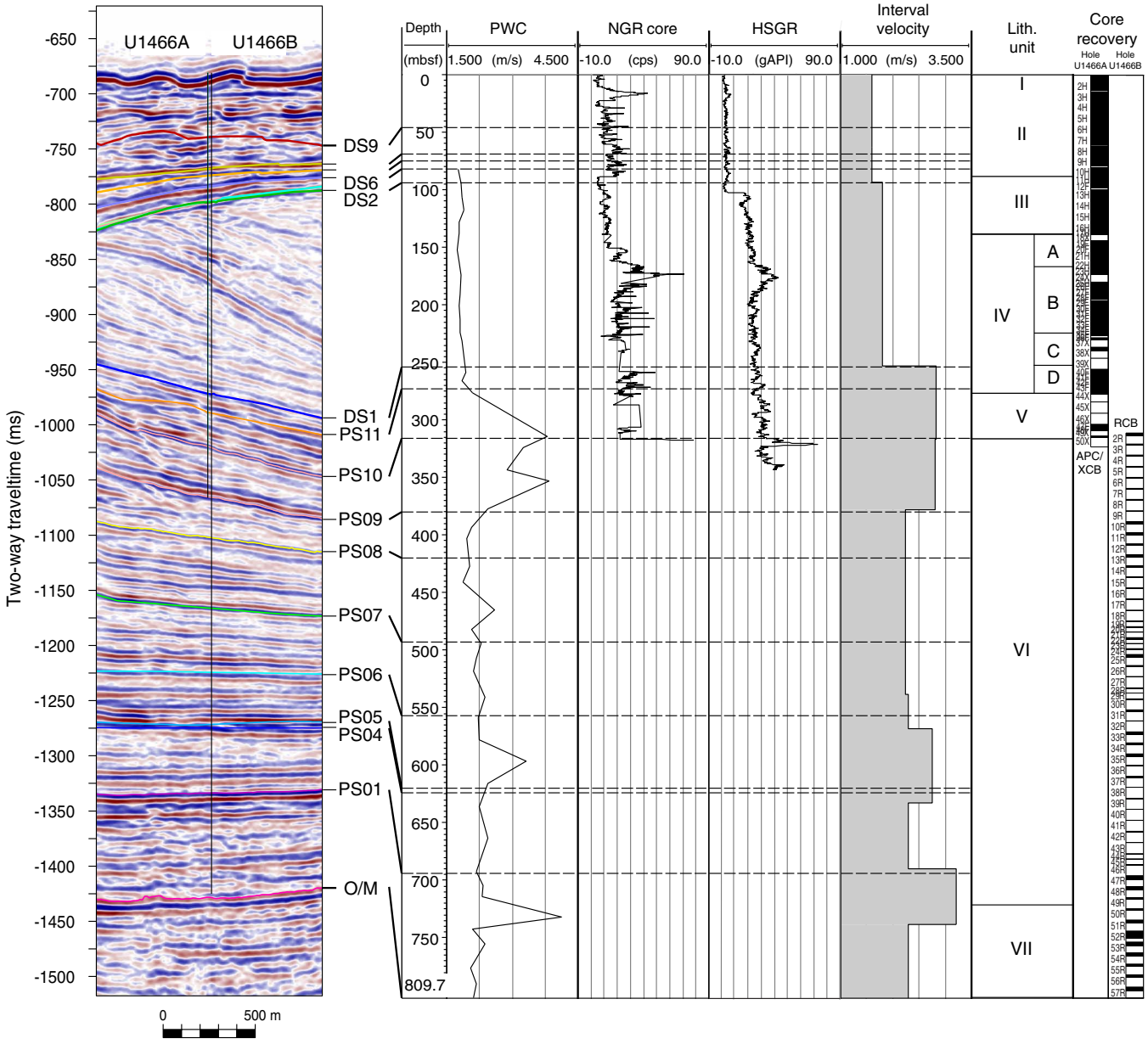

Figure F17. Age-depth plot, Site U1467. The age constraint for the base of the recovered sediments from <13.3–13.4 Ma is based on several reliable events which must occur below the base of Hole U1647C. The green dotted correlation line and sedimentation rates are based on biostratigraphic data alone, and magnetostratigraphic data has been added to show good coherence between these data sources. Plotted paleomagnetic events are chron tops. L = last occurrence, F = first occurrence. *G.*rp = *Globigerinoides ruber* pink, *E.h* = *Emiliania huxleyi*, *P.l* = *Pseudoemiliania lacunosa*, S *sG* = Start small *Gephyrocapsa* event, *C.m* = *Calcidiscus macintyrei*, *G.f* = *Globigerinoides fistulosus*, *D.b* = *Discoaster brouweri*, *G.limbata* = *Globorotalia limbata*, *D.p* = *Discoaster pentaradiatus*, *D.a* = *Dentoglobigerina altispira*, *S.a* = *Sphenolithus abies*, *G.m* = *Globorotalia margaritae*, *R.p* = *Reticulofenestra pseudoumbilicus*, *D.q* = *Discoaster quinqueramus*, *G.d* = *Globoquadrina dehiscens*, *N.a* = *Nicklithus amplificus*, *G. lenguaensis* = *Globorotalia lenguaensis*, S *sR* = Start small *Reticulofenestra* event, *P.m* = *Paragloborotalia mayeri*, *F.f* = *Fohsella fohsi*, *C.n* = *Coronocyclus nitescens*.

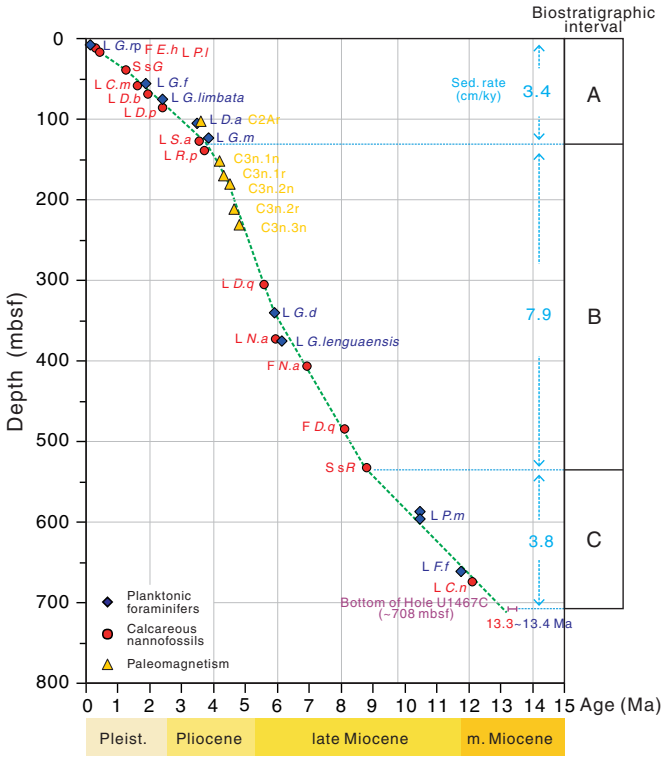

Figure F18. Variations in concentrations of Cl^-, Na^+, and K^+, Holes U1467A–U1467C.

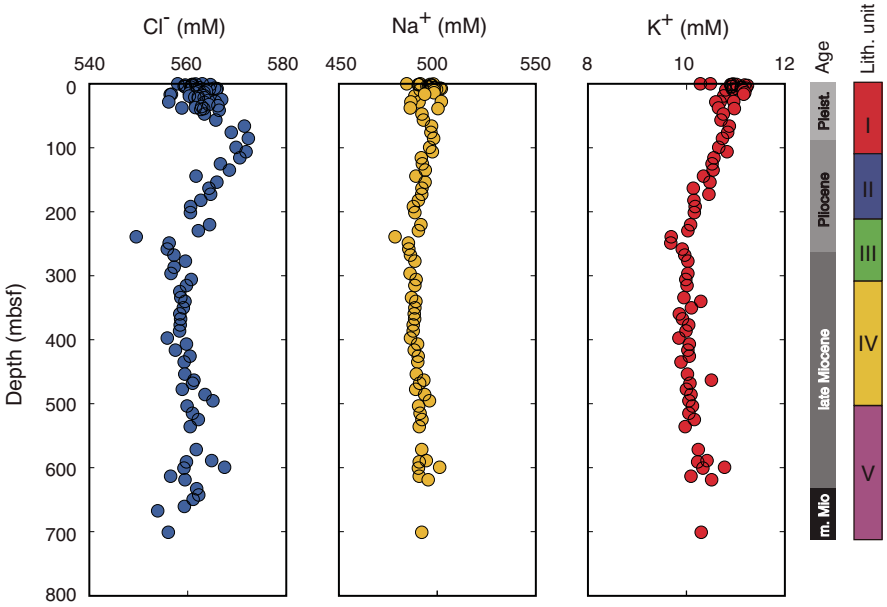

Figure F19. Summary of downhole logs recorded by the triple combo tool string, Hole U1467E. Downhole logs (marked Log) are on the logging depth scale (WMSF); all other data are on the core depth scale (CSF-A). MAD = moisture and density. Magnetic susceptibility: gray dots = WRMSL, blue dots = MSP. Resistivity: R3 = medium resistivity reading of HRLA, R5 = deepest resistivity, RT = true resistivity, modeled from all depths of investigation.

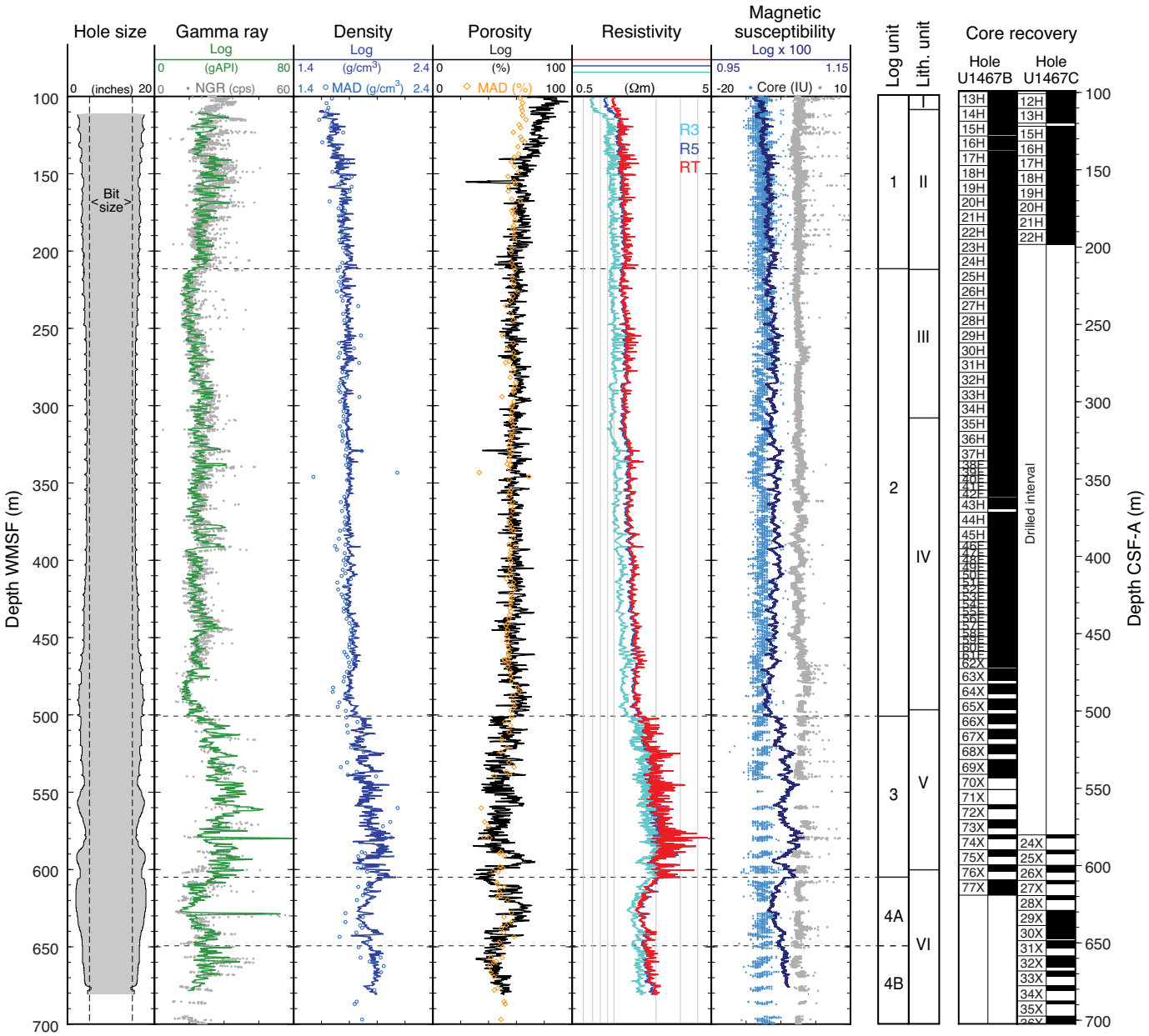

Figure F20. Thin section photomicrographs of *Amphistegina* sp. grainstone (359-U1468-7H-2, 48–50 cm). A. 1 = *Amphistegina* sp., 2 = red algal lithoclast cemented by bladed cements in plane-polarized light. B. Same view in cross-polarized light.

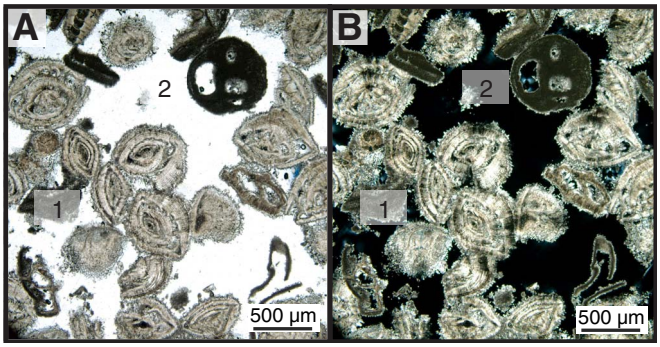

Figure F21. Core close-up photographs (359-U1468A-17F-1, 47–68 cm). A. Fining-upward layers from very coarse grained rudstone to fine-grained packstone with an erosional surface at each succession. The top of this section is the Subunit IIA/IIB boundary. B. Very coarse grained rudstone between 56 and 65 cm (red line) in A showing large components (≈1 cm) such as rip-up clasts, large benthic foraminifers, echinoid spines, and lithoclasts.

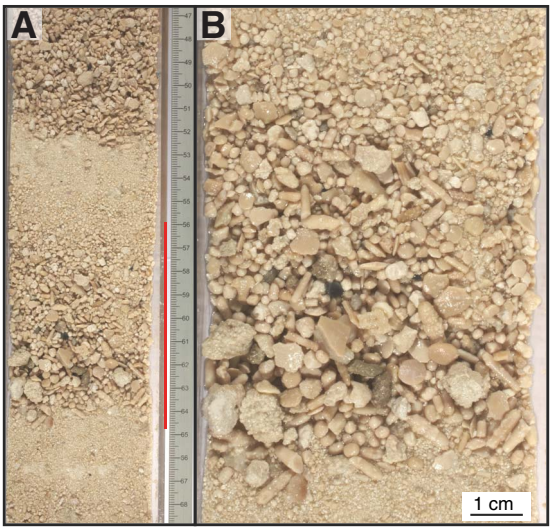

Figure F22. Light–dark alternations in coccolith-rich lower Miocene deposits (359-U1468A-99X).

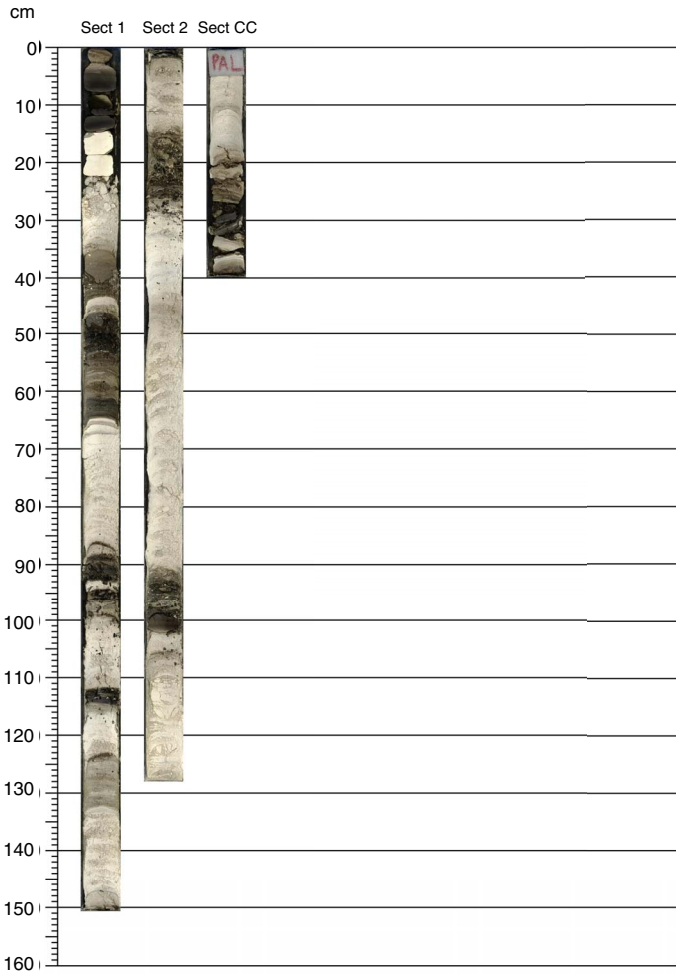

Figure 23. Triple combo downhole logs, Hole U1468B. Downhole logs are on the logging depth scale (WMSF), whereas core data (NGR, density and porosity, and MS [WRMSL and MSP]) and core recovery from Hole U1468A are on the core depth scale (CSF-A). HSGR = total spectral gamma ray; GR EDTC = total gamma ray from EDTC. R3 = medium resistivity reading of HRLA, R5 = deepest resistivity, RT = true resistivity, modeled from all depths of investigation.

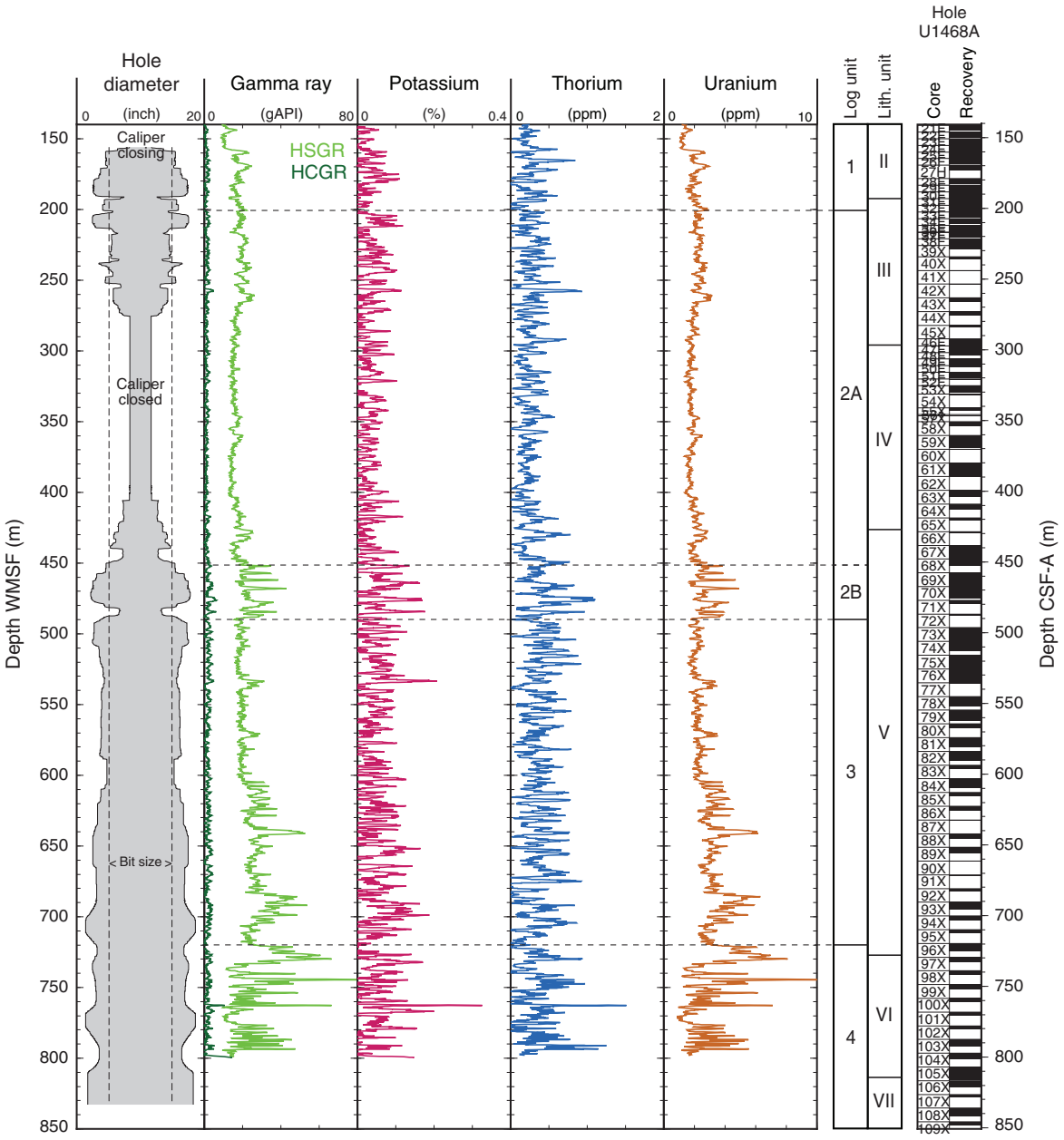

Figure F24. Seismic section of Site U1468 displaying the drowned Kardiva platform and burial by drift sequences. Light blue lines = platform sequence (PS) boundaries, orange lines = drift sequence (DS) boundaries, dark blue line = horizon that separates PSs and DSs. CDP = common depth point. O/M = Oligocene/Miocene boundary.

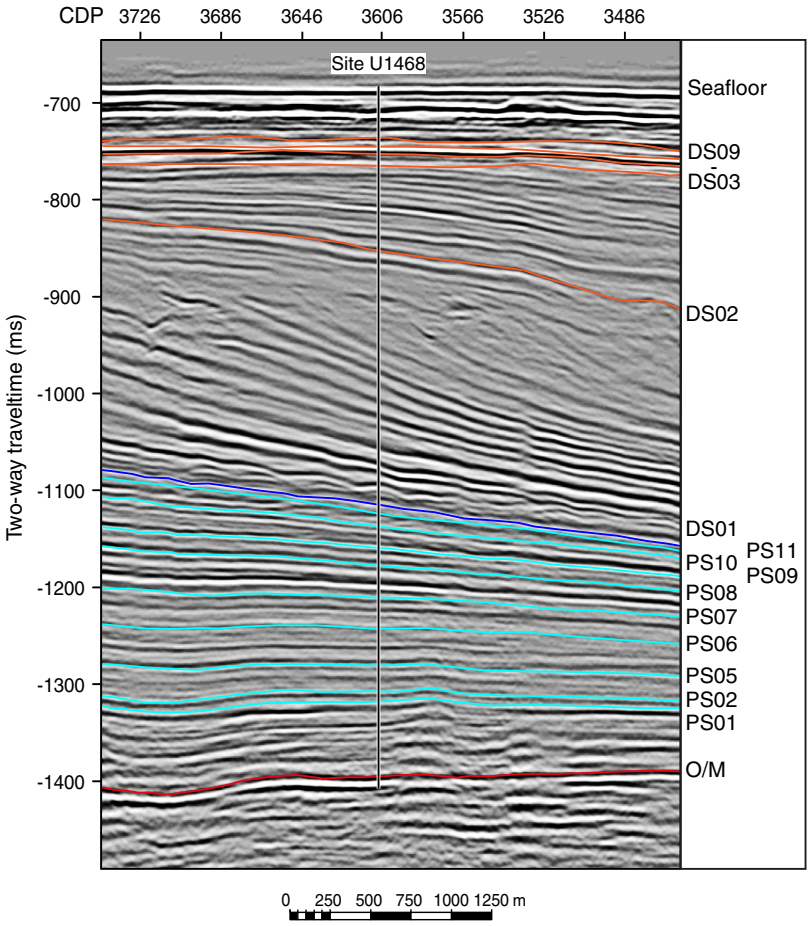

Figure F25. Lithostratigraphic Unit II/III boundary (359-U1469B-4R). A. Close-up of transition from white foraminiferal rudstone (Unit II) to grayish brown dolomitized floatstone (dolostone) (Unit III). (1) Boring and (2) coral fragment. B. Bioclastic grainstone from Unit II with benthic foraminifers. C. Dolomitized floatstone from Unit III showing (3) encrusting red algae and (4) coral fragment. Scale bars = 1 cm.

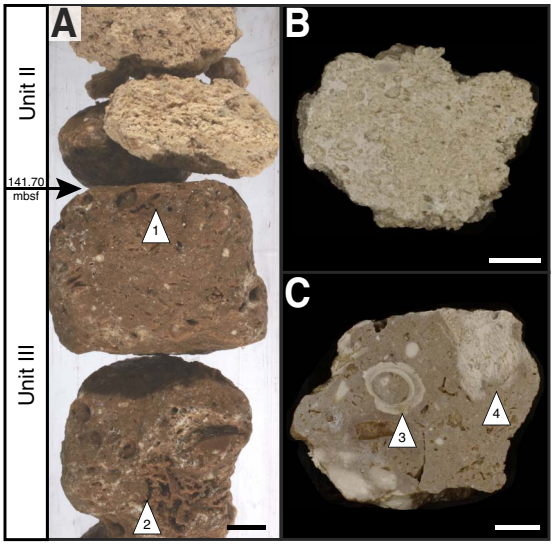

Figure F26. Physical property measurements, Site U1469. Detail of seismic Line 32 (SO236) shows position of Site U1469 and bases of seismic sequences (DS = drift sequence). Interval velocity is model for time-depth conversion.

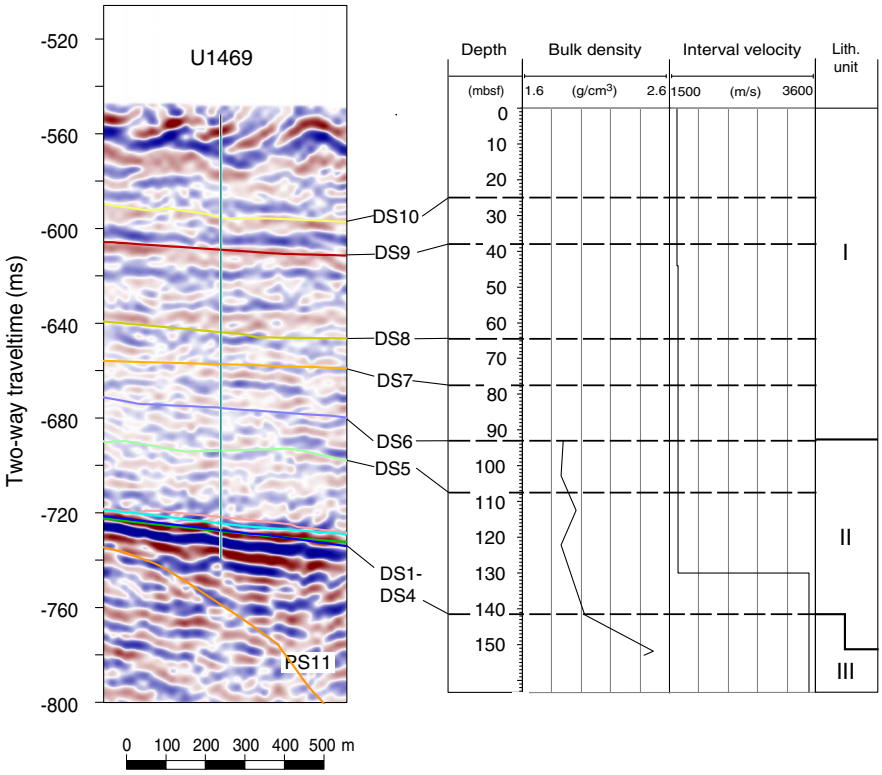

Figure F27. Age-depth plot showing changes in sedimentation rate, Site U1470. L = last occurrence, F = first occurrence. *G.rp* = *Globigerinoides ruber* pink, *E.h* = *Emiliania huxleyi*, *P.l* = *Pseudoemiliania lacunosa*, S *sG* = Start small *Gephyrocapsa* event, *G.f* = *Globigerinoides fistulosus*, *D.b* = *Discoaster brouweri*, *G.l* = *Globorotalia limbata*, *D.p* = *Discoaster pentaradiatus*, *D.a* = *Dentoglobigerina altispira*, *S.a* = *Sphenolithus abies*, *G.d* = *Globoquadrina dehiscens*.

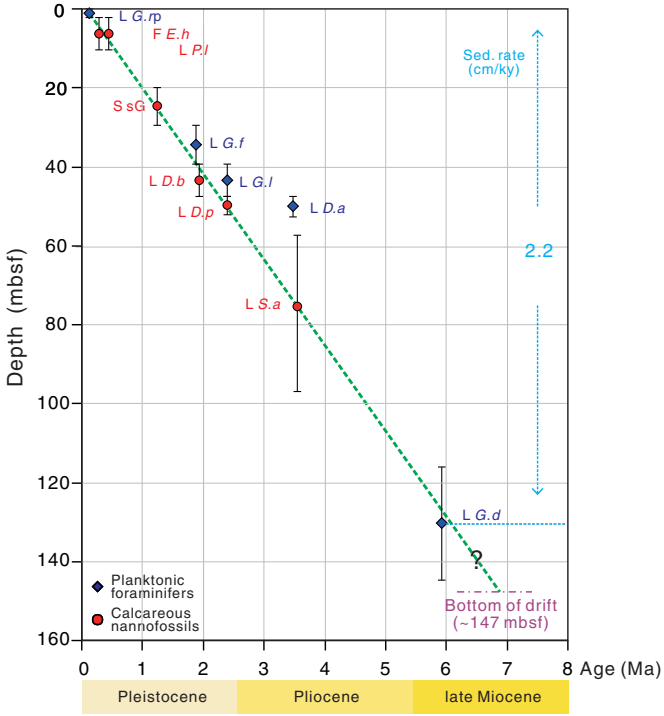

Figure F28. Variations in concentrations of Cl^-, Na^+, and K^+ in IW, Hole U1470A.

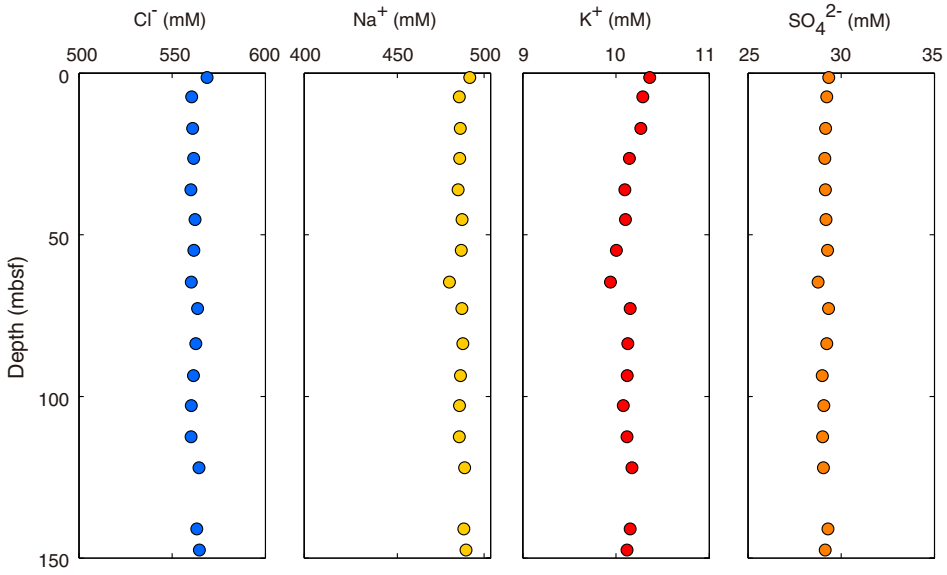

Figure F29. Physical property measurements, Site U1470. Detail of seismic Line 32 (SO236) shows position of Site U1470 and the bases of seismic megasequences (DS = drift sequence, PS = platform sequence). NGR is from core samples. Interval velocity is model for time-depth conversion.

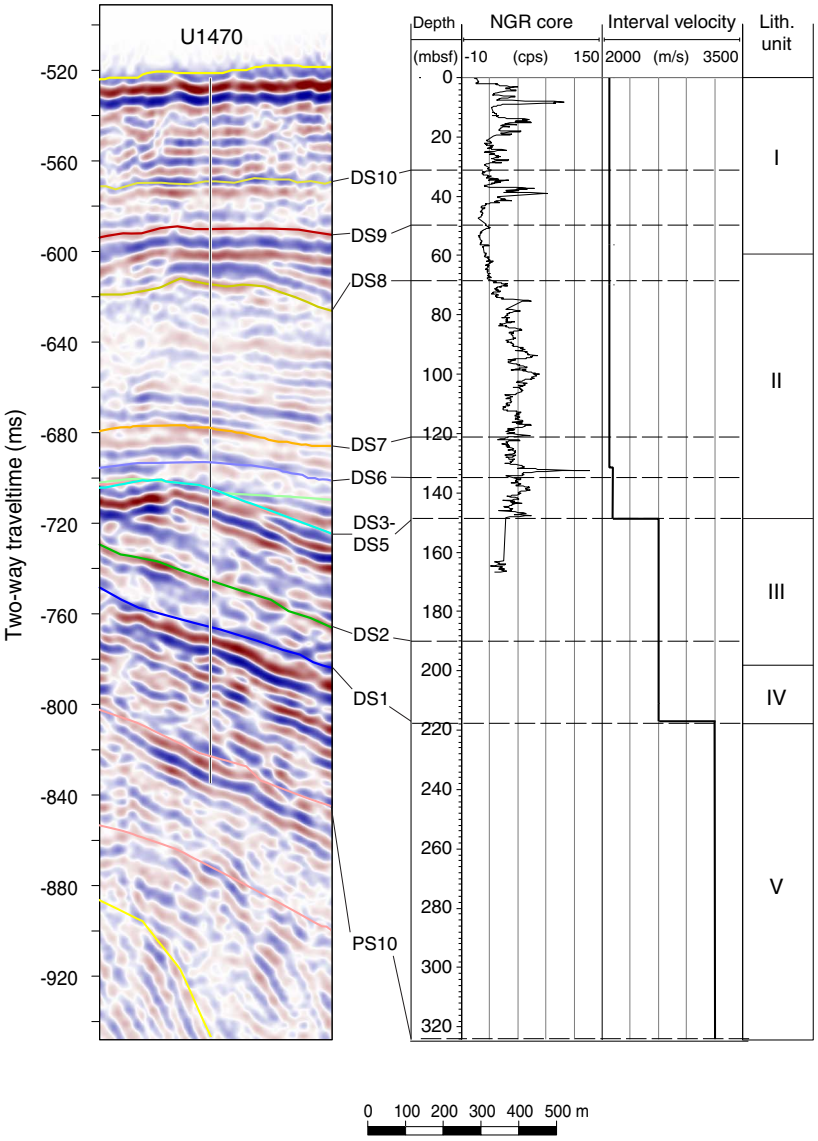

Figure F30. Components, porosity, and cementation in Unit V (TS 359-U1471A-38X-1). (A) plane-polarized light and (B) cross-polarized light photomicrographs of degraded foraminifers punctuated by (1) intraparticle, (2) moldic, and (3) interconnected vuggy porosity; (4) porosity is partially filled by celestine (blue color).

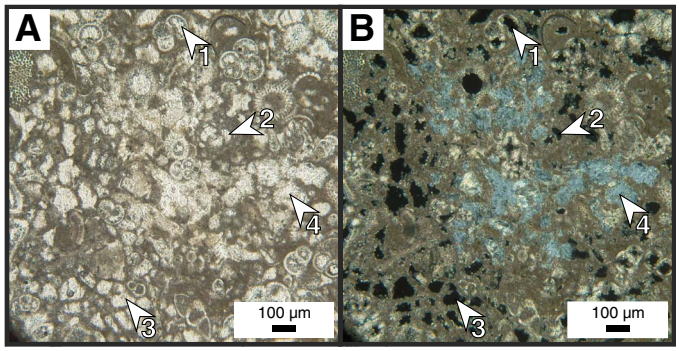

Figure F31. Sedimentary features, Unit VIII. A. Alternations between white and dark gray layers (359-U1471E-35R-3). B. Glauconitic rims around burrows (arrow), (34R-6). C. Fine pseudolamination structure (36R-2). Insert photomicrograph of lamination illustrates the discontinuous internal structure, possibly tapered and flattened burrows.

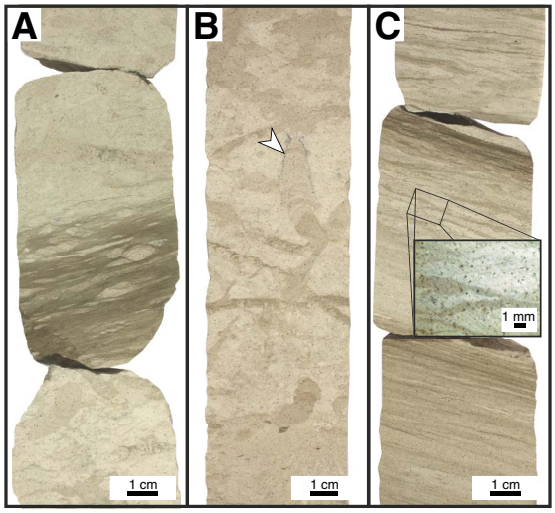

Figure F32. Relative concentrations of aragonite (Arag), high-Mg calcite (HMC), low-Mg calcite (LMC), dolomite (Dol) and quartz (Qtz) as determined using X-ray diffraction, Site U1471. Cel = celestine.

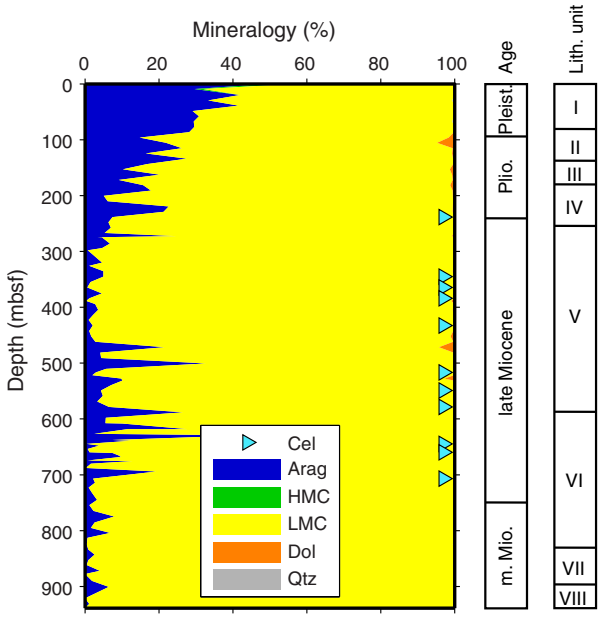

Figure F33. Close-up photographs (359-U1472A-4H-1). A. Unit I floatstone with grainstone matrix (3–46 cm). Red box = B. B. Floatstone (35.5–45.5 cm) showing large components such as solitary coral, intraclasts, echinoid fragments, and mollusk fragments. Red box = C. C. Solitary coral.

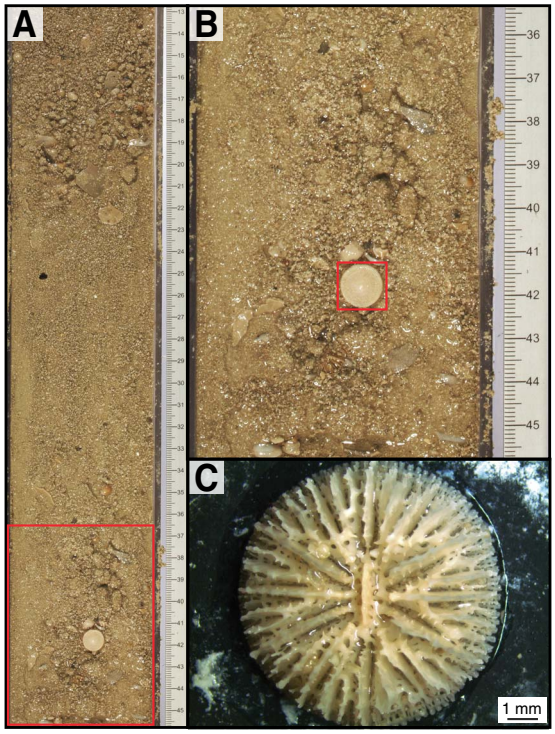

Figure F34. Operations and core recovery diagram, Expedition 359. Eight sites (U1465–U1472) were drilled using the APC, XCB, and RCB systems. Five sites were logged. Percentages at bottom of holes are core recovery (see Table **T1**). See **Site U1471** in Operations for more information on MDHDS testing.

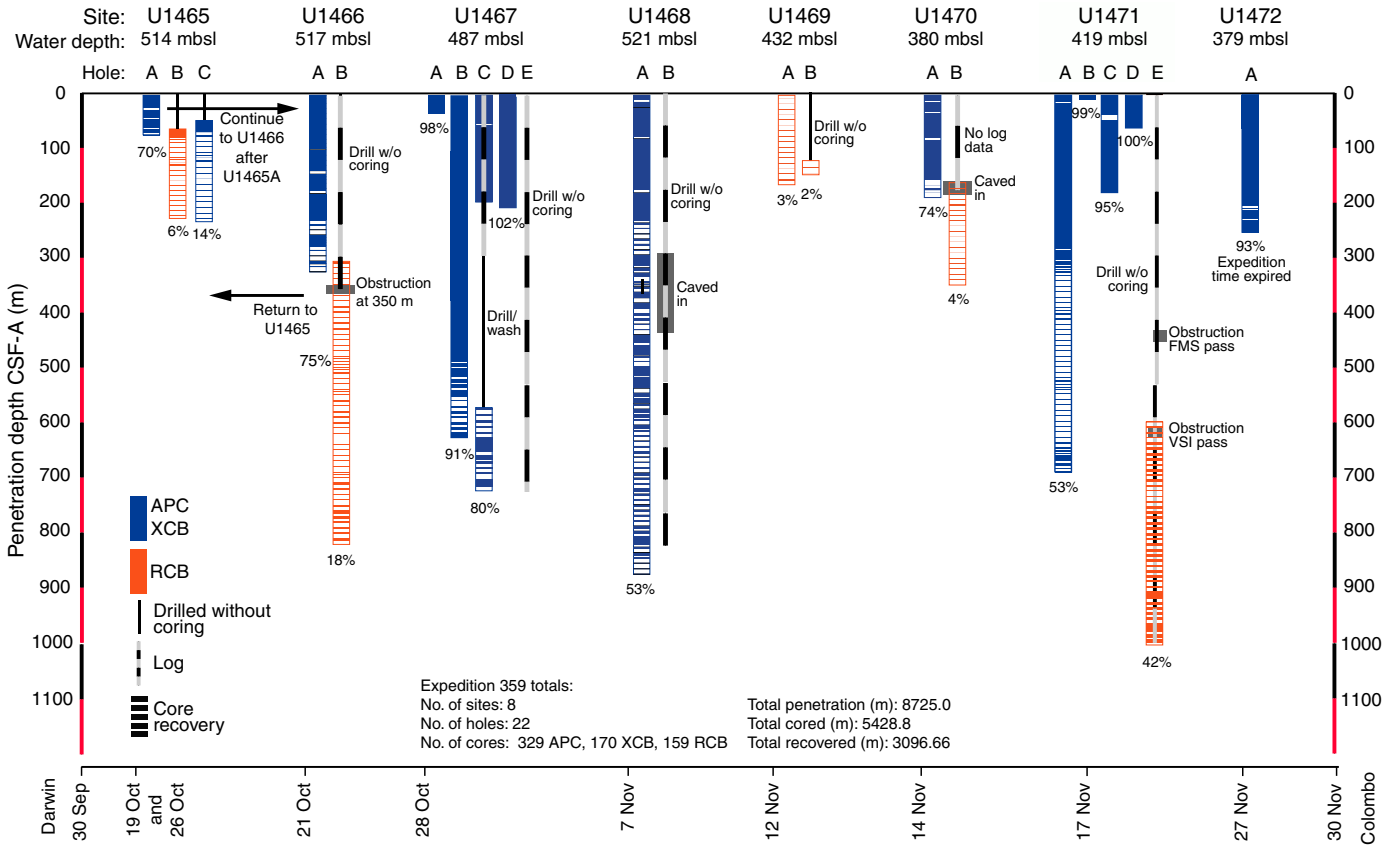

Site:	U1465	U1466	U1467	U1468	U1469	U1470	U1471	U1472
Proposed site:	(MAL-1A)	(MAL-2A)	(MAL-9A)	(MAL-3A)	(MAL-8A)	(MAL-5A)	(MAL-7A)	(MAL-6B)
Holes (#):	3	2	5	2	2	2	5	1
Cores (#):	58	106	137	110	20	42	151	34
Cored (m):	410.2	821.9	1180.8	873.7	190.5	364.8	1335	251.9
Recovered (m):	87.38	332.33	1061.32	458.7	4.86	147.13	771.19	233.75
Total penetration (m):	531.1	1135.9	2278.2	1749.4	312.5	533.7	1932.3	251.9
Logging:	NA	Triple combo only	Triple combo, FMS, VSI	Triple combo only	NA	NA	MHDHS test Triple combo, VSI, FMS	NA